Regulation of myelination in the developing and regenerating CNS

Inaugural-Dissertation

Zur Erlangung des Doktorgrades

der Mathematisch-Naturwissenschaftlichen Fakultät

der Heinrich-Heine-Universität Düsseldorf

vorgelegt von

Christine Baksmeier

aus Speyer

Düsseldorf, Dezember 2018

aus der Klinik für Neurologie

der Heinrich-Heine-Universität Düsseldorf

Gedruckt mit der Genehmigung der

Mathematisch-Naturwissenschaftlichen Fakultät der

Heinrich-Heine-Universität Düsseldorf

Berichterstatter:

Univ.-Prof. Dr. Goebels

(Klinik für Neurologie der Heinrich-Heine-Universität Düsseldorf)

Univ.-Prof. Dr. Proksch

(Institut für pharmazeutische Biologie und Biotechnologie der Heinrich-Heine-Universität Düsseldorf)

Tag der mündlichen Prüfung: 19.06.2019

Data of this thesis has been published:

In a published manuscript:

Winter M, **Baksmeier** C, Steckel J, Barman S, Malviya M, Harrer-Kuster M, Hartung H-P, Goebels N. Dose-dependent inhibition of demyelination and microglia activation by IVIG. 2016, Annals of clinical and translational neurology 3(11):828–843.

Published manuscripts not included in this thesis:

Malviya M, Barman S, Golombeck KS, Planagumà J, Mannara F, Strutz-Seebohm N, Wrzos C, Demir F, **Baksmeier** C, Steckel J, Falk KK, Gross CC, Kovac S, Bönte K, Johnen A, Wandinger KP, Martín-García E, Becker AJ, Elger CE, Klöcker N, Wiendl H, Meuth SG, Hartung HP, Seebohm G, Leypoldt F, Maldonado R, Stadelmann C, Dalmau J, Melzer N, Goebels N. NMDAR encephalitis: passive transfer from man to mouse by a recombinant antibody. Annals of clinical and translational neurology 4(11):768-783.

As oral presentation:

Meike Winter, Christine **Baksmeier**, Melanie Harrer-Kuster, Manish Malviya, Hans-Peter Hartung, Norbert Goebels. Intravenous immunoglobulin protects from antibody-mediated demyelination. 9th Meeting of the Biological-Medical Research Center of the Heinrich Heine University of Düsseldorf (2014, Düsseldorf, Germany)

As poster contribution:

Winter, M.W. (Meike), **Baksmeier**, C.B. (Christine), Harrer Kuster, M.H.K. (Melanie), Goebels, N.G. (Norbert). IVIG protects from antibody-mediated demyelination. International Symposium Remyelination – by endogenous and exogenous cells. (2013, Groningen, Netherlands)

Winter, M., **Baksmeier**, C., Goebels, N. IVIG protects oligodendrocytes in an organotypic slice culture model for demyelination. Federation of European Neuroscience Societies. (2014, Milan, Italy)

Meike Winter, Christine **Baksmeier,** Melanie Harrer-Kuster, Manish Malviya, Hans-Peter Hartung, Norbert Goebels. IVIG protects oligodendrocytes in an organotypic slice culture model for demyelination. Current Topics in Myelin Research (2015, Kassel, Germany)

C. **Baksmeier**, M. Winter, J. Steckel, M. Harrer-Kuster, N. Goebels, H.- P. Hartung. Intravenous immunoglobulin protects oligodendrocytes in an organotypic slice culture model for demyelination. XII European Meeting on Glial Cells in Health and Disease (2015, Bilbao, Spain)

Table of contents

Abstract

Intravenous immunoglobulin (IVIG) is a preparation of polyclonal immunoglobulin (Ig) derived from the pooled blood plasma of thousands of healthy donors. While IVIG is a well-tolerated treatment for several autoimmune disorders, which are associated with antibody and complement deposition, clinical trials in multiple sclerosis with different dosing schemes yielded controversial results. Therefore, the aim of the present study was to investigate the effector mechanisms of IVIG at the interface between the central nervous system (CNS) and the immune system using the *ex vivo* model of organotypic slice cultures (OSCs).

Cerebellar OSCs were prepared using transgenic mice expressing green fluorescent protein (GFP) in oligodendrocytes and myelin. Treatment of OSCs with complement and anti-myelin oligodendrocyte glycoprotein (MOG) antibody induced extensive immune-mediated demyelination. After the removal of anti-MOG antibody and complement from the culture medium, OSCs underwent spontaneous remyelination. De- and remyelination were monitored by fluorescence microscopic live cell imaging and confocal microscopy. The treatment of OSCs with IVIG preserved myelin and oligodendrocyte integrity in a dose dependent manner. Results were confirmed via gene expression analysis and flow cytometry. Following anti-MOG antibody and complement treatment, microglia moved towards the site of demyelination. This migration was inhibited by IVIG treatment. While rising complement concentrations overruled the protection of oligodendrocytes, increasing concentrations of anti-MOG antibody had no impact on the protective properties of IVIG. The protective effect of IVIG was not caused by competitive binding of IVIG and anti-MOG antibody. Antibody staining of Contactin associated protein (Caspr) in OSCs verified the presence of intact Nodes of Ranvier and thereby functionality of myelin. While confocal analysis revealed a positive staining for Caspr in untreated OSCs, Caspr staining was absent in demyelinated OSCs and reappeared after remyelination. In OSCs which were treated with IVIG during demyelination not only myelin, but also Caspr expression was preserved. IVIG treatment during remyelination resulted in a small but significant enhancement of early remyelination. Unlike uncleaved IVIG, neither a monoclonal humanized IgG antibody nor the equimolar amount of IVIG-derived Fab fragments caused protection of oligodendrocytes and myelin. In contrast, Fc fragments from a human polyclonal IgG preparation were as potent as intact IVIG.

In conclusion, IVIG and Fc fragments prevented OSCs from immune-mediated demyelination, while Fab fragments and monoclonal humanized IgG antibody did fail. The present data indicate that IVIG thereby interacts with complement factors and presumably also with local immune cells like microglia.

Zusammenfassung

Intravenöses Immunglobulin (IVIG) besteht aus polyklonalem Immunglobulin (Ig), welches aus dem Blutplasma von mehreren tausend gesunden Spendern gewonnen wird. Obwohl IVIG bereits seit längerem zur Behandlung von Antikörper und Komplement-vermittelten Autoimmunerkrankungen eingesetzt wird, erzielten klinische Multiple Sklerose Studien kontroverse Ergebnisse. Daher war es das Ziel der vorliegenden Arbeit, *ex vivo* die Effektormechanismen von IVIG an der Schnittstelle zwischen dem zentralen Nervensystem (ZNS) und dem Immunsystem zu untersuchen.

Dazu wurden organotypische Schnittkulturen (OSCs) aus dem Cerebellum von transgenen Mäusen präpariert, welche grün-fluoreszierendes Protein (GFP) in Oligodendrozyten und im Myelin exprimieren. Die Behandlung der OSCs mit anti-Myelin-Oligodendrozyten-Glykoprotein (MOG) Antikörper und Komplement induzierte eine umfangreicher immunmediierte Demyelinisierung. Durch das Entfernen des anti-MOG-Antikörpers und des Komplements wurde eine spontane Remyelinisierung in den OSCs hervorgerufen. De- und Remyelinisierung wurden mit Hilfe von Fluoreszenzmikroskopie und konfokaler Mikroskopie dokumentiert. Die Behandlung der OSCs mit IVIG führte dosisabhängig zum Schutz der Integrität von Myelin und Oligodendrozyten. Diese Ergebnisse wurden, sowohl auf der Ebene der Genexpression, als auch mit Hilfe von Durchflusszytometrie bestätigt. Durch die Behandlung der OSCs mit anti-MOG-Antikörper und Komplement migrierten Mikroglia zu den demyelinisierten Bereichen. Diese Migration wurde durch die Behandlung mit IVIG vermindert. Während der Schutz der Oligodendrozyten mit steigender Komplementkonzentration abnahm, hatte die Erhöhung der anti-MOG-Antikörperkonzentration keinen Einfluss auf die protektiven Eigenschaften von IVIG. Der schützende Effekt von IVIG wurde nicht durch eine kompetitive Bindung zwischen IVIG und anti-MOG-Antikörper vermittelt. Intakte Ranvier'sche Schnürringe und somit die Funktionalität des Myelins konnte durch Antikörperfärbungen des paranodalen Proteins Caspr nachgewiesen werden. Während in unbehandelten und remyelinisierten OSCs Caspr mittels konfokaler Mikroskopie detektiert wurde, konnte das paranodale Protein nicht in demyelinisierten OSCs nachgewiesen werden. Durch die Zugabe von IVIG während der Demyelinisierung, wurde zusätzlich zum Myelin, auch die Caspr-Expression geschützt. IVIG führte zu einer kleinen, aber signifikanten Verbesserung in der frühen Remyelinisierung. Anders als durch ungespaltenes IVIG, wurden Oligodendrozyten und Myelin nicht durch einen monoklonalen humanisierten IgG Antikörper oder durch die equimolare Menge aus IVIG gewonnenem Fab Fragment geschützt. Im Gegensatz dazu wirkten Fc Fragmente aus einer humanen polyklonalen IgG-Präparation genauso potent wie intaktes IVIG.

Zusammenfassend schützten IVIG und Fc Fragmente OSCs vor immun-mediierter Demyelinisierung, während Fab Fragmente und ein monoklonaler humanisierter IgG Antikörper keine Wirkung erzielten. Die vorliegenden Daten weisen auf eine Interaktion von IVIG mit Komplementfaktoren und wahrscheinlich auch mit lokalen Immunzellen, wie Mikroglia, hin.

1 Introduction

1.1 Multiple Sclerosis

Multiple sclerosis (MS) is one of the most common chronic inflammatory diseases of the central nervous system (CNS). MS affects almost 2.5 million people worldwide and it usually manifests clinically during early adulthood. Acute inflammation is a main characteristic of the disease and results in fully or partially reversible episodes of neurologic impairment, called relapses.

1.1.1 Etiology

Although the etiology of MS is still enigmatic, there is evidence that genetic factors as well as environmental factors are involved. For yet unknown reasons, women are more often affected than men (Orton et al., 2006). The overall prevalence of MS varies for different regions of the world and in many cases increases with latitude. Thus, the prevalence rates in Scotland at the end of the 20th century were higher than those in Spain (Pugliatti et al., 2002). Interestingly, emigrants moving from countries with high MS risk to a low risk area acquire the lower risk of their new country when they move before the age of 15 or 16, while emigration at a later age does not change the individual risk for the formation of the disease (Dean and Kurtzke, 1971). Vitamin D sufficiency, as a protective factor for MS (Munger et al., 2004), supports the latitude hypothesis. However, the geographic distribution of MS cannot completely be explained by latitude. While 1983 the southern part of Norway was characterized by a high MS prevalence, the prevalence in the northern part was much lower, in the same period. The lower MS prevalence in the northern part of Norway might be explained by the native Sami population, which has a different genetic background than the rest of the European population (Pugliatti et al., 2002). Genome-wide association studies identified more than 200 risk genes for MS, among them several genes which are involved in the regulation of the immune system. The highest risk was determined for the DRB1*15:01 allele of the human leukocyte antigen (HLA), in the class II major histocompatibilty complex (MHC). Genetic studies showed that the prevalence of MS rises with increasing degree of relationship to the affected relative. While about 0.1% of the general population is affected by the disease, first degree-relatives like siblings have a risk of about 3%. According to epidemiological studies, the concordance in monozygotic twins is between 25% and 30% (Kuusisto et al., 2008; Willer et al., 2003), indicating that disease development is influenced by genetic factors. On the other hand, the lack of full concordance between monozygotic twins points out that also environmental factors play a pivotal role in disease formation. Besides the influence of the latitude, also cigarette smoking and viral infections are thought to influence the development of MS.

Among others, Epstein-Barr virus (EBV), Human Herpes Virus 6 and varicella zoster virus have been suggested to be involved the pathogenesis of MS, but so far, only an infection with EBV has been shown to increase the risk of disease. Although over 90% of the population is infected with EBV, epidemiological studies revealed a 10-fold increased risk for MS among EBV-positive individuals and an at least 20-fold increased risk among individuals with a rather late occurring EBV infection (Thacker et al., 2006).

1.1.2 Clinical Manifestation

Although the manifestation of MS is quite heterogeneous, the disease starts in 85-90% of the cases with a relapsing-remitting (RR) form, which is characterized by inflammatory events followed by recovery. In 50% of the cases, the initial relapsing-remitting form transforms within 15 years into a secondary progressive (SP) disease course (Scalfari et al., 2014) which is associated with the accumulation of irreversible neurodegeneration. SP-MS, which is in some cases still accompanied by relapses, subsequently leads to neurological impairment. The remaining 10-15% of MS patients develop directly after disease onset a primary progressive (PP) manifestation of the disease, which is characterized by a slow but continuous deterioration of neurological deficits without relapses. The latency period between two relapses is variable and can differ between patients and the course of the disease. The reasons for the differences in the progression of the disease are not known yet. Like the latency period, also the symptoms are highly variable and differ from patient to patient. Symptoms include motor deficits like coordination problems as well as sensory dysfunction of speech and vision. Furthermore, patients may suffer from fatigue, depressions, cognitive impairments and mental disturbances (Sa et al., 2011). MS is diagnosed according to the criteria which have been described by McDonald et al., 2001 and revised several times (Polman et al., 2005; Polman et al., 2011; Thompson et al., 2018). According to the McDonald criteria, the diagnosis of MS is based on the demonstration of dissemination of symptoms and lesions in space and time. Therefore, paraclinical tests like magnetic resonance imaging and the detection of oligoclonal Immunoglobulin (Ig) bands in the cerebrospinal fluid (CSF) are commonly used.

1.1.3 Pathogenesis

Histologically, MS is characterized by demyelinating lesions in the central nervous system (CNS). While they are mostly located in the white matter of the brain, they can also be found in grey matter and cortex (BROWNELL and HUGHES, 1962). Although it is not clear which immune component is the key player in the formation of MS, its pathology is characterized by oligodendrocyte death, demyelination and axonal transection. The latter is most likely the major cause for irreversible neurological impairment (Trapp et al., 1998). Moreover, the temporary disruption of the blood brain barrier (BBB) is a substantial hallmark of the disease, indicating the active access of immune cells to the CNS. According to histological studies, T- and B-cells, macrophages as well as immunoglobulin and complement deposits have been shown to be present in MS lesions in different proportions.

1.1.3.1 CD4+ T-cells

Many years ago, Ben-Nun et al., 1981 discovered that the transfer of activated myelin-specific T-cells to healthy animals is sufficient to induce a passive form of experimental autoimmune encephalitis (EAE), a model commonly used to mirror CNS inflammation. Further EAE studies revealed that CNS inflammation is induced via MHC class II-mediated mechanisms, indicating a participation of CD4+ cells (Zamvil et al., 1985). However, the central role of CD4+ T-cells in EAE may not mirror the situation in human MS patients because myelin-specific CD4+T- cells were also shown to be present in the blood of healthy subjects (Burns et al., 1983). A further argument, which points towards a contribution of CD4+ T-cells is the association of several MHC class II alleles with an increase in MS susceptibility. Surprisingly, the reduction of CD4+ T-cells by the intravenous treatment with an antibody directed against these T-cells did not lead to a change of the number of active lesions in patients (van Oosten et al., 1997).

1.1.3.2 CD8+ T-cells

There are also several arguments for the involvement of CD8+ T-cells in the pathogenesis of MS. Studies from Booss et al., 1983 measured a higher proportion of CD8+ T-cells than CD4+ T-cells in MS lesions. Furthermore, single cell polymerase chain reaction (PCR) analysis revealed that CD8+ T-cells are clonally expanded in lesional tissue and that these clones can also be found in CSF and blood of the same MS patients (Babbe et al., 2000; Skulina et al., 2004). Moreover, oligodendrocytes and neurons, cells which are severely affected in MS, express MHC class I but not MHC class II and can therefore be recognized by CD8+ but not by CD4+ T-cells (Jurewicz et al., 1998; Medana et al., 2000).

1.1.3.3 B-cells and antibodies

Evidence for the involvement of B-cells in the pathophysiology of MS is provided by their clonal expansion in the CSF of patients (Colombo et al., 2000). Terminally differentiated B-cells (plasma cells) produce intrathecal immunoglobulins (Büdingen et al., 2010; Obermeier et al., 2008), which can be detected as oligoclonal bands (OCB) in the CSF of more than 90% of MS patients (Delmotte and Gonsette, 1977). In contrast, immunoglobulins, which are present in the serum of MS patients remain polyclonal. The pattern of OCBs is exclusive for each patient (Delmotte and Gonsette, 1977) and remains stable over a period of years (Walsh and Tourtellotte, 1986) indicating that B-cellls can survive in the CSF/CNS compartment. Several studies point towards an important role of antibodies in the formation of MS. Antibody and complement depositions as well as degenerated myelin were found in pattern II lesions of biopsies and autopsies of MS patients (Lucchinetti et al., 2000). Furthermore, antibodies from patient derived expanded B-cell clones have been shown to bind to neural antigens and to cause complement mediated demyelination in slice cultures (Blauth et al., 2015; Liu et al., 2017). Additionally, B-cells have been proposed to contribute to the pathogenesis of MS by antibody-independent mechanisms, including the secretion of cytokines and the transport and presentation of autoantigens (reviewed by Wekerle, 2017). This is supported by the fact that CD20-targeting antibodies like Rituximab are successfully used in patients with RR-MS (Hauser et al., 2008), although they spare antibody producing plasma cells.
So far, it is an open question to what extent humoral and cellular mechanisms contribute to the development of MS. However, since one of the four common lesional patterns in MS is characterized by antibody and complement deposition (Lucchinetti et al., 2000) there is clear evidence that antibodies play an important role, at least in a subset of patients.

1.1.3.4 Microglia and Astrocytes

Under physiological conditions, astrocytes have several functions. Among others, they contribute to the maintenance of the BBB, provide other cells with nutrients and control water and glutamate homeostasis. Under pathological conditions, astrocytes build a glial scar in demyelinated lesions. In the past, the glial scar has been described as a rather late mechanism in MS pathology with little or no role in lesion formation and repair (Brosnan and Raine, 2013). However, more recently, the glial scar has been proposed to serve as a functional barrier that restricts the entry of inflammatory cells into the CNS (reviewed by Sofroniew, 2015). Furthermore, astrocytes have been shown to induce local inflammatory responses as well as to promote tissue repair (Farina et al., 2007).

Similar to astrocytes, also the influence of microglia on the course of MS has been discussed controversially. In the healthy brain resting microglia actively scan their surrounding (reviewed by Hanisch and Kettenmann, 2007) and maintain the homeostasis of the CNS. In the diseased brain the previously small and ramified microglia develop an amoeboid shape and play different roles. On the one hand, activated microglia cause neurodegeneration and demyelination through the secretion of pro-inflammatory factors like tumor necrosis factor alpha (TNFα) or interleukin 1 beta (IL-1β). On the other hand, microglia contribute to the protection of neural tissue through anti-inflammatory factors like Interleukin-10 (IL-10) (Kwilasz et al., 2015). Regeneration is enhanced by the secretion of growth promoting factors like neuronal growth factor (NGF), brain-derived neurotrophic factor (BDNF), glial cell line derived neurotrophic factor (GDNF) (Batchelor et al., 2002; Liang et al., 2010) and through the clearance of myelin debris (Kotter et al., 2006; Neumann et al., 2009).

1.1.4 Remyelination

The disease progression of demyelinating disorders like MS is characterized by the loss of myelin and subsequently by the degeneration of axons. The diagnosis of MS mostly begins when the first neurological symptoms occur. Since these symptoms are caused by a massive loss of myelin, strategies for remyelination are urgently needed to protect axons. After demyelination, mature Schwann cells in the PNS still have the ability to proliferate and thereby to contribute to remyelination. In contrast, after demyelination in the CNS preexisting mature oligodendrocytes are postmitotic and incabable of remyelination (Keirstead and Blakemore, 1997). Consequently, successful remyelination in the CNS is enabled uniquely by oligodendrocyte precursor cells (OPCs). During embryonic development, OPCs originate from neural progenitors, undergo proliferation, migration and finally differentiation into postmitotic, premyelinating and myelinating oligodendrocytes. Although in the adult brain proliferative OPCs remain present throughout the whole life (Chang et al., 2000), remyelination is often incomplete in earlier stages and absent in later stages of the chronic form of the disease. Furthermore, successfully rebuilt myelin is thinner and has shorter internodes than the initial myelin sheath (Ludwin and Maitland, 1984). Apart from the thickness and lengths of internodes, de- and remyelination processes also influence the structures of the node of Ranvier, the paranode and the juxtaparanode. The formation of these structures is critical for rapid and correct signal transduction in myelinated axons. Under physiological conditions, the distinct cylindrical structure of the paranode is formed by the adhesion molecules contactin 1, neurofascin 155 (NF155) and contactin-associated protein 1 (Caspr) **(Figure 1)**. While in demyelinated MS lesions the expression pattern of the Caspr protein is diffuse or absent (Coman et al., 2006; Wolswijk and

Balesar, 2003), in remyelinated lesions Caspr reappeared in the paranodal region due to the formation of new myelin sheaths (Wolswijk and Balesar, 2003).

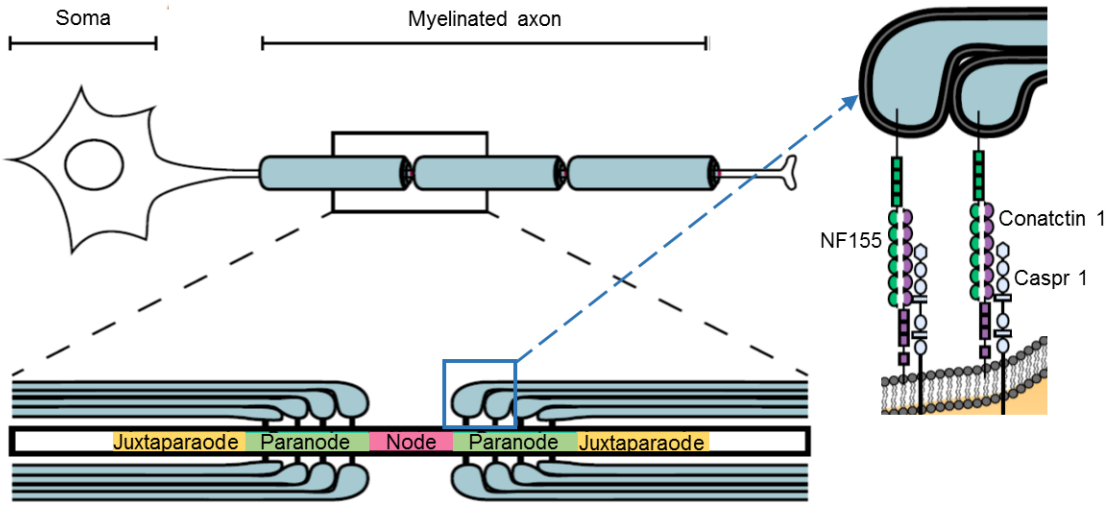

Figure 1. Schematic view of the different domains of a myelinated axon.
The node of Ranvier is flanked first by the paranode and then by the juxtaparanode. Each domain is characterized by a unique protein expression. The paranodes are formed by the glial adhesion molecules neurofascin 155 (NF155) and by the axonal adhesion molecules contactin 1 and contactin-associated protein 1 (Caspr). Adapted from Arancibia-Carcamo and Attwell, 2014.

Even though the circumstances of failed remyelination have not been fully clarified yet, a multitude of factors has been shown to play a role. While some studies point towards a deficit in OPC migration (Boyd et al., 2013), others identified insufficient differentiation of OPCs (Cui et al., 2013; Kotter et al., 2006) or missing receptiveness of axons (Chang et al., 2002) as main obstacles on the way to remyelination. Several factors have been identified to inhibit oligodendrocyte differentiation in the adult brain (reviewed by Kremer et al., 2011). For example, the leucine rich repeat and immunoglobin-like domain-containing protein 1 (LINGO-1), which is expressed in oligodendrocytes, negatively regulates the myelination of axons through the Nogo receptor 1 (NgR1) signalling pathway (Mi et al., 2005). Hence, the identification of molecules which are able to neutralize oligodendroglial differentiation inhibitors represents a promising approach for the development of drugs, which favour remyelination.

1.1.5 Medication and drug development

Since the cause of MS is not clarified yet, current treatment focuses on the alleviation of symptoms as well as on the modulation and suppression of the immune system. During acute attacks, patients are treated with compounds like corticosteroids, which ameliorate and shorten acute attacks but do not modulate the long-term course of the disease (Filippini et al., 2000). Interferon-β1 is used based on its immunomodulatory properties including the inhibition of T-cell proliferation and the prevention of T-cell entry into the CNS. Another immunomodulatory drug is the MBP analogon Glatiramer acetate which inhibits the activation of T-cells and competes with the antigens of myelin (Teitelbaum et al., 1988). Both, Interferon-β1 and Glatiramer acetate reduce the relapse rate by about 30%. The proliferation of rapidly dividing cells like B- and T-cells is inhibited by Teriflunomide through the suppression of pyrimidine synthesis. Mitoxantrone is another drug which inhibits cell proliferation at the level of DNA synthesis. Due to its potentially severe side effects it is only used as second line treatment in highly active MS. In contrast, the fumaric acid ester dimethyl fumarate (DMF) activates the antioxidative Nrf2 (nuclear factor erythroid 2-related factor 2) pathway and is used to reduce inflammation. The phosphorylated form of the immune suppressive agent Fingolimod binds to the sphingosine-1-phosphate receptor 1 (S1PR1) on B- and T-cells. As a result, S1PR1 is internalized and B- and T-cells remain in the lymph nodes. A different type of medication is represented by monoclonal antibodies which are able to bind specifically to their designated target. The humanized monoclonal antibodies Natalizumab and Daclizumab modulate immune cell behaviour by the recognition of cellular surface proteins. The binding of Natalizumab to α4-integrin-expressing leukocytes inhibits their migration across the BBB. Through the recognition of the IL-2 receptor (CD25) of T-cells by Daclizumab blocks the receptor and thereby prevents T-cell activation. However, due to its severe adverse side effects Daclizumab has been recently withdrawn from the market. In contrast to the modulatory effect on immune cells mediated by Natalizumab and Daclizumab, the binding of the monoclonal antibodies Alemtuzumab, Rituximab and Ocrelizumab cause the depletion of their target cell types. Alemtuzumab recognizes CD52 on lymphocytes, monocytes and macrophages and mediates their depletion through antibody-depdendent cytotoxicity (ADCC) (Hu et al., 2009). The chimeric antibody Rituximab as well as the humanized Ocrelizumab selectively deplete B-cells by binding to CD20.

Based on immune suppressive and immunmodulatory mechanisms, current medication is able to delay the disease course and to cure the symptoms of MS. However, there is an urgent need for drugs, which stop neurodegenerative processes and induce functional repair.

1.2 Model systems for demyelination and remyelination

1.2.1 Animal models

The pathogenesis of MS is mainly investigated with the help of animal models, which mirror distinct hallmarks of the disease. Brain inflammatory is most frequently studied in the EAE model. EAE is induced in susceptible strains of rodents or nonhuman primates either by immunization with a myelin-specific peptide, emulsified in Complete Freund's adjuvants (active EAE), or by adoptive transfer of autoreactive T-cells specific for myelin (passive EAE). Besides inflammation, EAE depicts several other characteristics of MS, including immune-cell infiltration and demyelination. Nevertheless, a multitude of genetic and environmental factors cannot be mimicked by this animal model. As a result, treatments, which efficiently modulate EAE, do not necessarily improve the disease course of MS patients. Since the cause of MS is not known, a couple of other animal models have been developed to study demyelination in a different etiological and pathological context. These include toxin-induced (Lysolecithin, Cuprizone, Ethidiumbromide), as well as viral-induced (Theiler's murine encephalomyelitis virus) animal models. However, the underlying mechanisms of demyelination in these animal models are not fully understood and differ between the individual approaches.

1.2.2 *In vitro* and *ex vivo* models

Animal models have served as a useful tool for the understanding of MS, but due to their complexity and in order to reduce the number of animals and the extent of suffering, *in vitro* models are commonly used to study the processes of de- and remyelination. These models range from immortalized neural cell lines, over the (co-) culture of primary cells, to three-dimensional systems like neural spheroids. Although the above-mentioned *in vitro* methods are suitable for a first screening of eligible therapeutics, they are not able to depict the interaction between different CNS cell types in their natural three-dimensional context. As an approach for this problem, we have established in our group the *ex vivo* model of organotypic slice cultures. In this model, the complex spatial microarchitecture of the CNS is maintained, allowing the study of de- and remyelination processes, unimpaired by the BBB and by peripheral immune components.

1.2.3 *Ex vivo* model of organotypic slice cultures (OSCs)

For the long-term cultivation of OSCs two major techniques have been established. The “roller tube technique” developed by Gähwiler et al., 1997 is based on monolayer slices which are suitable for electrophysiological recordings. The “interface method” was established by Stoppini et al., 1991 and generates thicker OSCs in which the cytoarchitecture remains intact. According to the name, OSCs are cultured on a semipermeable membrane, which allows the supply with culture medium from below and with oxygen from above. Pharmacological manipulations can be induced by addition of treatment substances directly to the culture medium. OSCs can be prepared from different brain regions, including the hippocampus, the spinal cord and the cerebellum (Stoppini et al., 1991).

1.2.3.1 Cytoarchitecture and demyelination of cerebellar OSCs

OSCs of the cerebellum have been shown to be an extremely useful *ex vivo* system in order to study de- and remyelination processes in a three-dimensional context. The cerebellum, which is usually prepared from embryonic or early postnatal rodents, is cut into slices and cultivated on semipermeable membranes. Within a few days, cerebellar OSCs attach to the membrane and flatten. Since the cytoarchitecture is already established, the early postnatal period is most suitable for the preparation of cerebellar OSCs. *In vivo*, the process of myelination is completed between P21 and P23 (Bouslama-Oueghlani et al., 2003; Foran and Peterson, 1992). In early postnatal cerebellar OSCs from rodents (P10), myelination is completed after 14 days *in vitro*, which closely resembles the *in vivo* situation (Birgbauer et al., 2004). The grey matter of the cerebellum consists of several layers. In the postnatal but still developing cerebellum, the external granule layer (EGL) builds the outermost layer (Altman and Das, 1966). The EGL contains precursors of granule cells (GC) prior to their migration to the inner cortex (premigratory cerebellar granule cells) **(Figure 2)** and is followed by the molecular layer (ML), the Purkinje cell layer (PCL) and the internal granular layer (IGL). While the IGL is characterized by cell bodies of cerebellar granule cells, their unmyelinated axons form synapses with Purkinje cell dendrites and build the parallel fibres in the ML. The cell bodies of the Purkinje cells are located in the PCL. During the preparation, afferent axons like mossy and climbing fibres as well as some of the efferent projecting neurons from Purkinje cells are destroyed through cutting. Nevertheless, the myelinated dendrites of the mostly surviving Purkinje cells serve as an excellent model for the investigation of CNS damage and repair. Comparable to the situation in animal models, there are several ways to induce demyelination in OSCs. One the one hand, toxic substances like lysolecithin (Birgbauer et al., 2004) or gut bacteria toxin epsilon (Wioland et al., 2015) can induce demyelination; on the other hand,

dysmyelination can be monitored via the preparations of OSCs from MBP deficient shiverer mice (Bin et al., 2012). Apart from the rather artificial toxic models of demyelination, immune-mediated demyelination can be induced by antibody and complement (Harrer et al., 2009) which have been found in pattern II lesions of biopsies and autopsies of MS patients (Lucchinetti et al., 2000). The preparation of OSCs from transgenic mice which express green fluorescent protein (GFP) in oligodendrocytes and myelin enables the investigation of de- and remyelination processes in living OSCs (Harrer et al., 2009).

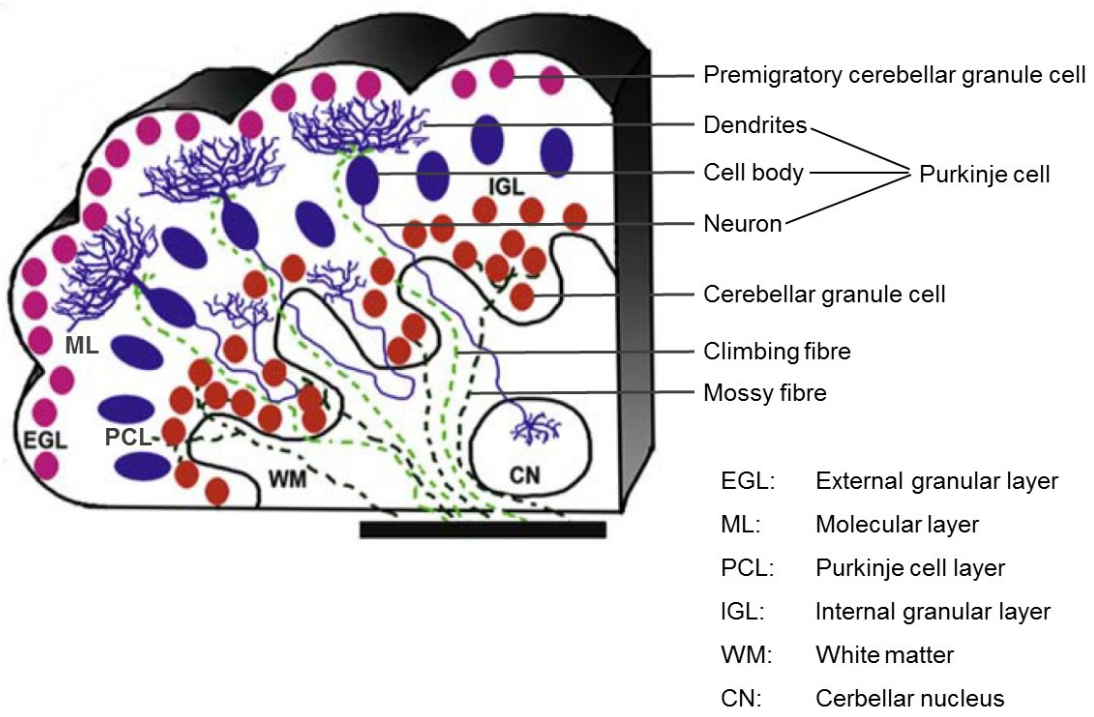

Figure 2. Schematic view of the main architecture of a cerebellar OSC.
The layered structure of the grey matter: The EGL contains premigratory cerebellar granule cells. The ML is dominated by dendrites of Purkinje cells (PC), which are innervated by axons of cerebellar granule cells. Cell bodies of PC and cerebellar granule cells are located in the PCL and IGL, respectively. The CN, which is embedded in the white matter receives *in vivo* excitatory and inhibitory inputs. *Ex vivo*, excitatory inputs from afferent mossy and climbing fibres are destroyed due to the slicing, inhibitory inputs from efferent projecting PC neurons are spared if nuclear neurons are located within the OSC. PC neurons, which do not have a target, might become self-inneravted. Adapted from Lossi et al., 2009.

1.3 Intravenous immunoglobulin (IVIG)

IVIG is a preparation of normal immunoglobulin G that is derived from the plasma of thousands of healthy donors. These preparations are composed of normally occurring antibodies with a rather broad reactivity as well as of specific antibodies, which are produced following antigen exposure. Due to its beneficial effects, the administration of IVIG has been

established as effective therapy of autoimmune and inflammatory disorders. In the field of neurology, IVIG has proven to serve as a basic therapy for several disorders of the peripheral nervous system (PNS), among them Myasthenia gravis (reviewed by Gilhus et al., 2011), autoimmune neuropathies like Guillain Barré Syndrome, Multifocal motor neuropathy and Chronic inflammatory demyelinating polyradiculoneuropathy (reviewed by Buttmann et al., 2013). Interestingly, autoreactive antibodies as well as complement deposition have been shown to be involved in the pathogenesis of all of the above mentioned diseases (reviewed by Léger et al., 2015; Mathey et al., 2015; Ruff and Lisak, 2018; Yuki and Hartung, 2012). Complement and antibody deposition have also been present in pattern II lesions of MS biopsies and autopsies (Lucchinetti et al., 2000). However, in contrast to the just mentioned diseases, clinical studies of IVIG treatment in MS patients did not show definite results. While some studies revealed beneficial effects of IVIG in RR-MS (Achiron et al., 1992; Achiron et al., 1998; Fazekas et al., 1997; Lewańska et al., 2002; Sorensen et al., 1998; Teksam et al., 2000), in other studies IVIG was not able to reduce or to ameliorate relapses (Fazekas et al., 2008; Sorensen et al., 2004). The different outcomes of those rather small clinical studies might arise through varying inclusion criteria, differences in dosage and administration schedules and through the heterogeneity of the disease itself. In the recent past, IVIG has also been highlighted as an option for the treatment of inflammatory conditions of the CNS, like Neuromyelitis optica (Elsone et al., 2014) or Autoimmune encephalitis (reviewed by Fassbender et al., 2017). Both diseases have been shown to be associated with pathogenic autoantibodies. Complement deposition though has only been observed in neuromyelitis optica (Lucchinetti et al., 2002). For IVIG, several mechanisms of actions have been discussed (reviewed by Ballow, 2011; Gelfand, 2012; Hartung, 2008; Lünemann et al., 2015; Nimmerjahn and Ravetch, 2007; Schwab and Nimmerjahn, 2013). On the one hand, IVIG has been proposed to influence several types of immune cells, including T-cells (Aktas et al., 2001; Ephrem et al., 2008; Janke et al., 2006; Maddur et al., 2011; Mausberg et al., 2013; Othy et al., 2013), B-cells (Kessel et al., 2011; Tackenberg et al., 2009), NK-cells (Jacobi et al., 2009) and dendritic cells. (Kapur et al., 2017; Tha-In et al., 2006). On the other hand, IVIG has been related to effects of the humoral immune response. In this regard, some authors propose that IVIG acts through its variable Fab portion, for example through the anti-idiotypic neutralization of pathogenic autoantibodies (Rossi et al., 1989), through the binding of immunomodulatory proteins like cytokines (Hansen et al., 1995; Ross et al., 1995; Svenson et al., 1993; Svenson et al., 1998) and chemokines or through the neutralization of activated complement components (Basta et al., 2003). Furthermore, several modes of action have been attributed to the Fc portion of IVIG including the influence on Fc receptor functions and the inhibition of complement activation (Wada et al., 2001).

1.4 Aims of the study

Both the cellular and the humoral immune response are involved in MS pathogenesis. Humoral mechanisms include the intrathecal production of clonally expanded Immunoglobulins, detectable as oligoclonal bands and the deposition of antibodies and complement in pattern II lesions of MS patients (Luccinetti 2000). However, despite their presence in MS lesions, the impact of antibody and complement deposits on disease formation is hardly distinguishable from the cellular effector mechanisms, caused by infiltrating immune cells. Therefore, this study aims to:

1) Prove whether organotypic slice cultures of the mouse cerebellum can serve as a model to monitor antibody and complement-mediated CNS damage and subsequent repair in the absence of infiltrating immune cells.

2) Verify whether the OSC model is suitable to test substances for their ability to prevent CNS damage or to promote CNS repair by using IVIG as an example.

3) Dissect effector mechanisms of IVIG in the OSC model and to transfer the results to antibody and complement mediated diseases like MS.

2 Material and methods

2.1 Material

2.1.1 Laboratory devices

Table 1: List of laboratory devices

Device	Company
Accurate weighting scale	Kern, Balingen, Germany
Äkta protein purification system	GE Healthcare, Uppsala, Sweden
Autoclave Systec V-150	Systec, Linden, Germany
TC10 Automatic Cell Counter	Bio-Rad, Hercules, CA, USA
Binocular Microscope	Leica, Wetzlar, Germany
BD FACSCanto™ II flow cytometer	BD Bioscience, San Jose, CA,USA
Cell culture sterile bench	SKAN, Allschwill, Switzerland
Cell culture sterile bench, Hera Safe	Thermo Fisher Scientific, Waltham, MA, USA
Centrifuge, Galaxy MiniStar silverline	VWR, Radnor, PA, USA
Centrifuge 5417 R	Eppendorf, Hamburg, Germany
Centrifuge 5810 R	Eppendorf, Hamburg, Germany
Centrifuge Minispin	Eppendorf, Hamburg, Germany
CO_2 incubator, BBD 6220	Heraeus, Hanau, Germany
CO_2 incubator, Hepa Class 100	Thermo Fisher Scientific, Waltham, MA, USA
Confocal Laser Scanning Microscope, Leica SP8	Leica, Wetzlar, Germany
Confocal Laser Scanning Microscope, LSM 510	Carl Zeiss, Oberkochen, Germany
Electrophoresis System	Bio-Rad, Hercules, CA, USA
Forceps for tissue preparation	Fine Science Tools, Heidelberg, Germany
Freezers (-20°C)	Liebherr, Bulle, Switzerland
Freezer (-80°C)	Thermo Fisher Scientific, Waltham, MA, USA

Device	Company
Freezer (-80°C)	Sanyo, Moriguchi, Osaka Prefecture, Japan
Freezing container, CoolCellTM	Menlo Park, CA, USA
F-View fluorescence camera	Soft Imaging System, Munich, Germany
Gel documentation system	INTAS, Göttingen, Germany
Heating block, Thermostat plus	Eppendorf, Hamburg, Germany
Heating block, Thermomixer comfort	Eppendorf, Hamburg, Germany
Protein gel and western blot imaging system	Odyssey, LI-COR, Lincoln, NE, USA
Light microscope, Leica DMIL	Leica, Wetzlar, Germany
Liquid nitrogen tank	tec-lab, Taunusstein, Germany
Mastercycler®	Eppendorf, Hamburg, Germany
Mastercycler® gradient	Eppendorf, Hamburg, Germany
McIlwain Tissue Chopper	Mickle Laboratory, Guildford, UK
Mechanical shaker	Bibby Scientific Limited, Stone, UK
Mechanical shaker	Biometra, Göttingen, Germany
Microplate Reader	Tecan Group Ltd., Männedorf, Switzerland
Multi-channel pipette	Eppendorf, Hamburg, Germany
Multi pipette	Eppendorf, Hamburg, Germany
Nanodrop 2000 Spectrophotometer	Thermo Fisher Scientific, Waltham, MA, USA
Olympus BX51, fluorescence micro-scope	Olympus, Hamburg, Germany
Olympus U-RFL-T Burner	Olympus, Hamburg, Germany
Pipettes	Eppendorf, Germany
Pipetus	Hirschmann Laborgeräte, Germany
Protein Gel Electrophoresis Chamber	Bio-Rad, Hercules, CA, USA
7500 Pro Real-Time PCR Systems	Applied Biosystems, CA, USA

Device	Company
Refrigerators	Liebherr, Bulle, Switzerland
Scissors for tissue preparation	Fine Science Tools, Heidelberg, Germany
Single-channel pipettes	Eppendorf, Hamburg, Germany
TC10 Automatic Cell Counter	Bio-Rad, Hercules, CA, USA
Tissue homogenizer	Schuett-Biotec, Göttingen, Germany
Vortex	Scientific Industries Inc, Bohemia, NY, USA
Water bath	Memmert, Schwabach, Germany
Weighting scale	Kern, Balingen, Germany

2.1.2 Software

Table 2: Software used for data analysis and presentation

Software	Company
Citavi 5	Swiss Academic Software, Wädenswil, Switzerland
GraphPad Prism 5	GraphPad Software Inc., La Jolla, CA, USA
ImageJ	Rasband, W.S., ImageJ, U. S. National Institutes of Health, Bethesda, MD, USA
MAFFT	Kuraku et al., 2013
Odyssey Image Studio Lite	Odyssey, LI-COR, Lincoln, NE, USA
Office 2016	Microsoft Corporation, Redmond, WA, USA
Snap gene viewer	GSL Biotech LLC, Chicago, IL, USA

2.1.3 Chemicals and supplements

Table 3: List of chemicals and supplements

Chemicals and supplements	Company
Agarose	Sigma-Aldrich, St. Louis, MO, USA
Baby rabbit complement, lyophilized	Cedarlane, Burlington, Canada
BC Assay Protein Quantification Kit	Interchim, Montlucon, France
Blasticidin S HCl powder	Thermo Fisher Scientific, Waltham, MA, USA
BlueJuice™ Gel Loading Buffer	Thermo Fisher Scientific, Waltham, MA, USA
BSA	Merck, Darmstadt, Germany
Chloroform	Merck, Darmstadt, Germany
Dulbecco's PBS (1x), without Ca^{2+} + Mg^{2+}	Thermo Fisher Scientific, Waltham, MA, USA
DNase/RNase free dH_2O	Thermo Fisher Scientific, Waltham, MA, USA
EDTA	G-Biosciences, St. Louis, MO, USA
Ethanol (absolute for analysis)	Merck, Darmstadt, Germany
Ethidium bromide	Sigma-Aldrich, St. Louis, MO, USA
Fetal calf serum (FCS)	Thermo Fisher Scientific, Waltham, MA, USA
Fixable Viability Dye eFluor® 450	eBioscience, San Diego, CA, USA
GeneRuler™ DNA ladder Mix	Thermo Fisher Scientific, Waltham, MA, USA
GelCode® Blue Stain Reagent	Thermo Fisher Scientific, Waltham, MA, USA
Glucose	Sigma-Aldrich, St. Louis, MO, USA
GlutaMAX™	Thermo Fisher Scientific, Waltham, MA, USA
Glycine	Sigma-Aldrich, St. Louis, MO, USA
Glycogen	Ambion®, Thermo Fisher Scientific, Waltham, MA, USA
Goat serum	Sigma-Aldrich, St. Louis, MO, USA
HBSS with Ca^{2+} + Mg^{2+}	Thermo Fisher Scientific, Waltham, MA, USA

Chemicals and supplements	Company
HBSS without Ca^{2+} + Mg^{2+}	Thermo Fisher Scientific, Waltham, MA, USA
HEPES	Thermo Fisher Scientific, Waltham, MA, USA
Hoechst 33258	Thermo Fisher Scientific, Waltham, MA, USA
Horse serum, heat inactivated	Thermo Fisher Scientific, Waltham, MA, USA
Human-Albumin 20%	CSL Behring GmbH, Marburg, Germany
Human IgG, Fc fragment	Millipore, Billerica, MA, USA
Immu-Mount	Thermo Fisher Scientific, Waltham, MA, USA
Isofluran	Actavis, Parsippany-Troy Hills, NJ, USA
Isopropanol	Merck, Darmstadt, Germany
Kynurenic acid	Sigma-Aldrich, St. Louis, MO, USA
LB Broth Medium	Sigma-Aldrich, St. Louis, MO, USA
Minimal essential Medium (MEM)	Thermo Fisher Scientific, Waltham, MA, USA
Mini-Protean® TGX™ Precast Gels	Bio-Rad, Hercules, CA, USA
5x Hot-Start Taq PCR-Mastermix	Bio-Budget, Krefeld, Germany
Novex® Sharp Pre-Stained Protein Standard	Thermo Fisher Scientific, Waltham, MA, USA
NuPage MOPS SDS running buffer 20x	Invitrogen, Karlsruhe, Germany
Nutridoma™-SP	Roche, Basel, Switzerland
Opti-MEM™	Thermo Fisher Scientific, Waltham, MA, USA
PageRuler™ Plus Prestained Protein Ladder	Thermo Fisher Scientific, Waltham, MA, USA
Penicillin-Streptomycin	Thermo Fisher Scientific, Waltham, MA, USA
Paraformaldehyd	Carl Roth, Lauterbourg, France
Polyethylenimine (PEI)	Polysciences, Warrington, PA, USA
Privigen 100 mg/mL	CSL Behring GmbH, Marburg, Germany
Proteinase K	Qiagen, Hilden, Germany

Chemicals and supplements	Company
Recovery Cell Culture Freezing Medium	Thermo Fisher Scientific, Waltham, MA, USA
RNaseOUT™ Recombinant Ribonuclease Inhibitor	Thermo Fisher Scientific, Waltham, MA, USA
RPMI	Thermo Fisher Scientific, Waltham, MA, USA
SuperScript™ III Reverse Transcriptase	Thermo Fisher Scientific, Waltham, MA, USA
SDS	Sigma-Aldrich, St. Louis, MO, USA
S.O.C. Medium	Thermo Fisher Scientific, Waltham, MA, USA
Sodium chloride	Sigma-Aldrich, St. Louis, MO, USA
Streptavidin Alexa Fluor® 594	Thermo Fisher Scientific, Waltham, MA, USA
Tris/HCl	Carl Roth, Karlsruhe, Germany
Triton-X-100	Merck, Darmstadt, Germany
Trizol	Thermo Fisher Scientific, Waltham, MA, USA
Trypsin-EDTA (0,25%), phenol red	Thermo Fisher Scientific, Waltham, MA, USA
UltraPure™ TBE Buffer, 10X	Thermo Fisher Scientific, Waltham, MA, USA

2.1.4 Consumable material

Table 4: List of consumable material

Product	Company
Aerodisc syringe filters	Pall Corporation, NY, USA
Amicon® Ultra-15 Zentrifugen-Filtereinheiten 15 und 30K	Millipore, Billerica, MA, USA
Bacteria tubes	Greiner Bio-One, Frickenhausen, Germany
Cell culture flask 75 cm^2, 175 cm^2	Greiner Bio-One, Frickenhausen, Germany
Cell culture inserts pore diameter 0.4 µm	Millipore, Billerica, MA, USA

Product	Company
Cell strainer (70 µm, 100 µm)	Greiner Bio-One ,Frickenhausen, Germany
Combitips advanced	Eppendorf, Hamburg, Germany
Cover slips	Menzel Gläser, Braunschweig, Germany
Cryo.s™ Tubes	Greiner Bio-One, Frickenhausen, Germany
Disposable Pasteur Pipettes, 2.5 mL	Carl Roth, Karlsruhe, Germany
Filtropur vacuum filtration units 0.2 µm (250 mL, 500 mL)	Sarstedt, Nümbrecht, Garmany
HiTrap Protein G column	GE Healthcare, Uppsala, Sweden
Hypodermic needle	B. Braun, Melsungen, Germany
Microscope slides	Menzel Gläser, Braunschweig, Germany
Parafilm	Pechiney Plastic Packaging, Akron, OH, USA
Petri dishes uncoated (Ø 30 mm, 100 mm)	Greiner Bio-One, Frickenhausen, Germany
PCR tubes, Sapphire	Greiner Bio-One ,Frickenhausen, Germany
Plastic discs for tissue chopping	Ted Pella Inc., Redding, CA, USA
Razor Blades	AccuTec Blades, Verona, VA, USA
Slide-A-Lyzer™ Dialysis Cassettes	Thermo Fisher Scientific, Waltham, MA, USA
Syringes (5 mL, 10 mL, 20 mL, 50 mL)	B. Braun, Melsungen, Germany
TipOne® Pipette Tips (1000 µL, 100 µL, 10 µL)	Starlab, Hamburg, Germany
Tubes (2 mL, 1.5 mL, 0.5 mL)	Eppendorf, Hamburg, Germany
Tubes, (15 mL, 50mL)	Greiner Bio-One, Frickenhausen, Germany
Well Plates (6, 24, 96 wells)	Greiner Bio-One, Frickenhausen, Germany

2.1.5 Prokaryotic and eukaryotic cells

Table 5: Prokaryotic and eukaryotic cells

Prokaryotic cells	**Company**
Subcloning Efficiency™ DH5α™ Competent Cells	Thermo Fisher Scientific, Waltham, MA, USA
Eukaryotic cells	**Company**
FreeStyle™ 293-F-Cells (HEK-FS)	Thermo Fisher Scientific, Waltham, MA, USA

2.1.6 Kits

Table 6: Kits used for sample analysis

Kits	**Company**
Pierce™ Fab Preparation Kit	Thermo Fisher Scientific, Waltham, MA, USA
Neural Tissue Dissociation Kit – Postnatal Neurons	Miltenyi, Bergisch Gladbach, Germany
Human IgG ELISA Kit	Molecular Innovations, Peary, MI, USA
Mix-n-Stain CF™5 55 Antibody Labeling Kit	St. Louis, MO, Vereinigte Staaten
SensiFAST™ Probe Lo-ROX Kit	Bioline, Luckenwalde, Germany
PureLink® Quick Plasmid Miniprep Kit	Thermo Fisher Scientific, Waltham, MA, USA
PureLink® HiPure Plasmid Maxiprep Kit	Thermo Fisher Scientific, Waltham, MA, USA

2.1.7 Antibodies

Table 7: Primary antibodies used for immunohistochemical analysis

Target	Species	Reactivity	Company	Dilution
Caspr	rabbit	mouse	Abcam, Cambridge, UK	1:3000
CD68	rat	mouse	Biolegend, San Diego, CA, USA	1:200
Iba1	rabbit	mouse	Wako, Neuss, Germany	1:400
MBP	mouse	mouse	Merck Millipore, Billerica, MA, USA	1:500
NF200	mouse	mouse	Sigma-Aldrich, St. Louis, MO, USA	1:500
NF200	rabbit	mouse	Sigma-Aldrich, St. Louis, MO, USA	1:500

Table 8: Secondary antibodies used for immunohistochemical analyis

Conjugation	species	reactivity	company	dilution
Alexa Fluor® 647	goat	mouse	Abcam, Cambridge, UK	1:500
Alexa Fluor® 647	goat	rabbit	Abcam, Cambridge, UK	1:500
Cy3	goat	mouse	Merck Millipore, Billerica, MA, USA	1:500
Cy3	goat	rabbit	Merck Millipore, Billerica, MA, USA	1:500
Cy3	goat	rat	Merck Millipore, Billerica, MA, USA	1:500

Table 9: Antibodies used for flow cytometry

target	conjugation	reactivity	species	company	dilution
CD11b	PerCP-Cy5.5	mouse	rat	ebioscience	1:200

2.1.8 Primer

Table 10: Primer sequences for genotyping of PLP~GFP mice

Primer	sequence
Primer fw	AAG TTC ATC TGC ACC ACC G
Primer rv	GCT CAG GTA GTG GTT GTG G

Table 11: Primer and probe sets for quantitative real-time PCR

Gene	Product name
Glyceraldehyde 3-phosphate dehydrogenase (GAPDH)	Mm99999915_g1
Myelin basic protein (MPB)	Mm01266402_m1
Ionized calcium-binding adapter molecule 1 (Iba1)	Mm00479862_g1
2',3'-Cyclic-nucleotide 3'-phosphodiesterase (CNPase)	Mm01306640_m1
Neuron-glial antigen 2 (Ng2)	Mm00507257
Neurofilament 200 (NF200)	Mm01191456_m1

Table 12: Locus specific primer for the sequencing of pVitro1-hu818c5_IgG1k-emGFPbsd

Primer	Sequence
Light chain fw	GAG GCT AAT TCT CAA GCC TC
Light chain rv	CTG GTC TTT CCA GGT CTA GA
Heavy chain fw	TTT TGA GCG GAG CTA ATT CTC GGG
Heavy chain rv	GGA GGT GTG GGA GGT TTT TT

2.2 Methods

2.2.1 Animal husbandry

Mice were bred at the animal facility of the Heinrich-Heine-University of Düsseldorf under specific pathogen-free conditions. B. Zalc kindly provided PLP-GFP mice. In these mice, green fluorescent protein (GFP) is expressed under regulatory elements of the proteolipid protein (PLP) gene in oligodendrocytes and is located in the cytosol as well as in the myelin sheath (personal communication B. Zalc). M. Gliem kindly provided CX3CR1-GFP mice. In these mice, GFP is expressed under the promotor of the chemokine receptor CX3CR1, which is in the CNS dominantly expressed in microglia, resulting in green microglia (Jung et al., 2000).

2.2.2 Genotyping

To ensure that only PLP~GFP-positive (GFP^+) mice were used for breeding, all offspring was genotyped using the following protocol.

2.2.2.1 Isolation of deoxyribonucleic acid (DNA) from tail biopsies

Tail biopsies were lysed at 56°C for at least 4 hours or overnight in 500 µL tail lysis buffer **(Table 13)**, containing 10 µL proteinase K per reaction. Tubes with lysed tails were centrifuged for 10 minutes at 13.000 rpm to remove undigested tail material. The supernatant was transferred into a new 1.5 mL tube containing 500 µL isopropanol. Subsequently the DNA was precipitated by inverting the tube. After a centrifugation step at 13.000 rpm, the supernatant was discarded and the DNA pellet was washed with 200 µL 70% ethanol (v/v) by mixing thoroughly. Then the tube was centrifugated for 5 minutes at 13.000 rpm, the supernatant was discarded and the tube was air dried while standing inverted on a paper towel until ethanol had evaporated. Finally, the DNA was solved in 100 µL of ribonuclease (RNase) free, distilled water (dH_2O) and stored at 4°C until further use.

Table 13: Composition of tail lysis buffer for genotyping

Reagent	Volume
1 M Tris/HCl pH 7.5	50 mL
0.5 M Ethylenediaminetetraacetic acid (EDTA)	5 mL
20% Sodium dodecyl sulfate (SDS) (w/v)	5 mL
5 M NaCl	20 mL
dH_2O	420 mL

2.2.2.2 Polymerase chain reaction (PCR)

PCRs were performed using the following pipetting scheme and PCR program.

Table 14: Pipetting scheme for genotyping PCRs

Reagent	Volume
5x Hot-Start Taq PCR-Mastermix	4 µL
Primer fw	0,25 µL
Primer rv	0,25 µL
RNase free, dH_2O	13 µL
DNA	2 µL

Table 15: PCR program for genotyping PCRs

Process	Temperature	Time	cycles
Polymerase activation	94°C	10 min	1 cycle
Denaturation	94°C	45 sec	35 cycles
Annealing	57°C	30 sec	
Elongation	72°C	45 sec	
Elongation	72°C	10 min	1 cycle
Cooling	12°C	Forever	1 cycle

2.2.2.3 Agarose gel electrophoresis

For the detection of the respective PCR products, an agarose gel electrophoresis was performed. Agarose was dissolved (2% w/v) in 1x Tris-borate-EDTA (TBE) Buffer and 3 µL ethidium bromide per 50 mL agarose was added. A volume of 15 µL per amplified DNA sample was filled into the pockets of the agarose gel and a voltage of 140 Volt was applied for 40 minutes. During this time the DNA samples, as well as the marker DNA were separated according to their size. Samples from GFP^+ mice were identified through the presence of a PCR product with a size of 500 base pairs. DNA bands were visualized using a gel documentation system with the help of a UV-lamp.

2.2.3 Preparation of cerebellar OSCs from mice

Murine OSCs were prepared according to a modified protocol from Stoppini et al., 1991. Briefly, postnatal day (P) 9-11 pups were anaesthetised with isoflurane and killed by de-capitation. The cerebellum was removed and cut into 400 µm thick, sagittal sections using a McIllwain tissue chopper. OSCs were separated under a binocular microscope in ice-cold dissecting medium **(Table 16)**, incubated for 10 minutes in ice-cold washing medium **(Table 18)** and then plated on Millicell cell culture inserts with a pore diameter of 0.4 µm **(Figure 3)**. Before plating, each insert was placed in a well of a 6 well plate filled with 1 mL of OSC medium **(Table 17)**. The medium was changed the first day after preparation and thereafter every second to third day. For the first 3-5 days, OSCs were incubated at 37°C, 5% CO_2 and 90% relative humidity. Thereafter they were transferred to an incubator maintaining 33°C, 5% CO_2 and 90% relative humidity.

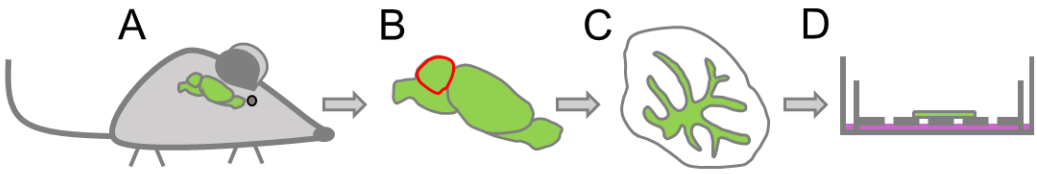

Figure 3. Preparation of cerebellar OSCs from mice.

(A) Mice were anesthetized and decapitated. The cerebellum was removed (red circle in **(B)**) and cut into 400 µm thick, sagittal OSCs. Thereafter, OSCs which were still connected to each other were separated under a binocular microscope **(C)**. Cell culture inserts were placed in medium-filled wells and OSCs were plated on top of the inserts **(D)**.

2.2.3.1 Media for OSC preparation and culture

All media were sterile filtered through a vacuum filtration unit.

Table 16: Composition of dissecting medium

Reagent	Volume
HBSS + Ca^{2+} + Mg^{2+} with penicillin/streptomycin (pen/strep) (100 U/mL and 100 µg/mL), kynurenic acid (1 mMol/L solved in 1-5 mL of NaOH)	500 mL
50% Glucose	5 mL
→ adjust to pH 7.2-7.4	

Table 17: Composition of OSC medium

Reagent	Volume
Heat inactivated horse serum	100 mL
HBSS + Ca^{2+} + Mg^{2+} with pen/strep (100 U/mL and 100 µg/mL)	100 mL
MEM with pen/strep (100 U/mL and 100 µg/mL)	200 mL
50% Glucose (w/v)	5 mL
100 x GlutaMAX™	4 mL

Table 18: Composition of washing medium

Reagent	Volume
HBSS + Ca^{2+} + Mg^{2+} with pen/strep (100 U/mL and 100 µg/mL)	250 mL
Minimal essential medium (MEM) with pen/strep (100 U/mL and 100 µg/mL)	250 mL
HEPES 1 M	12.5 mL

2.2.4 De- and remyelination experiments with OSCs

2.2.4.1 Immune-mediated demyelination

OSCs were allowed to adapt to *ex vivo* conditions for 5-7 days before experiments were performed. Immune-mediated demyelination was induced by adding hu818c5 antibody (2.5-40µg/mL) and pooled, normal baby rabbit serum (3-12% (v/v)) to the OSC medium. Since we used baby rabbit serum as a complement source, it will be hereinafter referred to as "complement". Hu818c5 is a recombinant humanized immunoglobulin G1 (IgG1) antibody directed against myelin oligodendrocyte glycoprotein (MOG; Linnington et al., 1984). The pooled, normal, lyophilized complement was reconstituted in 1 mL of ice-cold dH_2O and used for the treatment of OSCs within 30 minutes. OSCs were demyelinated for 2-3 days in the presence or absence of:

- 1-12 mg/mL IVIG (Privigen®)
- 6-12 mg/mL monoclonal IgG (Rituximab®)
- 4 mg/mL IVIG derived Fab fragments
- 6-12 mg/ml bovine serum albumin (BSA)
- 12 mg/mL human serum albumin (HSA)
- 1-2 mg/mL Fc fragments

All supplements were dialysed against or dissolved in HBSS + Ca^{2+} + Mg^{2+}.

2.2.4.2 Live imaging of de- and remyelination

Live imaging of de- and remyelination was achieved by regular, fluorescence microscopic documentation of each individual PLP~GFP^+ OSC. Fluorescence pictures were taken using the 4x objective of an Olympus BX51 fluorescence microscope and its color-view fluorescence camera. The exposure time was defined at the beginning and was maintained for the duration of the whole experiment. During the demyelination period, OSCs were imaged every day, during the remyelination period pictures from OSCs were taken only every second or third day.

2.2.4.3 Optical quantification of de- and remyelination

De- and remyelination processes were monitored according to the change in the GFP^+ area in OSCs. The GFP^+ area was documented for each time point via fluorescence microscopy. Using ImageJ software, these fluorescence microscopic pictures were quantified by measuring the GFP^+ area exceeding a defined threshold. For remyelination experiments, small GFP expressing cells were excluded from quantification via size

exclusion. Because of the normal variation in size and myelination, each OSC served as its own control. Therefore, the GFP^+ area of each slice was set to 100% at the beginning of the experiment. Pictures of the same OSC were processed in the same way for each observation time point. Images were contrast enhanced using the “background and contrast” tool in ImageJ to facilitate visibility in representative figures.

2.2.5 Immunohistochemical staining of OSCs

OSC were fixed by incubating the inserts in fixation buffer **(Table 19)** for 30 minutes at room temperature. Then the inserts which carried the OSCs were washed once in PBS and incubated in permeabilization buffer for 45 to 60 min. Thereafter, OSCs were washed three times for 15 minutes with PBS and incubated in blocking buffer for 1 hour. Primary antibody solution was prepared by diluting primary antibodies in antibody buffer, according to the manufacturer’s instructions. After three consecutive washes in PBS, the OSCs were cut out from the membrane, transferred to single wells of a 48-well plate, covered with primary antibody solution and incubated for 1-2 days at 4°C in the dark. Secondary antibody solution was prepared by diluting secondary antibodies in antibody buffer, according to the manufacturer’s instructions. After three consecutive washes in PBS, OSC were incubated over night with secondary antibody solution at 4°C in the dark. Subsequently, OSC were washed three times with PBS. To stain cell nuclei Hoechst was added (1:20.000) to the PBS in the second washing step. After the last washing step, OSCs were mounted on glass slides. For better preservation, the transition between cover glass and glass slide was sealed with varnish and the slides were thereafter stored at 4 °C. Fluorescence images were acquired by a Zeiss LSM 510 microscope using the ZEN black software. Confocal images were acquired by a Leica SP8 microscope using the LAS X software. Images were contrast enhanced using the “background and contrast” tool in ImageJ to facilitate visibility in representative figures.

Table 19: Buffers for immunostaining of OSCs

Buffer	composition
Fixation buffer	4% (w/v) paraformaldehyde in phosphate-buffered saline (PBS)
Permeabilization buffer	1% (v/v) Triton X-100 in PBS
Blocking buffer	10% normal goat serum in 0.2% Triton X-100 in PBS
Antibody buffer	1% goat serum and 0.2% Triton X-100 in PBS

2.2.6 Dissociation and staining of OSCs for flow cytometry

For quantification of living oligodendrocytes and microglia, OSCs from PLP-GFP mice were dissociated by enzymatic digestion using the "Neural Tissue Dissociation Kit – Post-natal Neurons" according to the manufacturer's instructions. Subsequently the cell pellet was resuspended in 100-200 µl PBS and washed twice with PBS. All centrifugation steps were performed for 5 min at 2000 x g in a 96 well plate and cells were always resuspended in 100 µl of the respective buffer. A flow cytometry antibody against the microglial protein cluster of differentiation molecule 11B (CD11b) and fixable viability dye (eFluor 450) were diluted in PBS according to the manufacturer's instructions and cells were stained for 30 min at 4°C in the dark. After two washes, cells were fixed in 4% PFA for 10 minutes at room temperature. After centrifugation, the pellet was resuspended in PBS and stored at 4°C until analysis by flow cytometry. GFP^+ cells not stained by viability dye were quantified as "living oligodendrocytes". CD11b positive cells not stained by viability dye were quantified as "living microglia". Living oligodendrocytes and living microglia were expressed in percent of all living and gated cells.

2.2.7 Quantitative real-time (RT) – PCR

2.2.7.1 Isolation of ribonucleic acid (RNA) from OSCs

RNA was isolated following a trizol protocol:

Single OSCs were homogenized in 1 mL of TRIZOL® Reagent. For better visibility of the RNA pellet 200 µg glycogen was added and the mixture was then incubated 5 minutes at room temperature. After addition of 200 µL chloroform, tubes were capped and shaken for 15 seconds vigorously by hand. Samples were incubated for 2-3 minutes at room tem-

perature and then centrifuged at 12.000 x g for 15 min at 4°C to induce separation into three phases:

- the lower red, phenol-chloroform phase, containing the DNA
- the white interphase
- the colourless aqueous phase, containing the RNA

The aqueous phase was transferred to a fresh tube and the RNA was precipitated by adding 500 µL isopropanol. Samples were incubated for 10 minutes at room temperature and centrifuged at 12.000 x g for 10 min at 4°C. The supernatant was removed and the RNA containing glycogen pellet was washed thoroughly with 1 mL of 75% ethanol (v/v). The tube was centrifuged at 7500 x g for 5 min at 4°C, the ethanol was removed and the pellet was air dried. Afterwards the pellet was dissolved in 20 µl RNase-free dH_2O. The RNA concentration was measured with the Nanodrop. To inhibit degradation, RNA was stored at -80°C until reverse transcription into complementary DNA (cDNA).

2.2.7.2 Reverse transcription of RNA into cDNA

RNA was transcribed into cDNA using the "SuperScript™ III Reverse Transcription Kit" according to the manufacturer's recommendations. RNA samples were brought to the same concentration by dilution in RNase free dH_2O to a maximum volume of 13 µL. First, oligo$(dT)_{20}$, dNTP Mix, RNA and RNase free dH_2O were heated for 5 minutes at 65°C, then the mixture was incubated for 1 minute on ice **(Table 20)**. Subsequently, First-Strand Buffer, Dithiothreitol (DTT), RNaseOUT® and SuperScript™ III RT were added. cDNA was synthesized for 50 minutes at 50°C. Heat inactivation was performed for 15 minutes at 70°C. Finally, the cDNA was diluted 1:5 in RNase free dH_2O and stored at -20°C until quantitative real-time PCR.

Table 20: Pipetting scheme for cDNA synthesis

Reagent	Volume
oligo$(dT)_{20}$	1 µL
dNTP Mix	1 µL
180 ng of RNA	x µL
RNase free dH_2O	13 µl – x µL
5 minutes at 65°C, 1 minute on ice	
5x First-Strand Buffer	4 µL
0.1 M DTT	1 µL
RNaseOUT®	1 µL
SuperScript™ III RT	1 µL
50 minutes at 50°C, 15 minutes at 70°C	

2.2.7.3 Quantitative real-time PCR

Quantitative real-time PCR (q-PCR) was performed with the "SensiFAST™ Probe Lo-ROX Kit" following using a 7500 Pro Real-Time PCR System. Primer Probe sets were purchased from Life Technologies. qPCRs were performed according to the pipetting scheme and programm in **Table 21** and **Table 22**. In each cycle, the probe hybridized with the complementary sequence of the already amplified gene copies. The hybridization activated a fluorescent reporter, the resulting fluorescence signal was measured after every cycle and documented in a fluorescent curve over the time. A threshold was defined in the linear part of the fluorescence curves. The corresponding value at the x-axis was named as Ct value and described the cycle number in which the defined threshold was reached. The higher the copy number of the target gene in the starting material (cDNA) the lower was the Ct value. To determine the expression of the target gene in relation to the general gene expression, the Ct value of a constitutively expressed housekeeping gene was included in the calculation. Thereby increased target gene production caused by overall higher cell activity was distinguished from distinct upregulation of the target gene. For this study, glyceraldehyde 3-phosphate dehydrogenase (GAPDH) was used a housekeeping gene. Up- or downregulation of a target gene in the treated group was depicted as n-fold expression of the same gene in the control group using the following formulas:

n-fold gene expression = $2^{-\Delta\Delta Ct}$

ΔΔCt = ΔCt (treated group) - ΔCt (control)

ΔCt = ΔCt (target gene) - ΔCt (housekeeping gene)

Table 21: Pipetting scheme for q-PCR

Reagent	Volume
SensiFAST™ LoROX Master Mix	10 µL
Primer & Probe	1 µL
RNase free dH_2O	5 µL
diluted cDNA	4 µL

Table 22: program for q-PCR

Process	Temperature	Time	cycles
Polymerase activation	95°C	2 min	1 cycle
Denaturation	95°C	10 sec	40 cycles
Annealing/Extension	60°	50 sec	

2.2.8 Preparation of Fab fragments

Fab fragments were prepared from whole IVIG using the "Pierce™Fab Preparation Kit" according to the manufacturer's recommendations.

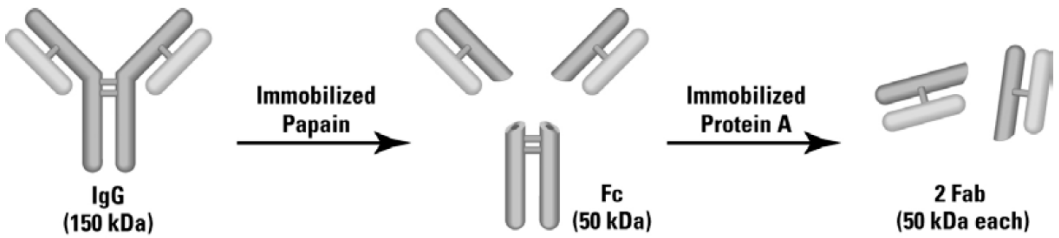

Figure 4. Preparation of Fab fragments from IVIG.
IVIG was cleaved by Papain, the Fc fragment was immobilized by the binding to a protein A column. (Figure taken from the manual: "Pierce™ Fab Preparation Kit")

2.2.9 Plasmid amplification for antibody production

2.2.9.1 Transformation

To induce immune-mediated demyelination, OSCs were treated with complement and the humanized anti MOG-antibody clone 818c5 (hu818c5). For recombinant production of this antibody by transfection of human embryonic kidney (HEK) cells, the corresponding plasmid **(Figure 5)** needed to be amplified. Therefore, competent *E.coli* cells (DH5α™) were transformed with the hu818c5 plasmid.

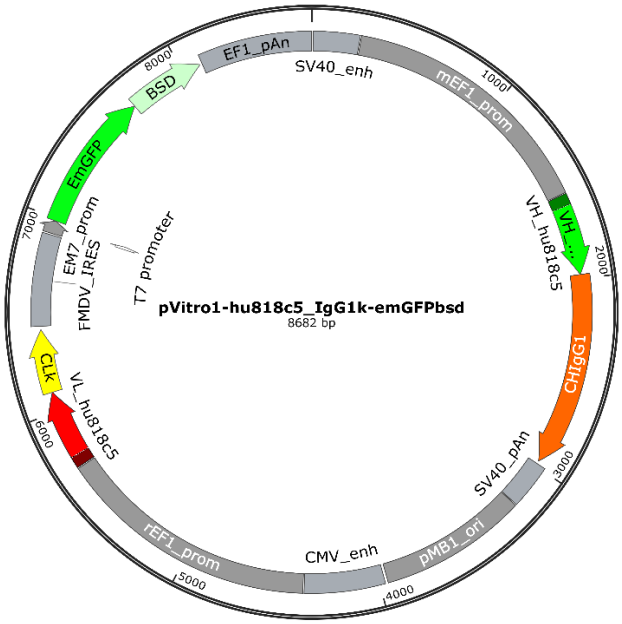

Figure 5. pVitro1-hu818c5 IgG1k emGFPbsd
Abbreviation: **BSD**: resistance to blasticidin; **EF1_pAn / SV40pAn**: polyadenylation signal; **SV40_enh / CMV_enh**: enhancer; **mEF1_prom**: mouse promoter; **VH_hu818c5**: variable domain of the heavy chain (hu818c5); **CHIgG1**: constant domain of the heavy chain; **pMBI_ori**: origin of replication for *E.coli*; **rEF1_prom**: rat promotor; **VL_hu818c5**: variable domain of the light chain (hu818c5); **CLk**: constant domain of the light chain; **FMDV_IRES**: internal ribosome entry site of the foot and mouth disease virus; **EmGFP**: emerald GFP. The plasmid pVITRO1-dV-IgG1/κ was purchased from Addgene. Jason Cline replaced the hygromycine resistance with EmGFP and BSD and inserted VH_hu818c5 and VL_hu818c5. Henrike Diel made the corresponding plasmid card using snap gene software. CHIgG1 and CLk were taken from pVITRO1-Trastuzumab-IgG1/k.

One vial DH5α™ cells (50 µL) and the hu818c5 plasmid were thawed on ice. The content of both tubes was collected by short centrifugation and 1 µL of Plasmid DNA was transferred to the DH5α™ cells. The cells were incubated with the Plasmid DNA for 30 minutes on ice, heat shocked for 30 seconds at 42°C and then again incubated for 2 minutes on ice. After addition of 250 µL of S.O.C. medium to the DH5α™ cells, they were incubated at 37°C and 300 rpm. After 2-3 hours, the bacteria suspension was plated on LB agar plates, which contained Blasticidin, to selectively support the growth of bacteria which internalized the hu818c5 plasmid. The agar plate was incubated over night at 37 °C. The next day, six single colonies were picked by a small pipette tip and each colony was transferred to a bacteria tube filled with 5 mL of LB medium. The bacteria suspension was incubated for 1-2 hours at 37°C and 300 rpm. After the addition of Blasticidin, the bacteria were allowed to grow over night and used thereafter to isolate the plasmid DNA.

2.2.9.2 Isolation of plasmid DNA (small scale)

For the isolation of hu818c5 plasmid DNA the “PureLink® Quick Plasmid Miniprep Kit” was used according to the manufacturer’s recommendations. All centrifugation steps were performed at 12.000 x g. A volume of 4 mL of the overnight culture was used for the small scale production, the remaining 1 mL was further stored at 4°C as starting material for the high scale production. The cells of the overnight culture (4 mL) were separated from the LB medium by centrifugation at room temperature. The LB medium was discarded and the pellet was resuspended in 250 µL of resuspension buffer. 250 µL of lysis buffer were added, the tube was mixed by inverting five times and incubated 5 minutes at room temperature. After addition of 350 µL of precipitation buffer, the tube needed to be inverted and the lysate was centrifuged for 10 minutes. After centrifugation, the supernatant was loaded onto a spin column, which was placed in a fresh 2 mL tube beforehand. The column was centrifuged for 1 minute, the flow through was discarded and the column was washed by adding 700 µL of wash buffer. The column was centrifuged for 1 minute and the flow through was discarded. The column was placed in a clean 1.5 mL recovery tube and 30 µL of TE buffer were pipetted in the center of the column. Subsequently, the column was incubated for 1 minute at room temperature and centrifuged for 2 minutes. The concentration of the eluted plasmid was measured using the Nanodrop. Therafter an aliquot was used for sequence confirmation.

2.2.9.3 Sequencing of plasmids

To confirm the sequence of the variable part of the heavy and light chain in the hu818c5 plasmid, 10 µL of plasmid were send together with 2 µL of locus specific primer to “Eurofins Genomics GmbH” for sequencing. Plasmids with the correct sequences were identified by comparison of the sequencing results to the original sequence using the online tool “MAFFT”. If several plasmids had the correct sequence, one was selected to prepare the overnight culture for the high scale plasmid production.

2.2.9.4 Isolation of plasmid DNA (high scale)

For the production of larger amounts of hu818c5 plasmid, the stored overnight culture (as described in section **2.2.9.2** was added to 300 mL of LB medium and incubated for 1 hour at 37°C at 250 rpm. After 1 hour, Blasticidin was added to a final concentration of 100 µg/mL to prevent the growth of bacteria without a hu818c5 plasmid. The culture was allowed to grow over night and used thereafter for the high scale isolation of plasmid DNA. The "PureLink® HiPure Plasmid Maxiprep Kit" was used according to the manufacturer's recommendations. The HiPure Maxi column was equilibrated with 30 mL of equilibration buffer, whereby the buffer was allowed to drain by gravity flow. The cells of the overnight LB culture were harvested by centrifugation at 4.000 x g for 10 minutes. The LB medium was removed and the bacteria pellet was resuspended in 10 mL of resuspension buffer until the suspension was homogeneous. Subsequently, 10 mL of lysis buffer were added, the tube was inverted 5 times and incubated for 5 minutes at room temperature. Then, 10 mL of precipitation buffer were added and the tube was immediately inverted until the lysate was homogeneous. The lysate was centrifuged at 8.000 x g for 10 minutes at room temperature and then the supernatant was loaded onto the equilibrated column. The solution was allowed to drain by gravity flow through. Then the column was washed by adding 60 mL of washing buffer. The flow through was discarded and a sterile 50 mL tube, containing 10 mL of ice-cold isopropanol, was placed under the column. The plasmid was eluted by 15 mL of elution buffer and precipitated while dropping into the isopropanol. The precipitate was mixed by inverting and then centrifuged at 8.000 x g for 1 hour. The supernatant was discarded, the DNA pellet was washed with 5 mL of 70% ethanol (v/v) and the tube was centrifuged for 10 minutes at 8.000 x g. Thereafter, the supernatant was removed, the pellet was air-dried and it was solved in 500-600 µl of RNase free dH_2O. The plasmid concentration was measured using the Nanodrop. The quality of the plasmid was confirmed by sequencing as described in section **2.2.9.3**.

2.2.9.5 Preparation and usage of a glycerol stock

For the preparation of a glycerol stock, 500 µL of an overnight bacteria culture were mixed with 500 µL glycerol in a cryoprotective tube and frozen at -80°C. For the following plasmid productions, the transformation procedure was replaced by spreading out a small volume of the glycerol stock on a Blasticidin LB agar plate. The next day, several single colonies were picked with a small pipette tip and each colony was transferred to a bacteria tube. Each tube was filled with 5 mL of LB medium and all tubes were incubated at 37°C and 300 rpm. Thereby an initial incubation for 1-2 hours without antibiotics was followed

by an overnight incubation with Blasticidin. Subsequently, the plasmid DNA was isolated as described in section **2.2.9.2**.

2.2.10 Culture and transfection of HEK cells for the production of recombinant anti-MOG antibody

2.2.10.1 Culture of HEK-Freestyle™ cells 293 (HEK-FS cells)

HEK-FS cells were cultured in T175 cm^2 flasks with 20 mL of HEK cell medium (**Table 23**) at 37°C and 90% humidity. When the confluency reached 90%, medium was removed and the cell layer was washed with 10 mL of HBSS without Ca^{2+} + Mg^{2+}. The HBSS was removed and 2 mL of tryspin-EDTA were added for 5 minutes to detach the cells from the cell culture flask. To inhibit the enzymatic reaction of trypsin-EDTA, 10 mL of HEK cell medium were added and cells were transferred into a 50 mL tube which was centrifuged at 500 x g for 10 minutes. The cell pellet was resuspended in fresh HEK cell medium and the cell suspension was then distributed on five fresh T175 cm^2.

Table 23: Composition of HEK cell medium

Reagent	Volume
Roswell Park Memorial Institute medium (RPMI) with pen/strep (100 U/mL and 100 µg/mL)	500 mL
Fetal calf serum (FCS)	50 mL
100 x GlutaMAX™	5 mL

2.2.10.2 Freezing of HEK-FS cells

For cryopreservation confluent HEK-FS cells were washed with PBS (without Ca^{2+} + Mg^{2+}) and incubated with trypsin-EDTA for 5 minutes at room temperature. The cells were resuspended in 10 mL of fresh HEK cell medium and an aliquot was counted while centrifuging the cell suspension for 5 minutes at 500 x g. Then the supernatant was removed and up to 10^7 cells were resuspended in 1 mL of Recovery™ cell culture freezing medium. One mL aliquots of cells were pipetted into cryoprotective tubes, the tubes were placed in a freezing container and frozen at -80°C overnight. Frozen tubes were transferred to the liquid nitrogen tank.

2.2.10.3 Thawing of HEK-FS cells

Cryopreserved HEK-FS cells were thawed as quickly as possible in the waterbath at 37°C and transferred to a tube containing 10 mL of prewarmed HEK cell medium. The tube was then centrifuged at 500 x g for 10 minutes. Subsequently, the cell pellet was dissolved in 20 mL of prewarmed HEK cell medium and plated on a T175 cm^2 flask. The first day after thawing, HEK-FS cells were divided into new cell culture flasks and cultured further on.

2.2.10.4 Transfection of HEK-FS cells with polyethylenimine (PEI)

One day prior to transfection 10-12 x 10^6 HEK-FS cells were plated per T175 cm^2 cell culture flask in normal HEK-FS cell medium. The next day two tubes were prepared:

Tube 1 20 µg plasmid (hu818c5) in a total volume of 500 µL Opti-MEM

Tube 2 60 µg PEI (three times the weight of the plasmid DNA) in a total volume of 500 µL of Opti-MEM™

Both tubes were incubated at room temperature for 5 minutes and then the content of tube 2 was transferred to tube 1, mixed shortly and incubated at room temperature for 30 minutes. Right before the end of the incubation time, the medium was removed from the HEK-FS cells, the PEI plasmid complex was added to 20 mL of fresh medium and transfection medium was given to the HEK-FS cells. 24 hours later, the transfection medium was changed to Nutridoma™ supplemented HEK cell medium **(Table 24)**. If necessary, half of the Nutridoma™ medium was changed every two days. After one week of antibody production, the cells were discarded. The collected medium was filled in 50 mL tubes and frozen at -20°C until protein purification.

Table 24: Composition of Nutridoma™ supplemented HEK cell medium:

Reagent	Volume
RPMI with pen/strep (100 U/mL and 100 µg/mL)	500 mL
Nutridoma SP	5 mL
100 x GlutaMAX™	5 mL

2.2.11 Purification and validation of recombinant anti-MOG antibody

2.2.11.1 Antibody purification by affinity chromatography

Antibody purification was performed with an Äkta protein purification system via affinity chromatography using a protein G column. The 50 mL tubes containing the collected Nutridoma^{TM} medium were thawed in cold water. To remove residual cells, the medium was centrifuged at 8.000 x g and the supernatant was then filtrated using a vacuum filtration unit. The filtrated Nutridoma^{TM} medium was adjusted to pH 7-8 by the addition of TrisHCl pH 8 (approximately 10% of the volume of the Nutridoma^{TM} medium). Before the Äkta was used for antibody purification, the system was washed with 20% non-denatured ethanol (v/v). The protein g column was installed and washed with 10 mL TrisHCl pH 7, before the antibody-containing medium was applied to the column with a flow rate between 0.1 and 1 mL/min. Once all medium run through, the column was again washed with 10 mL TrisHCl pH 7 before the antibody was eluted with 0,1 M Glycine Buffer pH 2,7 and collected in fractions of 5 mL. Immediately after elution, the pH of the eluted antibody solution was neutralized with TrisHCl pH 8. The antibody was dialysed against HBSS + Ca^{2+} + Mg^{2+} using a Slide-A-Lyzer™ Dialysis Cassette (cut off 10.000 kDa) according to the manufacturer's recommendations. Finally, the antibody solution was concentrated with an Amicon® Ultra-15 centrifugation unit (cut off 15.000 kDa). The antibody was aliquoted and stored at -20°C until concentration measurement.

2.2.11.2 Bicinchoninic acid assay (BCA)

For rough estimation of recombinant antibody concentration, a BC Assay was performed according to the enhanced protocol. The BSA standard was prepared according to **Table 25** and stored at -20°C for further use. For the assay, 25 µL of standards A-H, as well as the same volume of unknown samples were pipetted in duplicates in a transparent 96 well plate. The BC Assay working reagent was prepared from solution A and solution B in the ratio 1 to 50 and was mixed freshly for each experiment. 200 µL working reagent were added to the standards and unknowns. Thereafter the plate was incubated for 30 minutes at 37°C. The optical density (OD) at 562 nm was measured using a TECAN Reader. OD values from the BSA standard A-H were plotted against the protein concentration and a regression line was placed through the measured values. The linear equation of the regression line was used to calculate the protein concentrations of the unknown samples.

Table 25: Preparation of a BSA Standard for the BC Assay

Standard	2 mg/mL BSA stock	HBSS + Ca^{2+} + Mg^{2+}	Final protein concentration
A	100 µL	300 µL	500 µg/mL
B	100 µL	700 µL	250 µg/mL
C	300 µL of B	300 µL	125 µg/mL
D	100 µL of B	400 µL	50 µg/mL
E	48 µL of B	752 µL	15 µg/mL
F	16 µL of B	784 µL	5 µg/mL
G	6 µL of B	746 µL	2 µg/mL
H	0 µL	800 µL	0 µg/mL

2.2.11.3 Enzyme-linked immunosorbent assay (ELISA) for human IgG

For precise determination of recombinant antibody concentration, a human IgG ELISA was performed according to the manufacturer's recommendations.

Table 26: Preparation of the hu IgG standard for the ELISA

Standard	500 ng/mL hu IgG stock	Blocking Buffer	Final protein concentration
A	400 µL of stock	600 µL	200 ng/mL
B	500 µL of A	500 µL	100 ng/mL
C	500 µL of B	500 µL	50 ng/mL
D	400 µL of C	600 µL	20 ng/mL
E	500 µL of D	500 µL	10 ng/mL
F	500 µL of E	500 µL	5 ng/mL
G	400 µL of F	600 µL	2 ng/mL
H	500 µL of G	500 µL	1 ng/mL
I	500 µL of H	500 µL	0.5 ng/mL
J	400 µL of I	600 µL	0.2 ng/mL
K	0 µL -	500 µL	0 ng/mL

The lyophilized human IgG was reconstituted in 1 mL of blocking buffer (3% BSA (w/v) in Tris-buffered saline (0.1M Tris, 0.15M NaCl, pH7.4)) to generate the hu IgG stock solution (500 ng/mL). The hu IgG stock solution was used to prepare the hu IgG standards A-K according to **Table 26**. All steps of the ELISA were performed at room temperature. U known samples were diluted in blocking buffer to be in the linear range of the human IgG-standard curve. The results of the BC-Assay served as an indicator for an appropriate dilution. The provided and precoated 96 well plate was filled in duplicates with 100 µL of the respective standards and unknown samples. Then the plate was shaken at 300 rpm for 30 minutes to allow the IgG in the standard or unknown samples to bind to the capture antibody. In the mean time, 1x washing buffer was prepared by diluting the provided 10x washing buffer in dH_2O. After three consecutive washes with each 300 µL of 1x washing buffer per well, the primary antibody was reconstituted in 10 mL of blocking buffer. Then 100 µL of primary antibody were added to each well and the plate was shaken at 300 rpm for 30 minutes. Following three consecutive washes with 300 µL of 1x washing buffer, 100 µL of horseradish peroxidase-conjugated streptavidin (1:50,000 diluted in blocking buffer) were added to each well and shaken at 300 rpm for 30 minutes. Finally, all wells were washed three times with 1x washing buffer and incubated with 100 µL of 3,3',5,5'-Tetramethylbenzidine (TMB) substrate solution for 2-10 minutes. The reaction was stopped when the blue colour of the samples was visually in the same range of the standards by adding 50 µl of 1N HCl to each well. The OD at 450 nm was measured with a TECAN Reader. OD values were plotted against the amount of IgG in the standards and a regression line was placed through the linear part of the curve. The linear equation of the regression line was used to calculate the protein concentrations of the unknown samples.

2.2.11.4 Polyacrylamide gel electrophoresis (PAGE)

To control the recombinant antibodies and the cleaved Fab fragments for the correct protein size a Polyacrylamide gel electrophoresis was performed. PAGE allowed the separation of proteins according to their molecular weight. Therefore 13 µL of recombinant antibody were mixed with 5 µL NuPAGE® LDS probe buffer and 2 µL NuPAGE® sample reducing agent and denatured for 5 minutes at 95°C. The DTT, present in the reducing agent, destroyed disulfid linkages by reduction. The probe buffer contained Lithium dodecyl sulfate (LDS), which acted as chemical denaturant and destroyed hydrogen bounds of secondary and tertiary protein structures. In addition, the anionic detergent LDS, added negative charges to proteins in proportion to their molecular weight. The number of negative charges per protein determined the migration speed through the polyacrylamide gel towards the anode. As a result, proteins were separated according to their molecular weight. Mini-Protean® TGX™ Precast Gels were probed with 20 µL of reduced and dena-

tured recombinant antibody and the electrophoresis was performed at 150 Volt for 45 minutes. Afterwards, the gel was washed three times with dH_2O and stained for 1 hour with GelCode® Stain reagent. Unspecific staining was removed by washing the gel with dH_2O over night, shaking, at room temperature. Finally, gel documentation was performed using the Odyssey imaging system.

2.2.12 Statistical analysis

Statistical analysis was performed using the GraphPad Prism 5.00 software. Two groups were compared by student's t-test. For comparison of several groups a one-way analysis of variance with Dunnett's post hoc test was performed. Values were depicted as mean ± standard error of the mean (SEM). Significances were indicated as * for P values ≤ 0.05.

3 Results

3.1 Quantification of immune-mediated demyelination and spontaneous remyelination in organotypic slice cultures (OSCs) of the cerebellum

Immune-mediated demyelination of OSCs was induced by treatment with 5 µg/mL anti-MOG antibody and 6% complement as described previously (Harrer et al., 2009). After three days of demyelination, spontaneous remyelination was initiated through the replacement of the demyelination medium with OSC medium and monitored for one week. De- and remyelination were visualized by using transgenic mice expressing GFP under regulatory elements of PLP. The PLP-GFP expression was monitored in OSCs under standardized conditions by fluorescence microscopic digital photographs. Using ImageJ software, these photographs were analyzed by measuring the GFP-positive (GFP^+) area exceeding a defined threshold. The GFP^+ area is depicted as "mask of PLP-GFP" in **Figure 6**. In a second approach, small GFP expressing cells were subtracted from the GFP^+ area via size exclusion and visualized as "mask of PLP-GFP after size exclusion". In both approaches, serial pictures of the same OSC were processed identically. As each OSC served as its own control, its GFP^+ area at day 0 was defined as 100%. Representative fluorescence microscopic pictures as well as their quantification demonstrate that OSCs underlie progressive demyelination following anti-MOG antibody and complement treatment **(Figure 7)**. After a period of 7 days, OSCs show spontaneous and incomplete remyelination. In contrast, the GFP^+ area of untreated OSCs increased over the observed period, representing ongoing myelination. Although, the evaluation with size exclusion **(Figure 7 C)** results in lower values than the evaluation without size exclusion **(Figure 7 B)**, both evaluation methods show the same trend. The evaluation with size exclusion results after 3 days in a myelin reduction to a value of 4% (±1) compared to 12% (±2) without size exclusion. After 10 days, OSCs remyelinated up to a value of 43% (±4) with and 86% (±10) without size exclusion. Since in remyelination experiments, the size exclusion method is less prone to measure artefacts and since a value of 43% (day 10) mirrors better the incomplete remyelination **(Figure 7 A)**, the size exclusion method was used for all remyelination experiments.

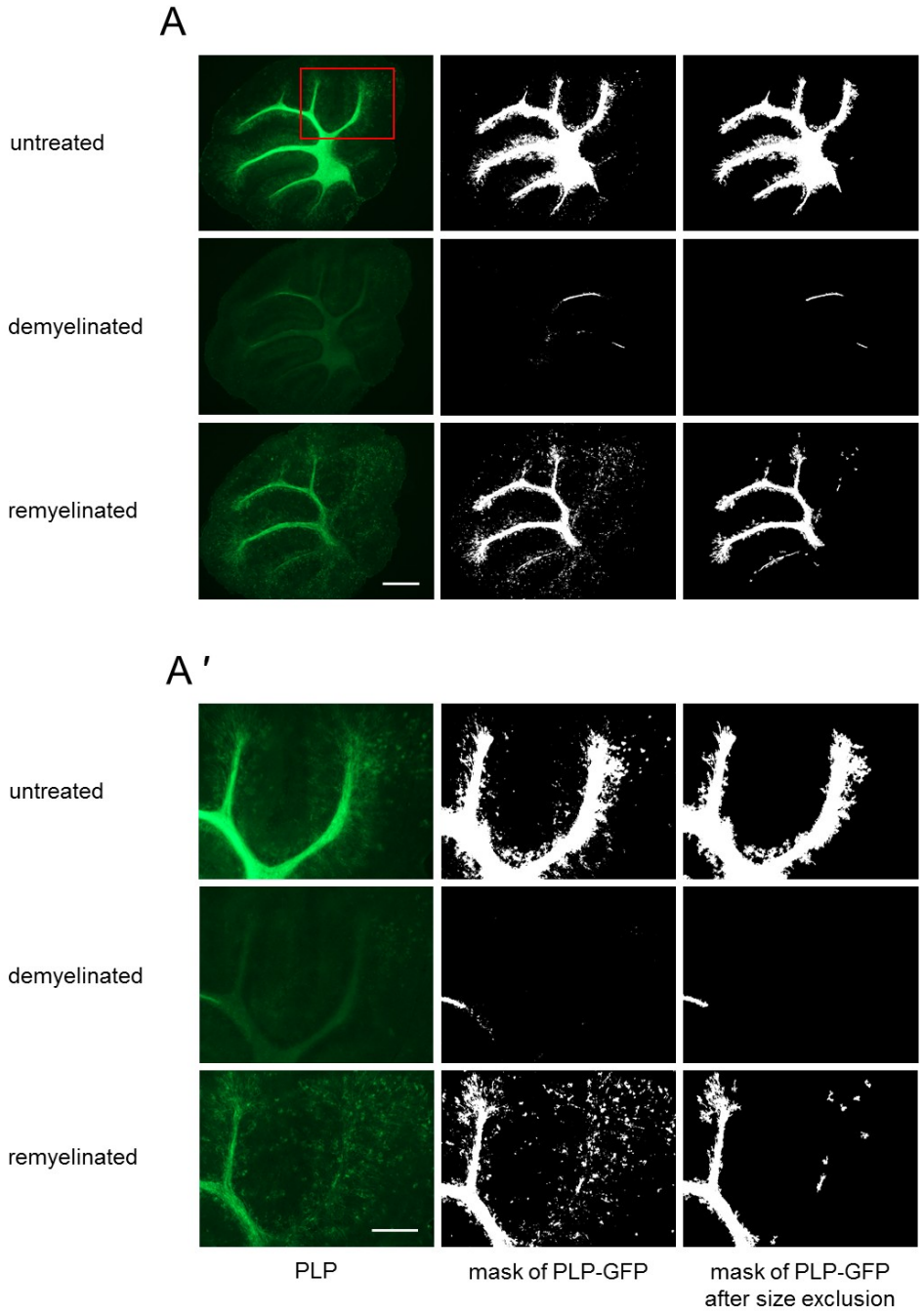

Figure 6. Quanitification of de- and remyelination.

OSCs were demyelinated with 5 µg/mL anti-MOG antibody and 6% complement for three days. Spontaneous remyelination of OSCs was initiated by a change to normal OSC medium for 7 days. De- and remyelination were visualized by using transgenic mice expressing GFP under regulatory elements of the myelin protein PLP. For the quantification of the relative myelin content of OSCs during de- and remyelination, PLP-GFP expression was documented in living OSCs, at different time points (daily during demyelination and 3 times a week during remyelination). **(A)** Representative quantification of an OSC before treatment and after de- and remyelination. Using ImageJ software, we assessed the area of the GFP signal exceeding a defined threshold (GFP^+ area) in digital images acquired by fluorescence microscopy. Pictures of the same OSCs at different time points were processed identically. As each OSC served as its own control, PLP-GFP expression was related to time point d 0 of each OSC. “Mask of PLP-GFP” represents the area above the defined threshold. “Mask of PLP-GFP after size exclusion” additionally excludes small, GFP expressing cells. **(A’)** Magnification of boxed area. Scale bars **(A)** 1 mm **(A’)** 0.5 mm.

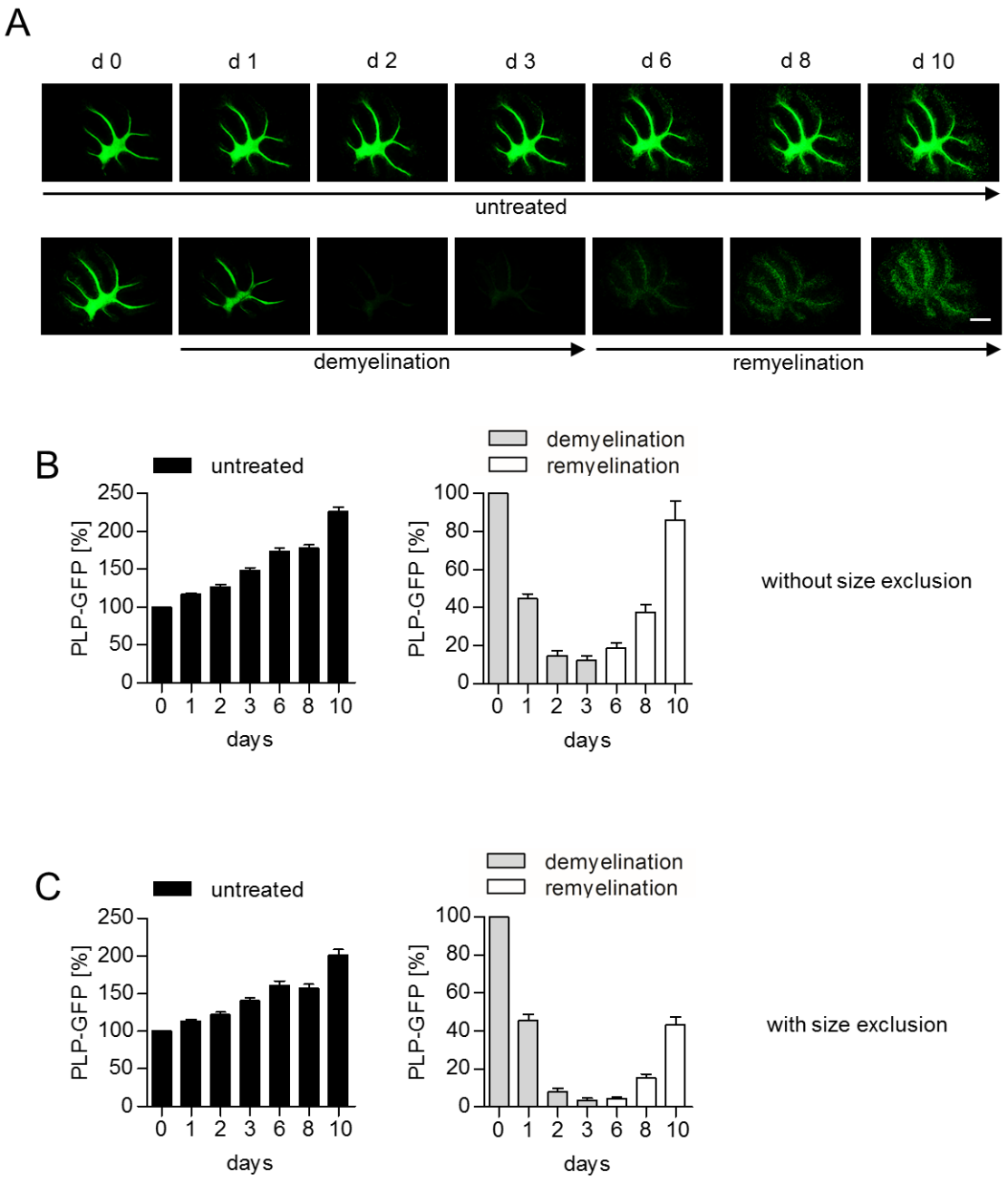

Figure 7. **Immune-mediated demyelination of OSC is followed by spontaneous remyelination.**
After 3 days of demyelination with 5 µg/mL MOG specific antibody and 6% complement, OSCs were cultured in normal OSC medium to induce remyelination. PLP-GFP expression was documented in living OSCs by fluorescence microscopy. Following de- and remyelination (d 3 and d 10), OSCs were fixed for further staining. **(A)** Representative images of PLP-GFP expression: Three days of immune-mediated demyelination result in a massive loss of myelin. Within 7 days, OSCs build spontaneously new myelin. Scale bar 1 mm. **(B)** and **(C)**: Quantification confirms that OSCs show spontaneous remyelination after immune-mediated demyelination. Untreated OSCs keep on myelinating during the duration of the experiment (n = 17-22 OSCs per group). While the quantification without size exclusion **(B)** counts the complete GFP^+ area, the quantification with size exclusion **(C)** excludes small GFP^+ cells and potential artefacts.

3.2 Re-expression of Contactin associated protein 1 (Caspr) after demyelination indiactes the functionality of the new built myelin

To analyze the functionality of myelin in the phase of de-and remyelination as well as in the untreated condition, the integrity of the paranodal junctions was examined. Therefore OSCs were fixed at the indicated time points and stained for the paranodal protein Caspr and the axonal protein NF200 (neurofilament) by immunohistochemistry. Analysis via confocal microscopy revealed that in untreated OSCs, the Caspr antibody stained short cylindrical structures, which are characteristic for the paranodes **(Figure 8).** While Caspr staining was absent in demyelinated OSCs, it reappeared following remyelination. In contrast to the short cylindrical staining pattern in the untreated condition, Caspr formed also longer aggregates in remyelinated OSCs.

3.3 Intravenous immunoglobulin (IVIG) inhibits immune-mediated demyelination in OSCs

To investigate the influence of IVIG on the demyelination process, OSCs were treated for 2 days with 5 µg/mL anti-MOG antibody and 6% complement in the presence and absence of different concentrations of IVIG. OSCs which were treated with IVIG during demyelination were protected from immune-mediated demyelination in a dose dependent way **(Figure 9 A+B)**. Incubation with higher concentrations of IVIG (6 & 12 mg/mL) protected more than 80% of the initial GFP^+ area after one day of demyelination. After two days, 58% (±12) and 80% (±13) of the GFP^+ area were protected in OSCs treated with 6 mg/mL or 12 mg/mL IVIG, respectively. In contrast, in OSCs which were not treated with IVIG, the GFP^+ area decreased to 45% (± 6) after one day and to 12% (± 4) after two days of demyelination. Lower concentrations of IVIG (1 & 3 mg/mL) also protected from demyelination, yet to a smaller degree.

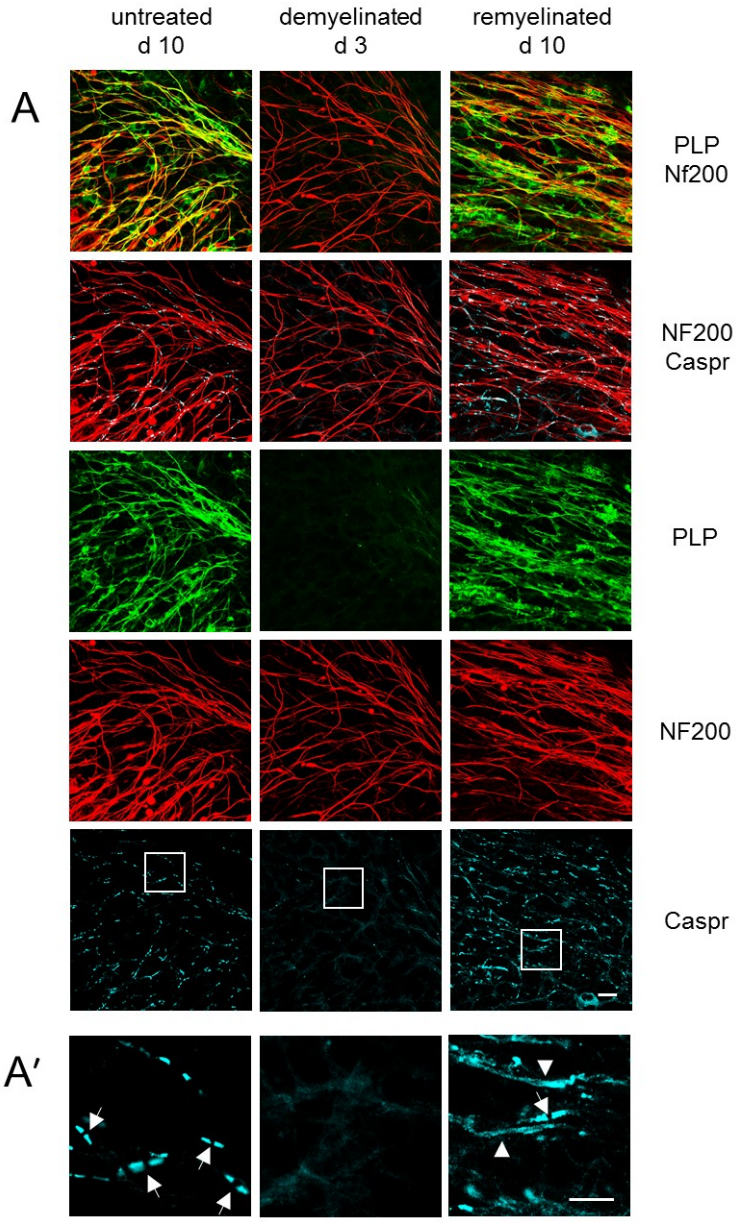

Figure 8. Spontaneous remyelination after immune-mediated demyelination is accompanied by Caspr re-expression.

OSCs were demyelinated for 3 days with 5 µg/mL anti-MOG antibody and 6% complement or left untreated as indicated. After demyelination OSCs were either fixed directly (d 3), or after a 7-day remyelination period (d 10). Fixed OSCs were stained for neurons (NF200) and the paranodal protein Caspr. Immunohistochemical stainings were analyzed by confocal microscopy. **(A)** Representative confocal images: In untreated OSCs, Caspr formed the distinct cylindrical structure of the paranode. After 3 days of demyelination, the myelin sheath was degraded and staining for the paranodal protein Caspr was negative. Seven days later, axons were remyelinated and Caspr was detectable again in paranodal regions. **(A')** Magnification of boxed area: While Capsr formed in untreated OSCs short cylindrical structures (arrows), in remyelinated OSCs also longer aggregates were present (arrowheads).Scale bars **(A)** 20 µm **(A')** 10 µm.

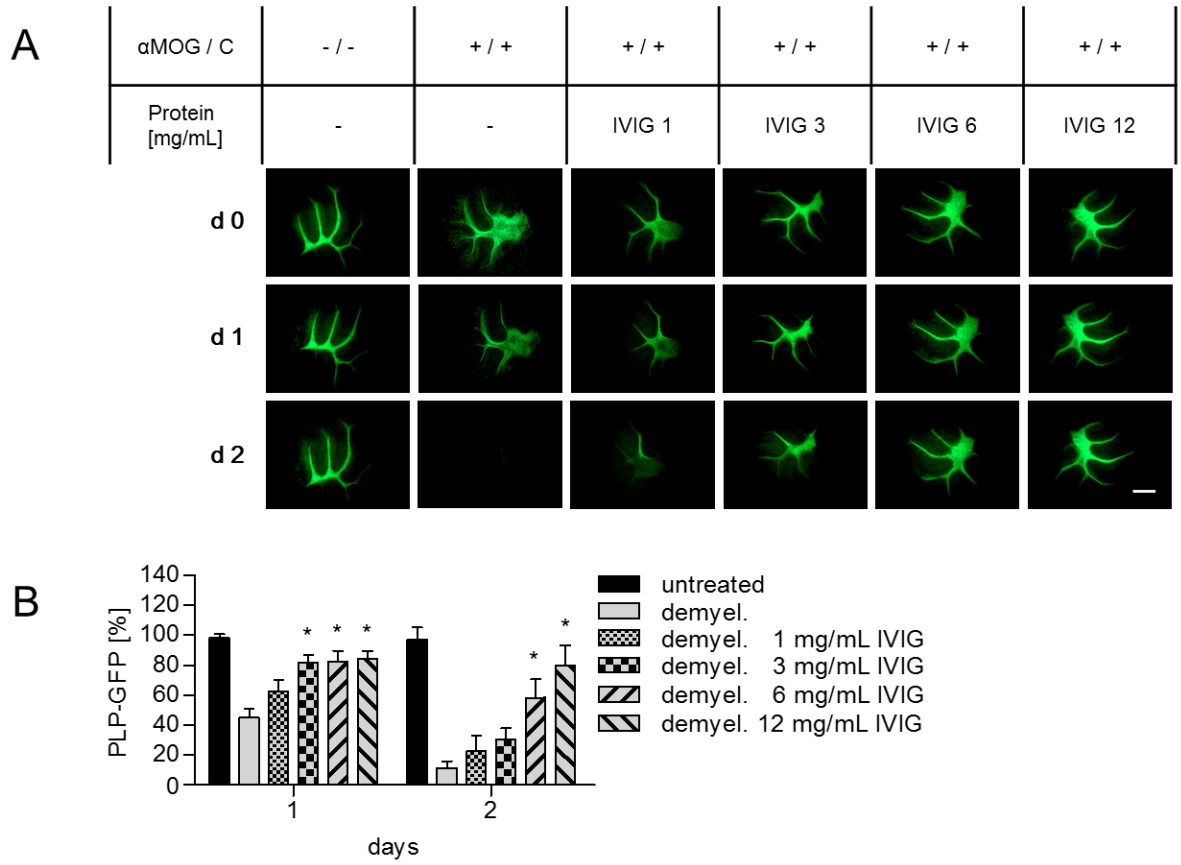

Figure 9. IVIG protects OSC from immune-mediated demyelination.

OSCs were treated as indicated and the GFP^+ area was documented by fluorescence microscopy in living OSCs at day 0, 1 and 2 of the experiment. After 2 days, OSCs were fixed for further immunohistochemical processing. Modified according to Winter et al., 2016 **(A)** Representative images of PLP-GFP expression: Intravenous immunoglobulin (IVIG) inhibited immune-mediated demyelination in a concentration-dependent manner. Scale bar 1 mm. **(B)** Quantification of PLP-GFP expression revealed that IVIG suppressed immune-mediated demyelination in a dose-dependent fashion (n = 6 OSC per group). Significances were calculated in respect to the demyelinated control using one-way analysis of variance and Dunnett's post hoc test. *P ≤ 0.05.

After two days of demyelination, OSCs were fixed and stained immunohistochemically with the neuronal marker NF200. **(Figure 10)**. Fluorescence microscopic images from untreated OSCs show myelinated axons. In contrast, microscopic analysis of demyelinated OSCs revealed that intact axons lost their myelin. In OSCs which were demyelinated in the presence of IVIG, the myelin was protected in a dose dependent way. While fluorescence microscopic images of demyelinated OSCs treated with 1 mg/mL IVIG only show little protection, myelin was increasingly preserved after treatment with 3, 6 and 12 mg/mL of IVIG.

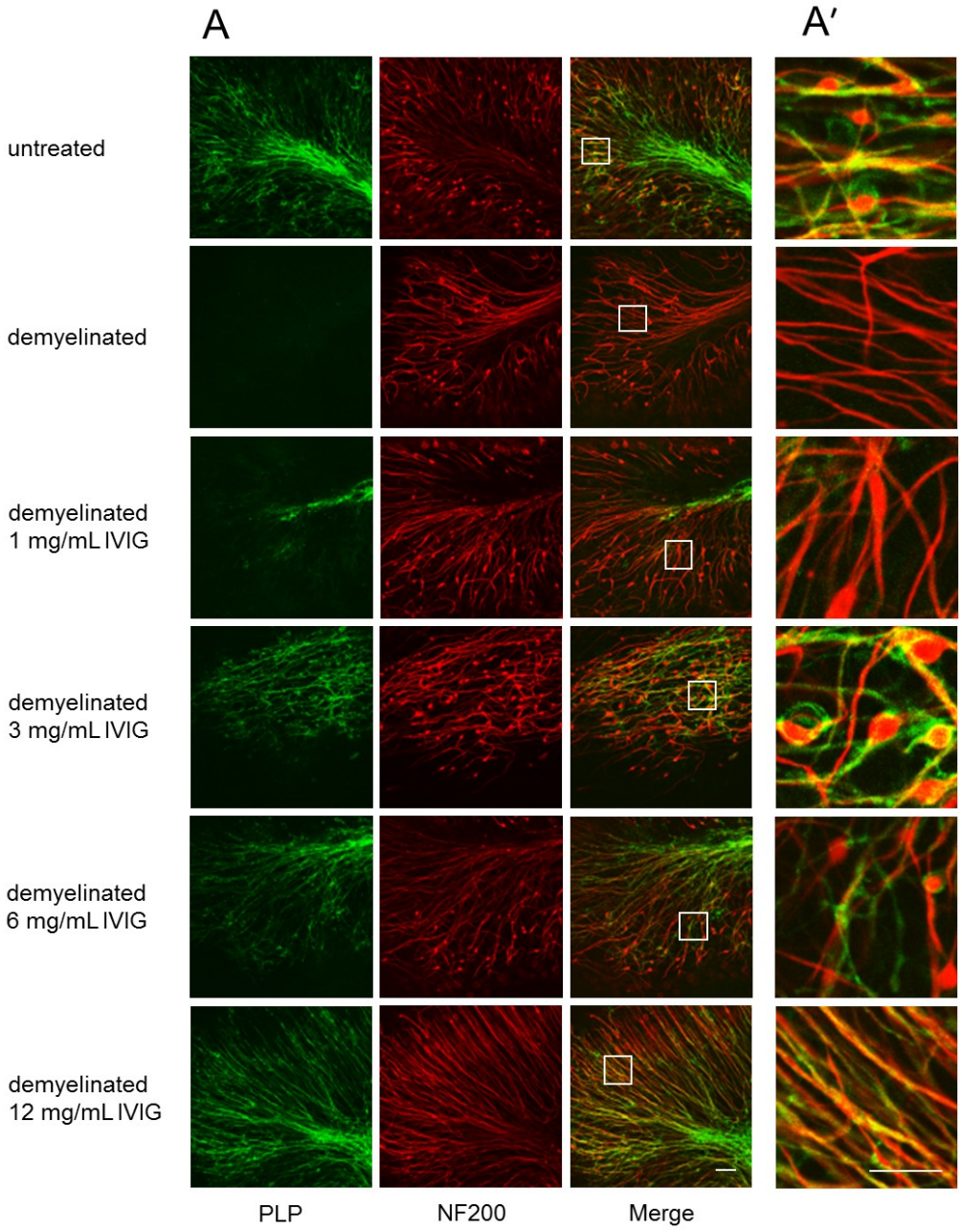

Figure 10. Fluorescence microscopic imaging confirmed that IVIG preserves the myelin sheath from immune-mediated demyelination.

OSC were treated as indicated, fixed after 2 days, stained for neurons (NF200) and analyzed via fluorescence microscopy. From Winter et al., 2016. **(A)** Representative microscopic images: IVIG protects the myelin sheath around axons in a dose dependent fashion. **(A')** Magnification of boxed area. Scale bars **(A)** 50 µm **(A')** 25 µm.

To verify that the solvent of IVIG as well as irrelevant bovine and human proteins do not protect OSCs from demyelination, OSCs were incubated with complement in combination with HBSS, BSA or HSA. The results of these experiments show that neither HBSS nor the protein controls protected from immune-mediated demyelination **(Figure 11)**.

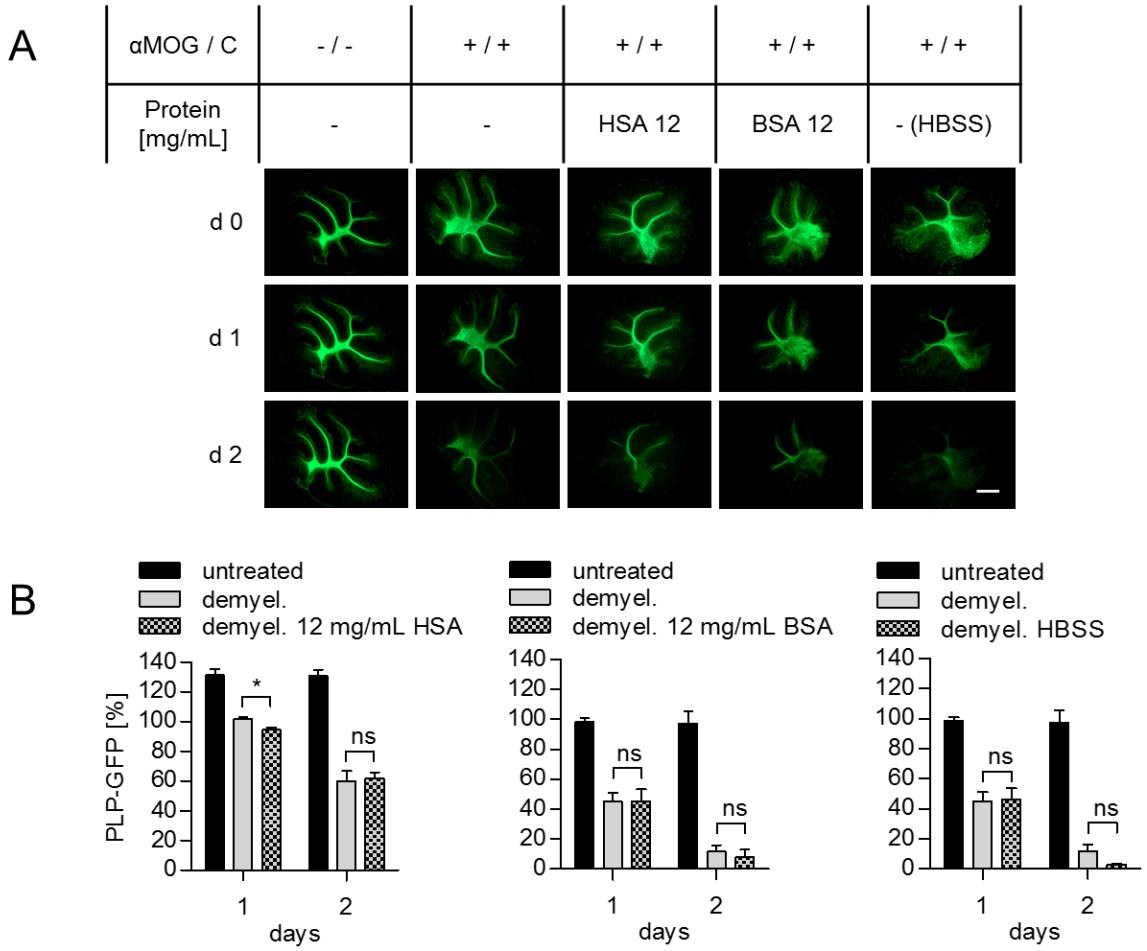

Figure 11. Control proteins or the solvent control do not protect from immune-mediated demyelination.

OSC were treated as indicated and the GFP$^+$ area was documented by fluorescence microscopy in living OSC at day 0, 1 and 2 of the experiment. Modified from Winter et al., 2016. **(A)** Representative images of PLP-GFP expression. Neither the addition of human serum albumin (HSA) nor the presence of bovine serum albumin (BSA) or the solvent control HBSS did inhibit demyelination. Scale bar 1 mm. **(B)** Quantification of PLP-GFP expression confirmed that the irrelevant proteins HSA and BSA, as well as HBSS did not suppress demyelination (n = 4-6 OSC per group). Significances between the demyelinated condition and the condition which was demyelinated in the presence of HSA, BSA or HBSS were calculated with the student's t-test. Control bars were included for better comparability. *P ≤ 0.05.

IVIG is a mixture of immunoglobulins from thousands of healthy donors. To ensure that the drug itself does not contain antibodies against oligodendrocytes/myelin, which might influence demyelination experiments via antibody dependent cellular cytotoxicity (ADCC) or complement dependent cytotoxicity (CDC), OSCs were incubated with 6 mg/mL IVIG in the presence or absence of complement. To prove that complement alone does not induce demyelination, OSCs were also incubated with complement only. As a result, neither the treatment with IVIG alone nor the addition of IVIG together with complement resulted in a significant reduction of the GFP$^+$ area of OSCs **(Figure 12)**. Also the incubation of OSCs with complement did not decrease the GFP$^+$ area significantly.

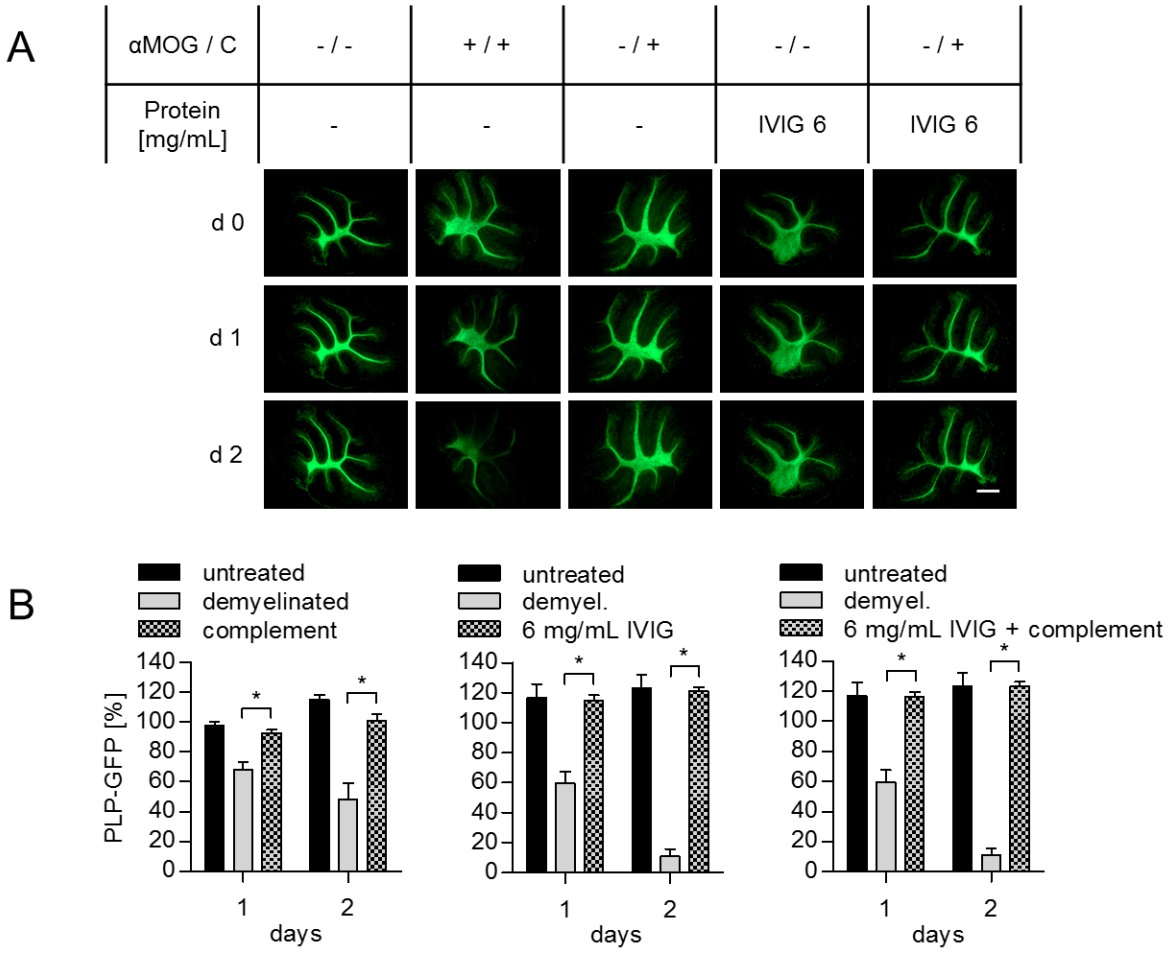

Figure 12. Complement and/or IVIG do not induce immune-mediated demyelination.
OSCs were treated as indicated and the GFP^+ area was documented by fluorescence microscopy in living OSC at day 0, 1 and 2 of the experiment. Modified according to Winter et al., 2016. **(A)** Representative images of PLP-GFP expression. The addition of complement, IVIG or complement and IVIG did not induce immune-mediated demyelination. Scale bar 1 mm. **(B)** Quantification of PLP-GFP expression confirmed that OSC treated with complement, IVIG, or complement and IVIG did not lead to demyelination (n = 6-8 OSC per group). Significances between the demyelinated condition and the condition which was treated with complement, IVIG, or complement and IVIG were calculated with the student's t-test. Control bars were included for better comparability. *P ≤ 0.05.

3.4 IVIG-mediated protection of oligodendrocytes in demyelinated OSC is reflected at the level of gene expression

The GFP expression under regulatory elements of the PLP gene allows the monitoring of the myelination grade on protein level. To investigate whether the protective effect of IVIG can be confirmed on mRNA level, OSCs were demyelinated in the presence or absence of 6 mg/mL IVIG. One and two days after demyelination, RNA was isolated from single OSCs, transcribed into cDNA and quantitative real-time PCR was performed. As an irrelevant protein control, OSCs were incubated with 6% complement and 6 mg/mL BSA. From

BSA treated OSCs RNA was isolated at day two only. To observe demyelination on the level of gene expression, the genes for myelin basic protein (MBP) and 2',3'-Cyclic-nucleotide 3'-phosphodiesterase (CNPase) were analysed **(Figure 13)**. Quantification of myelin gene expression revealed that demyelination as well as its protection by IVIG is mirrored on the level of gene expression: The mRNA expression of MBP was downregulated following demyelination. One day of demyelination resulted in 0.20-fold (± 0.04) mRNA expression and after two days, the expression was reduced to 0.15-fold (± 0.06). In OSCs which were treated with IVIG during demyelination, the expression of the MBP gene was less reduced then in the demyelinated condition (day 1: 0.41-fold ± 0.07; day 2: 0.36-fold ± 0.06).The difference between the two groups reached statistical significane at day 1. CNPase gene expression resembled the gene expression of MBP. After one day of demyelination, it was reduced to 0.28-fold (± 0.05). After the second day, CNPase gene expression was 0.31 fold (± 0.06). IVIG treatment led to a significant higher mRNA level at the first day of demyelination (0.49-fold ± 0.04). From the first to the second day of demyelination, the copy number was reduced to 0.43-fold (± 0.01) expression. Neither gene expression of the neuronal cytoskeleton subunit protein NF200, nor the expression of the oligodendrocyte precursor marker neuron-glial antigen 2 (Ng2) was significantly affected by demyelination or demyelination with IVIG treatment. To investigate the influence of demyelination and additional treatment with IVIG on microglia, the gene expression of Iba1 (Ionized calcium-binding adapter molecule 1) was analyzed. One day after demyelination, the Iba1 gene was down regulated to 0.17 fold (± 0.04) expression and stayed at that level until the second day of demyelination (0.15 fold ± 0.03). In OSCs, which were treated additionally with IVIG, down regulation of Iba1 mRNA was partly prevented (day 1: 38-fold ± 0.09; day 2: 0.40-fold ±0.1). Differences in mRNA expression between the demyelinated and the IVIG treated group did not reach statistical significance. The addition of BSA during demyelination of OSCs did not lead to a statistically significant change in the gene expression of the investigated genes.

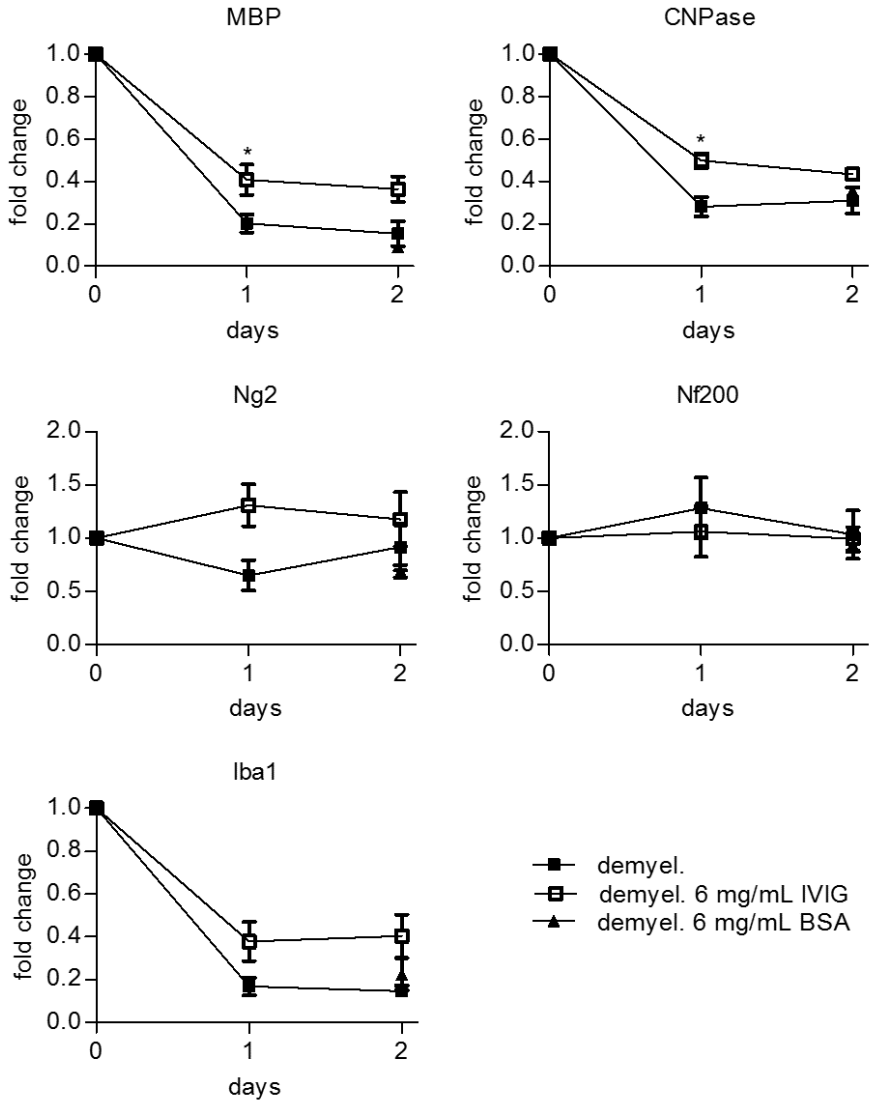

Figure 13. Analysis of gene expression confirms IVIG-induced protection of oligodendrocytes in demyelinated OSC.

OSC were demyelinated (closed squares), with and without 6 mg/mL IVIG (open squares) or 6 mg/mL BSA (triangles) or were left untreated. Gene expression was measured at day 1 and 2 day of the experiment by quantitative rtPCR. Values for BSA controls were assessed for day 2 only. The expression of indicated genes was normalized to GAPDH, relative to the untreated control. Gene expression of neuronal (NF200) and oligodendrocyte progenitor cell (Ng2) markers is hardly affected by demyelination +/- IVIG. In contrast, IVIG treatment protects against demyelination-induced reduction in gene expression of myelin (MBP, CNPase) and microglial (Iba1) gene expression (n = 3-6 OSC per group). Significances were calculated with the student's t-test. From Winter et al., 2016.

3.5 IVIG prevents immune-mediated oligodendrocyte death in anti-MOG antibody and complement-treated OSCs

To quantify the protective effect of IVIG more precisely, oligodendrocyte and microglia survival were investigated by flow cytometry **(Figure 14)**. Therefore, OSCs were demyelinated in the presence and absence of IVIG or BSA and dissociated enzymatically after one or two days of treatment. Single cell suspensions were stained with the microglia marker "cluster of differentiation molecule 11B" (CD11b) and with a viability dye (Fixable Viability Dye eFluor 450). Cells were fixed with 4% PFA and analysed by flow cytometry. GFP^+ cells not stained with viability dye were counted as "living oligodendrocytes". CD11b-positive cells not stained with viability dye were quantified as "living microglia". "Living oligodendrocytes" and "living microglia" were expressed in percent of all gated and living cells. In untreated OSCs, the percentage of living oligodendrocytes remained stable over the duration of the experiment (day 1: 41% ± 4; day 2: 44% ±3). In demyelinated OSCs, the percentage of living oligodendrocytes fell to 34% (± 4) at the first day and was significantly reduced to 16% (±5) at the second day of demyelination. The percentage of living oligodendrocytes in the BSA treated condition was significantly reduced to 25% (± 2) the first day and to 7 % (± 2) the second day after treatment. OSCs, which were treated with IVIG, did not lose living oligodendrocytes after one day of demyelination (41 % ±5). After two days of IVIG accompanied demyelination, the percentage of living oligodendrocytes was reduced to 29% (± 8). About 3-6% of the living cells were microglia. Their viability was not significantly affected by the demyelination with or without IVIG or BSA.

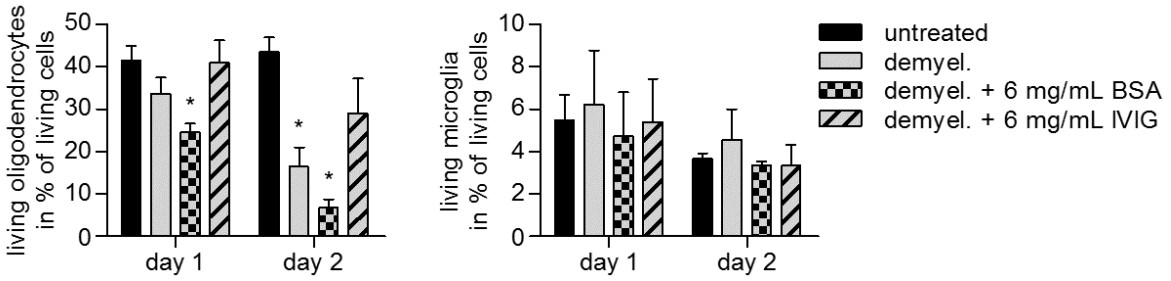

Figure 14. IVIG reduces oligodendrocyte death in OSC during immune-mediated demyelination.
OSCs were demyelinated with or without 6 mg/mL IVIG or 6 mg/mL BSA or were left untreated as indicated. After 1 and 2 days of demyelination, single cell suspensions of 4 OSC per condition were stained for viability (eFluor 450) and microglia (CD11b), fixed and analyzed by flow cytometry (oligodendrocytes n = 4, microglia n = 3). GFP^+ cells not stained for eFluor 450 were counted as "living oligodendrocytes". CD11b positive cells not stained by eFluor 450 were counted as "living microglia". Living oligodendrocytes and living microglia were expressed in percent of all living and gated cells. While demyelination with or without BSA significantly reduced the percentage of living oligodendrocytes, IVIG treatment protected oligodendrocytes significantly from dying. The viability of microglia was not significantly influenced by any treatment. Significances were calculated in respect to the untreated control using one-way analysis of variance and Dunnett's post hoc test. *P ≤ 0.05. From Winter et al., 2016.

3.6 IVIG protects the paranodal integrity during immune-mediated demyelination

In view of the knowledge that IVIG protects myelin in OSCs from immune-mediated demyelination by preventing oligodendrocytes from dying, it should be clarified whether the paranode as an essential element for the functionality of myelin is also preserved through IVIG treatment. Therefore, OSCs were demyelinated in the presence or absence of 6 mg/mL IVIG and subsequently stained for neurons and the paranodal protein Caspr. Confocal analysis of immunohistochemistry revealed that Caspr staining was reduced in IVIG-treated OSCs but still detectable in some parts. Caspr staining was absent in OSCs which were demyelinated in the absence of IVIG **(Figure 15)**.

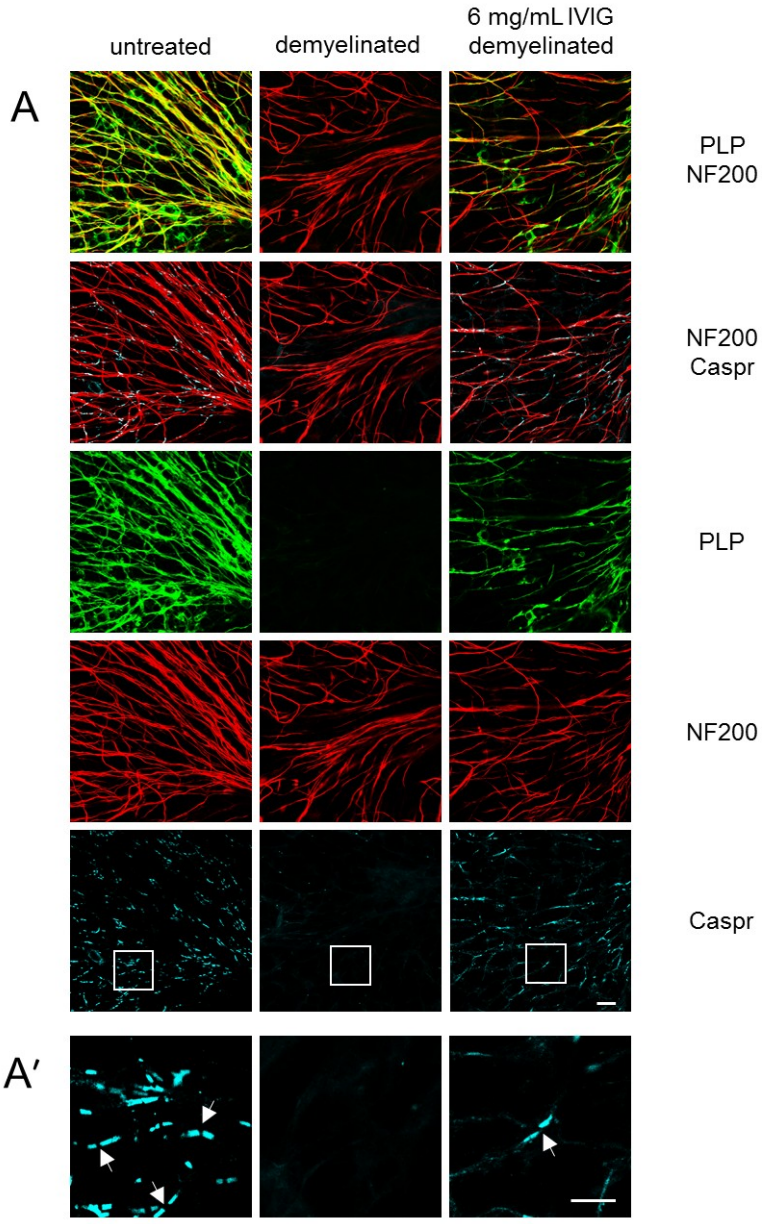

Figure 15. IVIG protects the paranodal integrity during immune-mediated demyelination.
OSCs were demyelinated for 3 days with 5 µg/mL anti-MOG antibody and 6% complement with or without 6 mg/mL IVIG, or left untreated as indicated. After demyelination, OSCs were fixed and stained for neurons (NF200) and the paranodal protein Caspr. Immunohistochemical stainings were analyzed by confocal microscopy. **(A)** Representative confocal images: In untreated OSCs, myelinated axons and intact paranodes were indicated by colocalization of PLP and NF200 as well as Caspr staining. While myelin and paranodes were absent in demyelinated OSCs the additional treatment with IVIG partly protected both structures. **(A')** Magnification of boxed area: Caspr formed the distinct cylindrical structure of the paranode (arrows). Scale bars **(A)** 20 µm **(A')** 10 µm.

3.7 IVIG-mediated inhibition of demyelination is independent of the anti-MOG-antibody concentration

To reveal whether the protective effect of IVIG is caused by its interaction with the anti-MOG antibody, OSCs were demyelinated with increasing concentrations of anti-MOG antibody, hypothesizing that this would overrule the IVIG-mediated protection. To test this assumption OSCs were demyelinated with 5, 20 and 40 µg/mL of anti-MOG antibody while the complement concentration was kept constant at 6%. The GFP^+ area was quantified after one, two and three days of treatment. In demyelinated OSCs it decreased irrespective of the used anti-MOG concentration **(Figure 16)**. Three days of treatment with 5, 20 and 40 µg/mL of anti-MOG antibody resulted in a GFP^+ area of 37% (± 5), 20% (± 1) and 28% (± 7), respectively. In contrast, OSCs were mostly spared from myelin loss in all IVIG-treated conditions. After three days, the quantification resulted in GFP^+ area of 64% (± 9), 72% (± 4) and 79% (± 8) in OSCs treated with 5, 20 and 40 µg/mL, respectively.

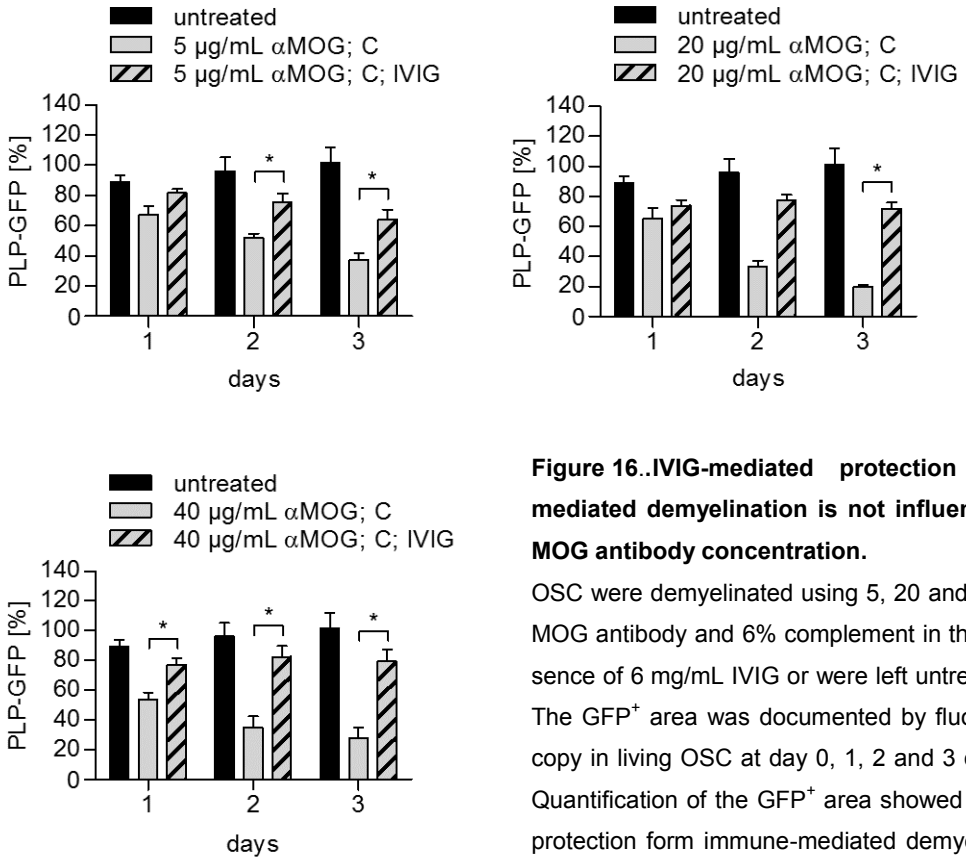

Figure 16..IVIG-mediated protection from immune-mediated demyelination is not influenced by the anti-MOG antibody concentration.

OSC were demyelinated using 5, 20 and 40 µg/mL of anti-MOG antibody and 6% complement in the presence or absence of 6 mg/mL IVIG or were left untreated as indicated. The GFP^+ area was documented by fluorescence microscopy in living OSC at day 0, 1, 2 and 3 of the experiment. Quantification of the GFP^+ area showed that IVIG-induced protection form immune-mediated demyelination is not influenced by increasing concentrations of the anti-MOG antibody (n = 4–6 OSC per group). Significances between the demyelinated condition with and without IVIG were calculated using the student's t-test. Control bars were included for better comparability. *P ≤ 0.05. Modified according to Winter et al., 2016.

After three days of demyelination, OSCs were fixed, stained for NF200 and analysed by fluorescence microscopy. The staining confirmed that myelin of IVIG treated OSCs is preserved at all concentrations of anti-MOG antibody **(Figure 17)**. In contrast, fluorescence microscopy of OSCs demyelinated without IVIG revealed myelin loss in all investigated concentrations of anti-MOG antibody.

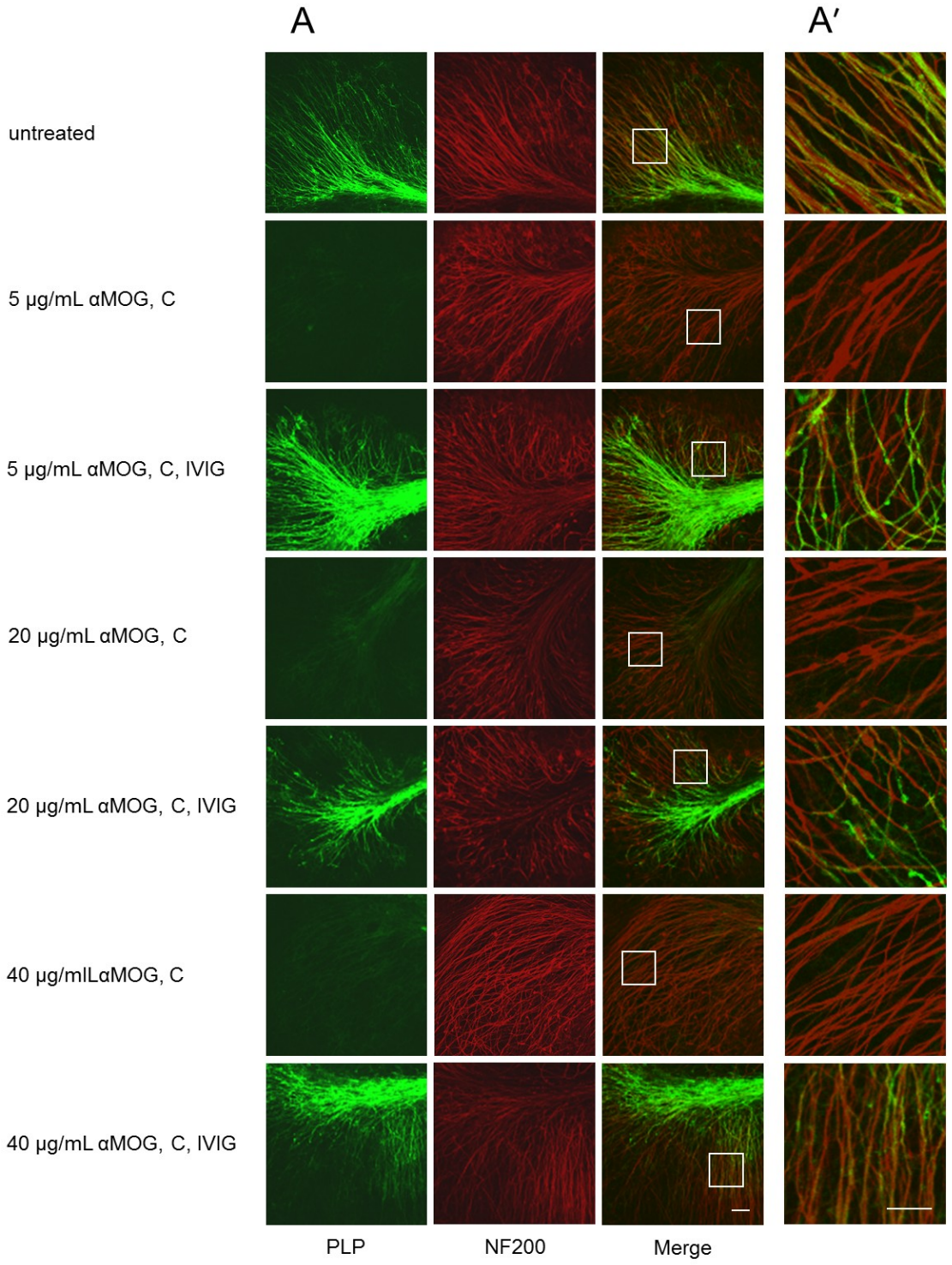

Figure 17. IVIG-induced myelin sheath protection is not dependent on the concentration of anti-MOG.

Figure 17: OSCs were treated as indicated, fixed after 3 days, stained for neurons (NF200) and analyzed via confocal microscopy. From Winter et al., 2016. **(A)** Representative microscopic images illustrate that 6 mg/mL IVIG preserved the integrity of myelin sheaths around axons at all concentrations of the anti-MOG antibody. **(A')** Magnification of boxed area. Scale bars **(A)** 50 µm, **(A')** 25 µm.

3.8 IVIG does not neutralize the binding of anti-MOG antibody

Moreover, it was investigated if IVIG prevents demyelination by binding to the myelin and by blocking the binding sites of the anti-MOG antibody. Therefore, OSCs were preincubated with 6 and 12 mg/mL IVIG or 12 mg/mL BSA for three days, fixed with 4% PFA and stained immunhistochemically with biotinylated anti-MOG antibody and Streptavidin Alexa Fluor®594. Pictures of PLP-GFP fluorescence and anti-MOG staining revealed that neither preincubation with BSA nor with IVIG reduced binding of the biotinylated anti-MOG antibody **(Figure 18)**.

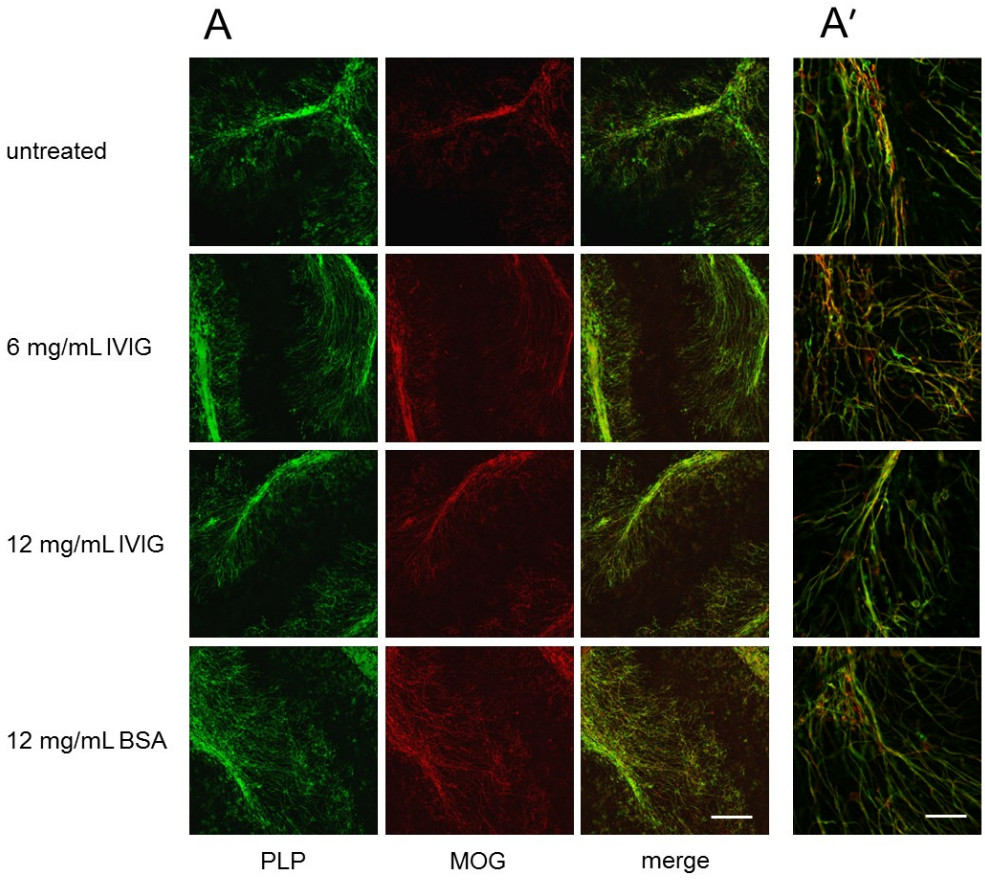

Figure 18. IVIG does not compete with the binding of anti-MOG antibody during demyelination.
OSCs were pretreated with or without IVIG or BSA for 3 days before fixation. Subsequently OSCs were stained with a biotinylated anti-MOG antibody. Confocal pictures illustrate that the anti-MOG antibody bound strongly to myelin irrespective of pretreatment with IVIG or BSA. Scale bars **(A)** 100 µm, **(A')** 50 µm. From Winter et al., 2016.

3.9 IVIG-mediated protection is overruled by rising complement concentrations

In order to determine whether IVIG prevents demyelination by interfering with complement deposition and/or activation, varying concentrations of complement were used for immune-mediated demyelination. The standard complement concentration of 6% was lowered to 3% and raised to 9% and 12%. Anti-MOG antibody concentration was kept constant at 5 µg/mL and IVIG was applied in the standard concentration of 6 mg/mL. While a complement concentration of 3% did not result in a considerable demyelination (GFP^+ area of 94% after three days), increasing complement concentrations led to extended demyelination **(Figure 19)**. In detail, three days of treatment with anti-MOG antibody together with 6%, 9% and 12% complement resulted in a GFP^+ area of 27% (± 6), 6% (± 2) and 5% (± 2) respectively. While IVIG significantly protected the demyelination induced with 6% complement at all investigated time points, the immunoglobulin was not able to maintain the same level of protection in OSCs demyelinated with 9% and 12% complement. In quantitative terms demyelination with 6%, 9% and 12% of complement together with anti-MOG antibody and IVIG resulted after three days in a GFP^+ area of 73% (± 6); 19% (± 4) and 16% (± 7).

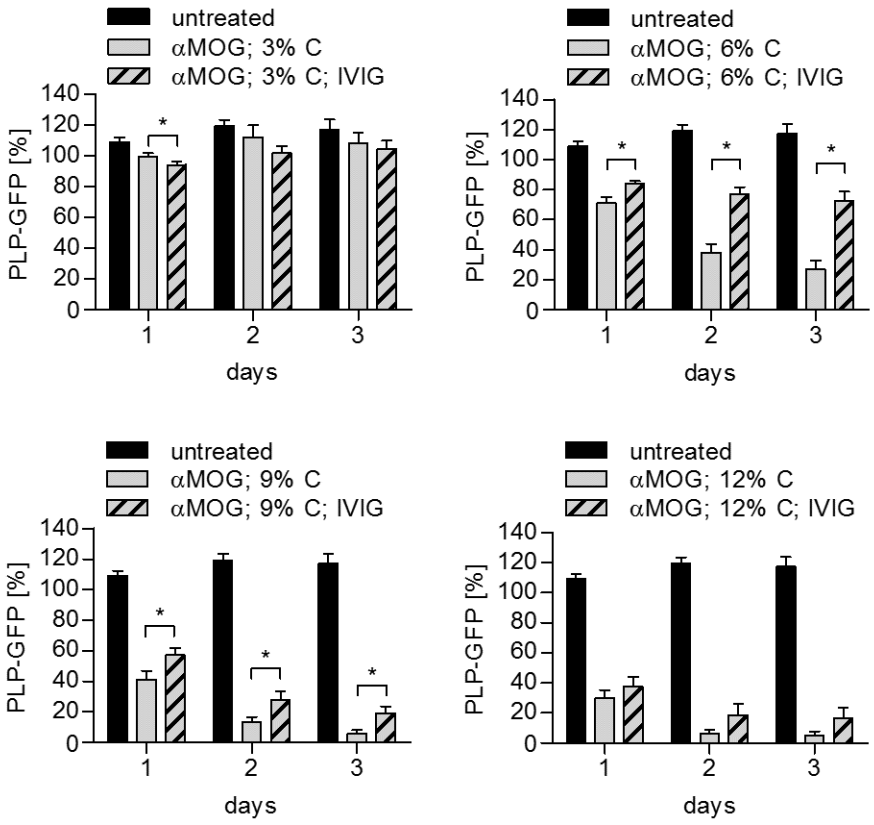

Figure 19. IVIG-mediated protection from demyelination is overruled by rising concentrations of complement.
OSCs were demyelinated using different concentrations of complement (3%, 6%, 9% and 12%) and 5 µg/mL anti-MOG antibody in the presence or absence of 6 mg/mL IVIG or were left untreated as indicated. The GFP^+ area was documented by fluorescence microscopy in living OSC at day 0, 1, 2 and 3 of the experiment. Quantification of PLP-GFP expression revealed that with increasing concentrations of complement, IVIG loses its protective effect (n = 10-12 OSC per group). Significances between the demyelinated condition with and without IVIG were calculated using the student's t-test. Control bars were included for better comparability. *P ≤ 0.05. Modified according to Winter et al., 2016.

After three days of treatment, OSCs were fixed, stained for neurons (NF200) and analysed by confocal microscopy. Immunohistochemical staining confirmed that rising complement concentration overrule the protection of IVIG in a dose dependent way **(Figure 20)**. Confocal images of OSCs demyelinated with 3 and 6% complement, reveal that axons were protected from immune-mediated demyelination by IVIG. In contrast, confocal images of OSCs demyelinated with 9 and 12% complement, do not show any IVIG-mediated protection from demyelination.

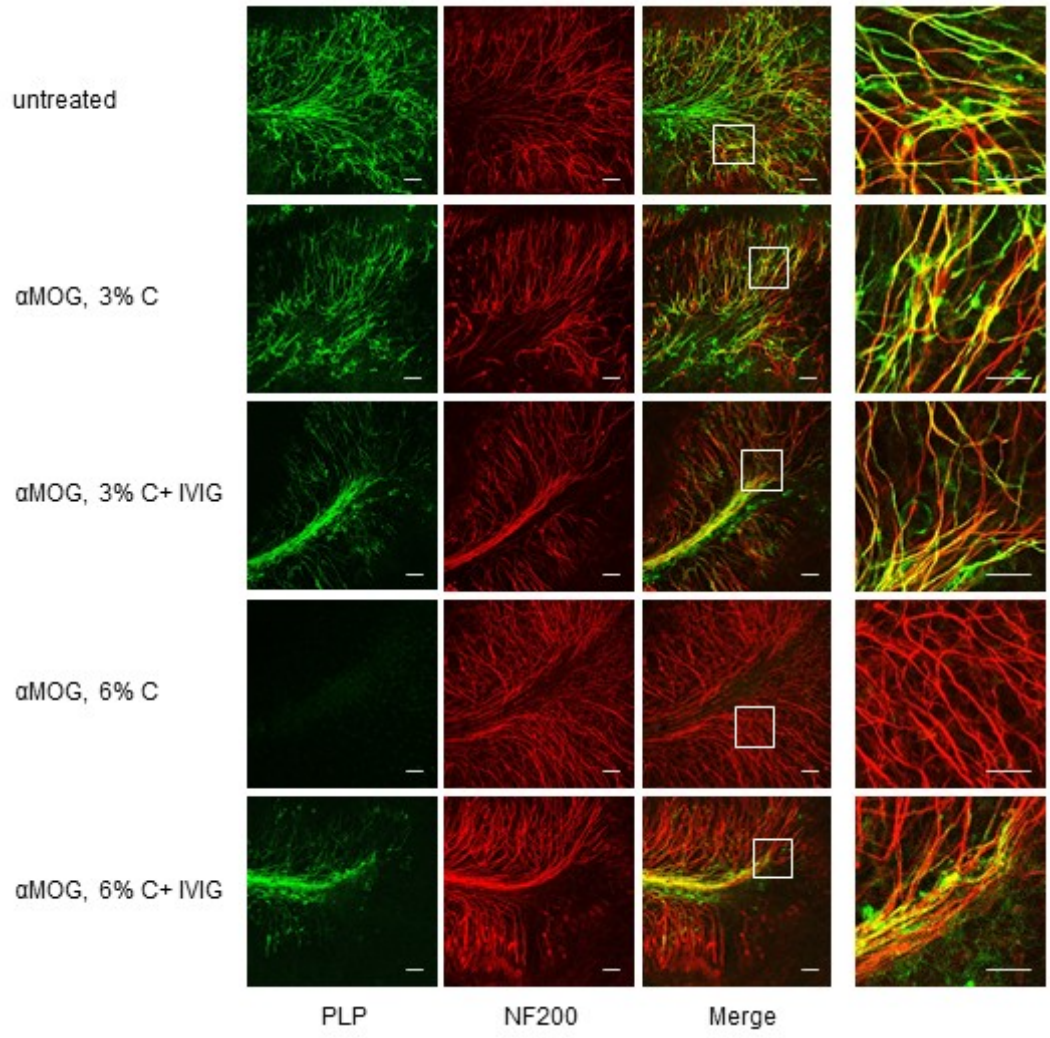

Figure 20.

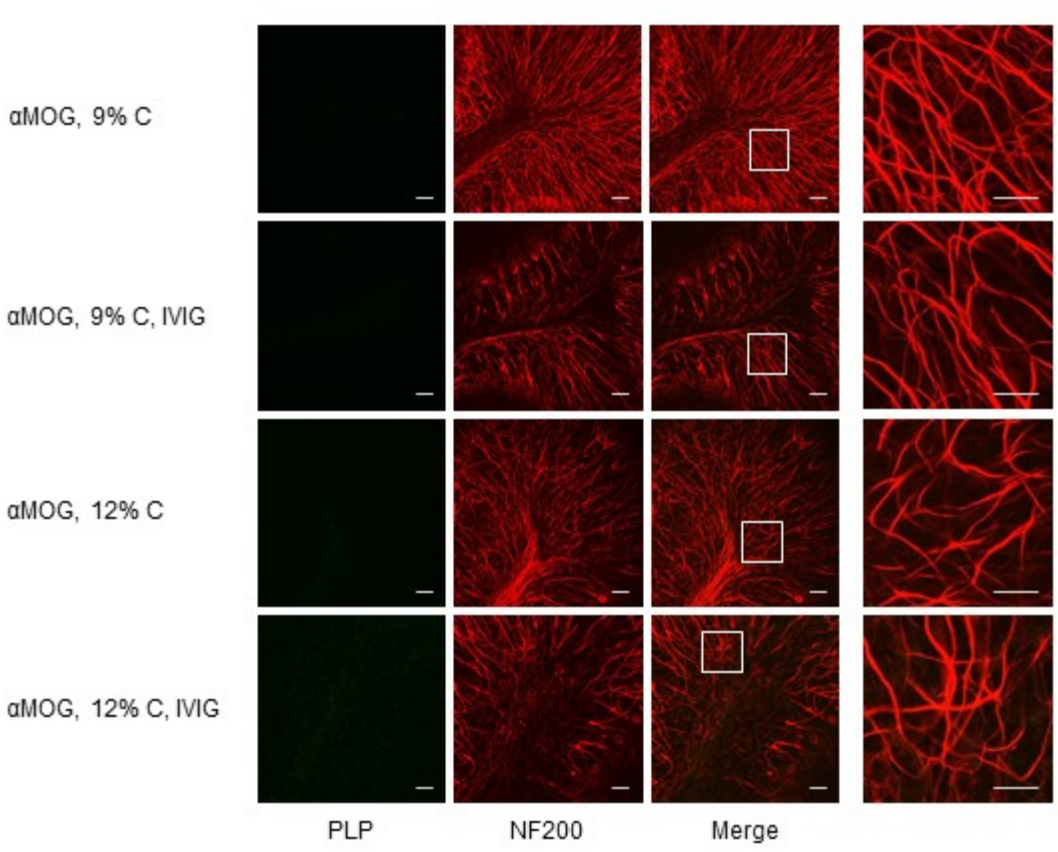

Figure 20. IVIG-induced myelin sheath protection is overruled by increasing complement concentrations.

OSC were treated as indicated, fixed after 3 days, stained for neurons (NF200) and analyzed via confocal microscopy. **(A)** Representative microscopic images illustrate that at complement concentrations above 6%, IVIG does not protect the myelin sheath from demyelination. **(A')** Magnification of boxed area. Scale bars **(B)** 50 µm, **(B')** 25 µm.

3.10 IVIG-mediated inhibition of demyelination is not mediated by Ig-variable regions

To investigate which part of IVIG mediates the protective properties, OSCs were demyelinated only with the antigen-binding Fab fragments of IVIG. Fab fragments were derived by cleavage of IVIG with papain, immobilisation of Fc fragments by Protein A and subsequent elution of Fab fragments. **Figure 21A** shows a SDS gel loaded with Fab fragments or whole IVIG in native or denatured condition. The first lane depicts denatured IVIG. The most prominent bands are located at 25 and 50 kDa, representing the heavy and the light chain of the immunoglobulins. Weak bands at 150 and 100 kDa visualize a small amount of native or partly denatured immunoglobulins. The second lane shows denatured Fab fragments, which have the size of 25 kDa. The native IVIG is represented by the 150 kDa band in the third lane. Lane four depicts native Fab fragments which have a size of 50 kDa. The 25 kDa band shows that some of the Fab fragment was already denatured.

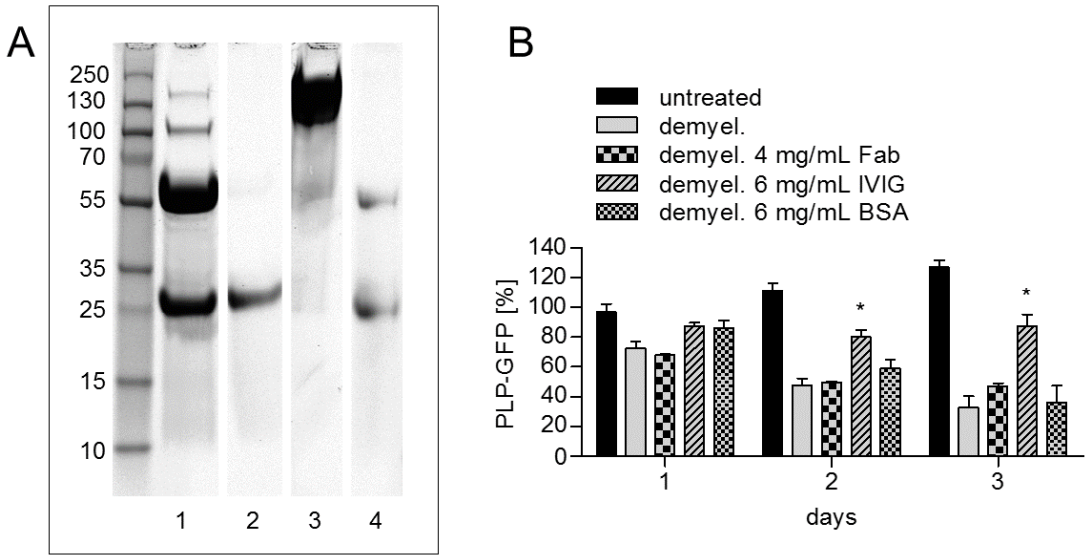

Figure 21. The Fab fragment is not responsible for IVIG-mediated inhibition of demyelination.
IgG-variable regions (Fab) were cleaved from whole IVIG by papain. From Winter et al., 2016. **(A)** To prove the purity of the Fab preparation, the Fab fragments as well as IVIG were separated by SDS-PAGE. 1 = denatured IVIG; 2 = denatured Fab; 3 = native IVIG; 4 = native Fab. **(B)** OSCs were demyelinated with or without 6 mg/mL IVIG, 4 mg/mL Fab fragment or 6 mg/mL BSA or were left untreated as indicated. The GFP^+ area was documented by fluorescence microscopy in living OSC at day 0, 1, 2 and 3 of the experiment. Quantification of PLP-GFP expression revealed that IVIG but not Fab fragments or BSA inhibit immune-mediated demyelination (n = 3 OSCs per group). Significances were calculated in respect to the demyelinated control using one-way analysis of variance and Dunnett's post hoc test. *P ≤ 0.05.

For the experiment, OSCs were demyelinated with 6% complement und 5 µg/mL anti-MOG antibody with or without 6 mg/mL IVIG or the equimolar amount of Fab fragment (4 mg/mL). As irrelevant protein control, OSCs were demyelinated in the presence of 6 mg/mL BSA. As shown in the previous experiments, IVIG significantly inhibited demyelination **(Figure 21B)**. In this experiment, three days of IVIG treatment resulted in a GFP^+ area of 87% (± 8). In contrast, exposure to Fab fragments did not protect from demyelination, as PLP-GFP expression fell down to 47% (± 2) after three days. Equally, PLP-GFP expression of OSCs which were demyelinated in the presence or absence of BSA decreased to 36% (± 11) and 33% (± 8), respectively. After three days of treatment, OSCs were fixed, stained with an antibody for NF200 and analysed via laser scanning microscopy. Microscopic images confirm the quantitative evaluation since myelin was only protected in IVIG treated OSCs and not in those which were demyelinated with and without Fab fragments or BSA **(Figure 22)**.

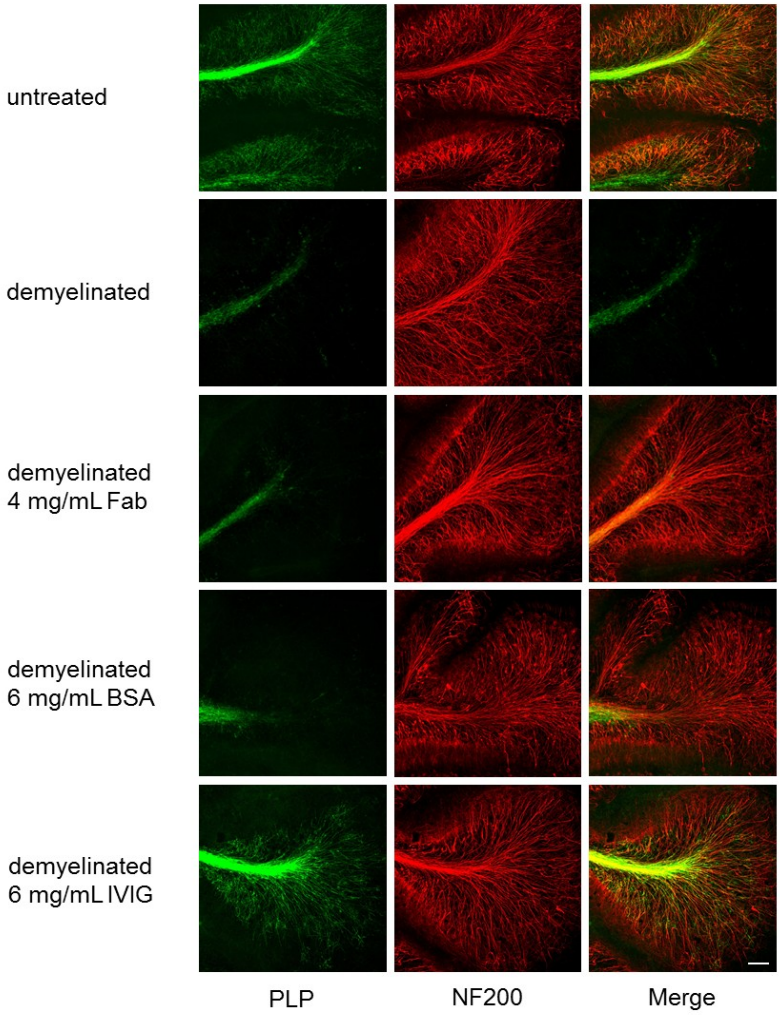

Figure 22. Fab fragment does not preserve axons from demyelination.
OSC were treated as indicated, fixed after 3 days, stained for neurons (NF200) and analyzed via laser scanning microscopy. Representative microscopic images reveal that IVIG but not Fab or BSA protect axons from immune-mediated demyelination. Scale bar 50 µm. Modified according to Winter et al., 2016.

3.11 Myelin protection by IVIG depends on the Fc and, not the Fab fragment

In further experiments, the effect of Fc fragments on demyelination was investigated. For this purpose, during demyelination, OSCs were incubated with 6 mg/mL IVIG in comparison to 2 and 1 mg/mL human Fc fragments (huFc) derived from a polyclonal preparation of human immunoglobulin. The concentrations of Fc fragments corresponded to the equimolar and half of the equimolar amount of 6mg/mL IVIG. Incubation of OSCs with 1 mg/mL of Fc fragments during demyelination resulted in myelin protection comparable to those achieved by 6 mg/mL of IVIG **(Figure 23)**. Incubation of OSCs with 2 mg/mL Fc fragment during demyelination showed an even better myelin protection than with 6 mg/mL IVIG. In numbers, GFP^+ area of OSCs demyelinated with and without BSA fell down to 25% (± 2) and 13% (± 5) after three days, respectively. OSCs treated with IVIG

expressed after three days 58% (± 6) GFP and OSCs incubated with 1 and 2 mg/mL Fc fragment reached a PLP-GFP expression of 59.0% (± 6) and 85% (± 2), respectively.

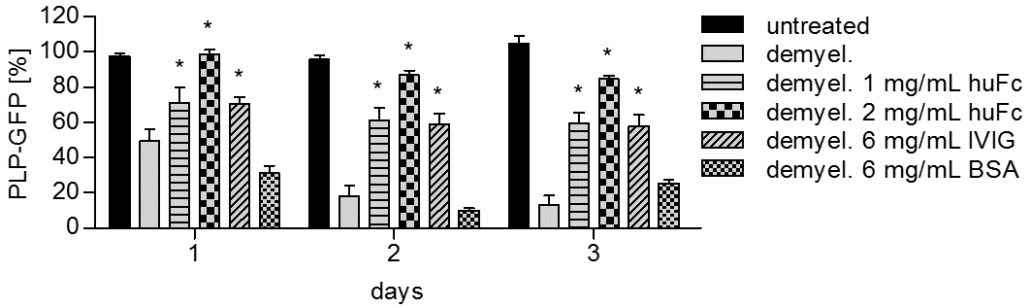

Figure 23. IVIG-induced protection from demyelination is Fc-mediated.

OSCs were demyelinated with or without 6 mg/mL IVIG, 6 mg/mL BSA or 1 and 2 mg/mL human polyclonal Fc fragment or were left untreated as indicated. GFP^+ area was documented by fluorescence microscopy in living OSCs at day 0, 1, 2 and 3 of the experiment. Quantification of the PLP-GFP expression revealed that Fc fragments inhibit demyelination even stronger than whole IVIG at the equimolar concentration of 2 mg/mL (n = 4-13 OSCs per group). Significances were calculated in respect to the demyelinated control using one-way analysis of variance and Dunnett's post hoc test. *P ≤ 0.05. Modified from Winter et al., 2016.

After three days of treatment, OSCs were fixed, stained for neurons (NF200) and analysed by confocal microscopy. Immunohistochemical staining confirmed that 1 and 2 mg/mL Fc fragment, as well as 6 mg/mL IVIG protect axons from demyelination **(Figure 24)**. In contrast, myelin was not protected in OSCs demyelinated with or without 6 mg/mL BSA.

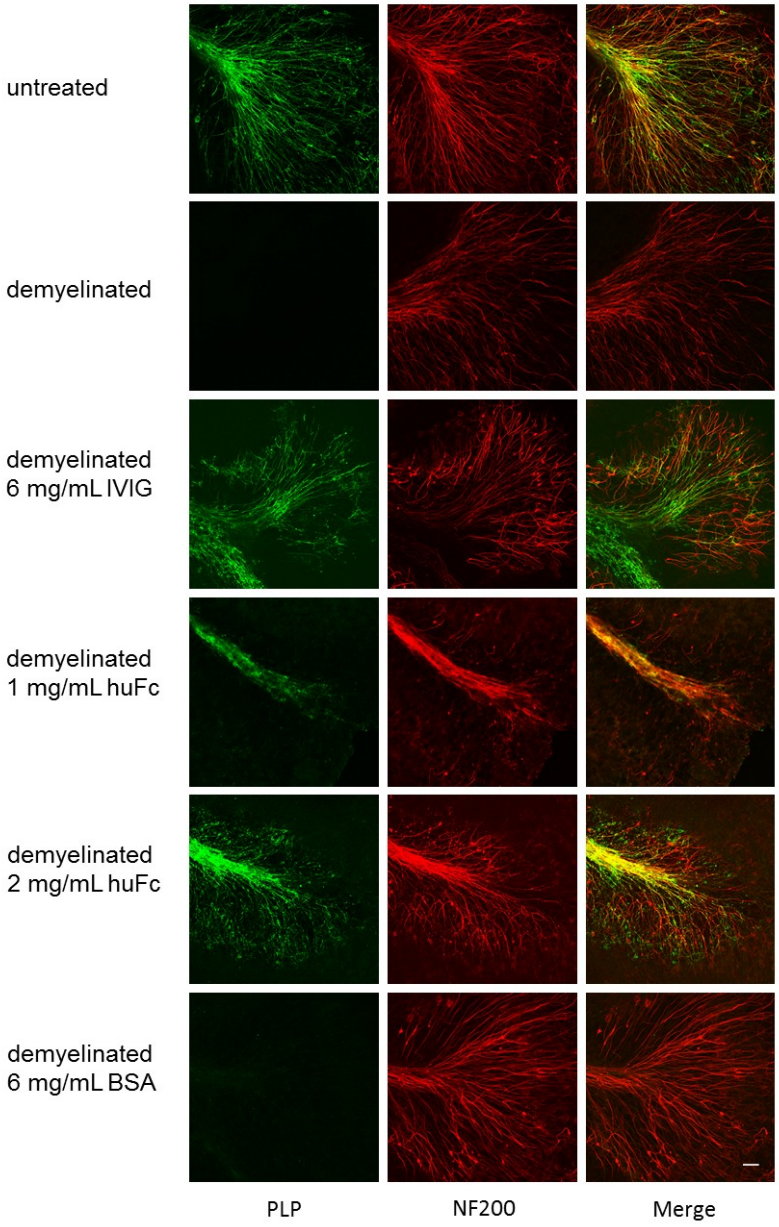

Figure 24. Fc fragments protect axons from demyelination.

OSC were treated as indicated, fixed after 3 days, stained for neurons (NF200) and analyzed via confocal microscopy. Representative microscopic images illustrate that Fc fragments and IVIG but not BSA prevent axons from immune-mediated demyelination. Scale bar 50 µm. Modified according to Winter et al., 2016.

3.12 IVIG-mediated protection seems to depend on specific modifications of the Fc terminus or the composition of isotypes

Since previous experiments showed that the protection of IVIG is mediated through the constant Fc fragment and not through the variable Fab fragment, the question was raised whether a monoclonal immunoglobulin would also prevent demyelination. To answer this question, OSCs were incubated with the monoclonal antibody Rituximab for three days during demyelination in a concentration of 6 and 12 mg/mL. The GFP^+ area was documented daily, quantified at the end of the experiment and compared between Rituximab and IVIG treated OSCs. Evaluation of this experiment showed that neither 6 mg/mL nor 12 mg/mL Rituximab prevented demyelination **(Figure 25)**. In numbers, OSCs which were treated for three days during demyelination with either 6 mg/mL Rituximab or 6 mg/mL IVIG showed a GFP^+ area of 35% (± 10) and 94% (± 18), respectively. The higher concentration of 12 mg/mL Rituximab or 12 mg/mL IVIG resulted in a GFP^+ area of 55% (± 3) and 92% (± 2), respectively. In OSCs, which were solely demyelinated, the GFP^+ area was decreased to 54% (± 8).

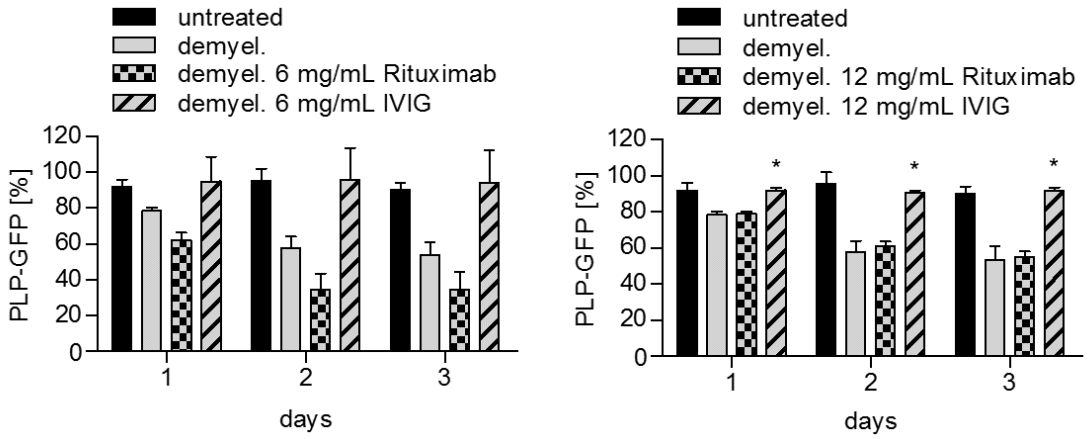

Figure 25. Monoclonal IgG does not protect OSCs from demyelination.

OSCs were demyelinated with or without Rituximab, or IVIG or were left untreated as indicated. The GFP^+ area was documented by fluorescence microscopy in living OSC at day 0, 1, 2 and 3 of the experiment. Quantification of the PLP-GFP expression revealed that IVIG but not the monoclonal Rituximab inhibits immune-mediated demyelination in OSC (n = 4–5 OSC per group). Significances were calculated in respect to the demyelinated control using one-way analysis of variance and Dunnett's post hoc test. *P ≤ 0.05. From Winter et al., 2016.

Following three days of demyelination in the presence and absence of IVIG or Rituximab, OSCs were fixed, stained for neurons (NF200) and analysed via laser scanning microscopy. Microscopic images confirm that 6 and 12 mg/mL IVIG, but not the same amounts of the monoclonal Rituximab protect axons from demyelination **(Figure 26)**.

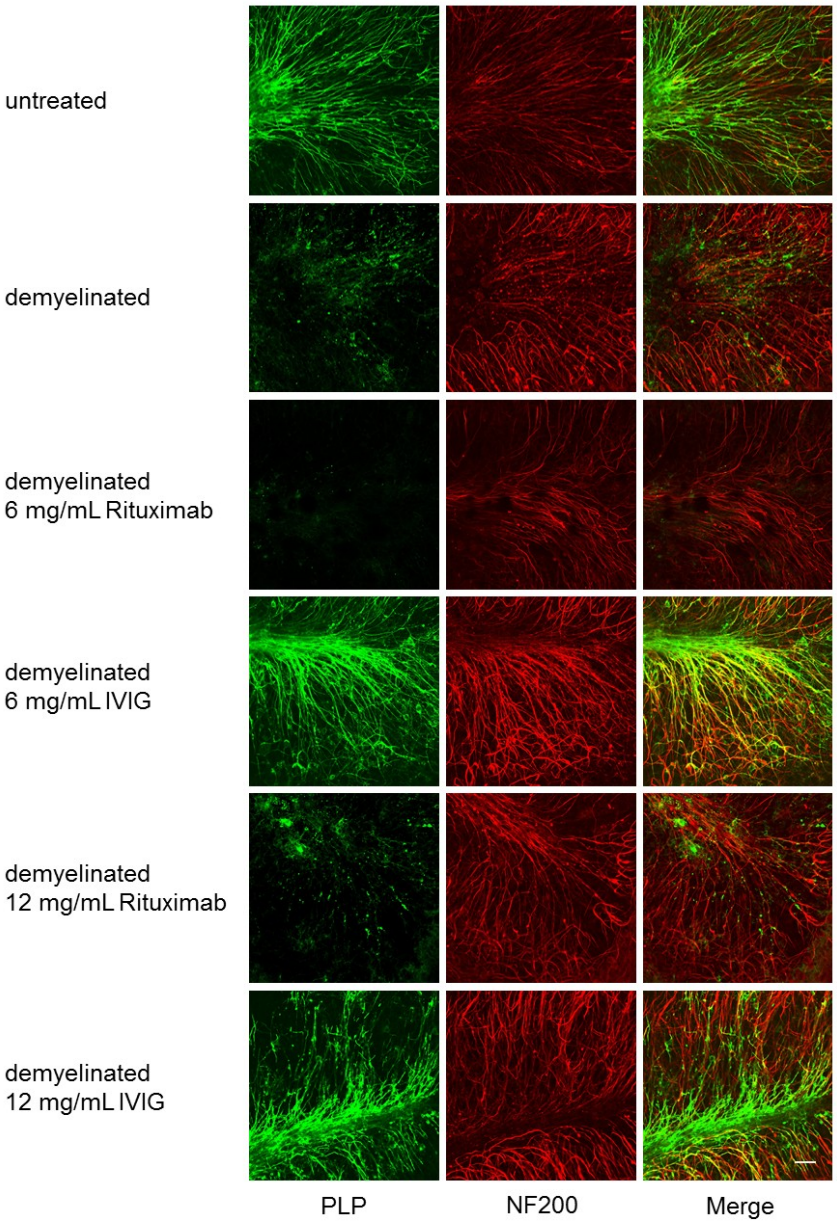

Figure 26. Monoclonal IgG does not preserve axons from demyelination.

OSC were treated as indicated, fixed after 3 days, stained for neurons (NF200) and analyzed via confocal microscopy. Representative confocal images: IVIG but not the recombinant monoclonal antibody Rituximab protects axons from demyelination. Scale bar 50 µm. Modified from Winter et al., 2016.

3.13 Influence of IVIG on remyelination

As IVIG protects axons from demyelination, it should be investigated whether it has also the potential to remyelinate axons. Therefore, OSCs which were demyelinated for three days were allowed to remyelinate for one week in the presence of 6 mg/mL IVIG. OSCs incubated in the usual OSC medium served as a control for spontanous remyelination. IVIG had a small but significant positive effect after three days of remyelination **(Figure 27)**. While the remyelination control showed a GFP^+ area of 4% (± 1) at day 6 of the experiment, OSCs treated with IVIG reached even a GFP^+ area of 7% (± 2). At later time points the differences between the two treatment groups did not reach statistical significance. After one week, remyelination resulted in both groups in a GFP^+ area of about 40%.

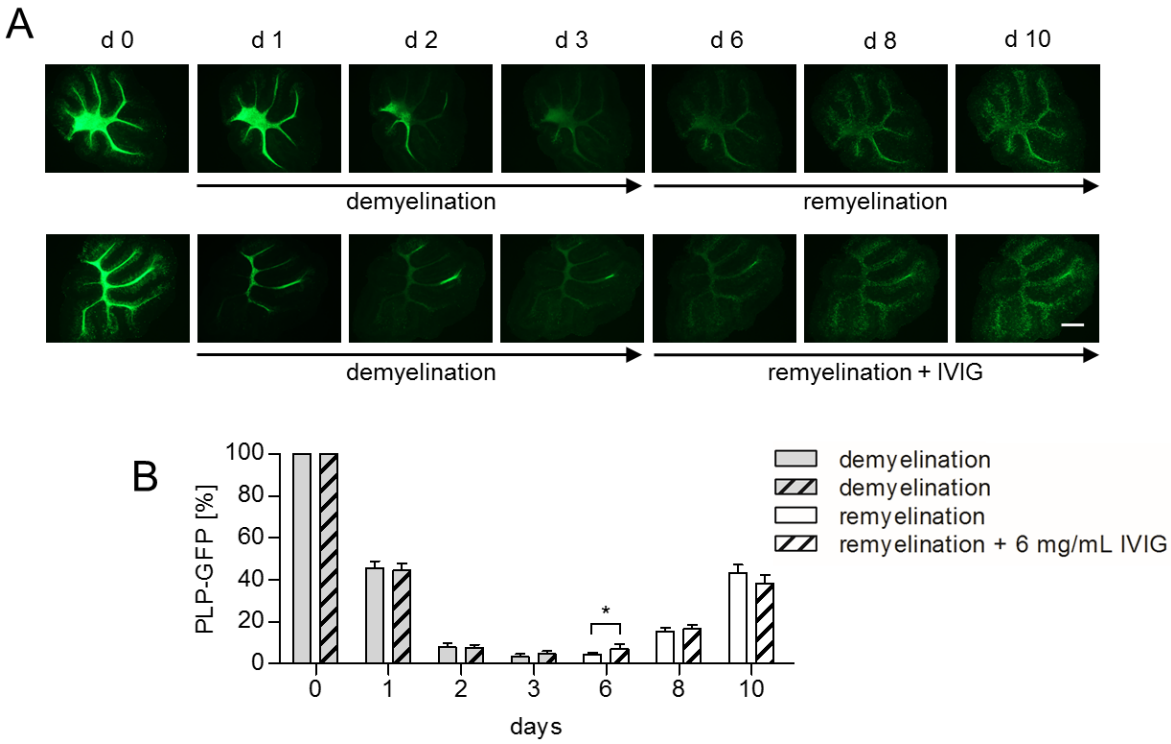

Figure 27. IVIG might promote early remyelination.

After 3 days of demyelination, OSCs were allowed to remyelinate in normal OSC medium with and without 6 mg/mL IVIG. The GFP^+ area was documented in living OSC by fluorescence microscopy, daily during demyelination and 3 times a week during remyelination. **(A)** Representative images of PLP-GFP expression: Three days of immune-mediated demyelination resulted in the loss of myelin. OSC treated with or without IVIG built spontaneously new myelin within 7 days. Scale bar 1 mm. **(B)** Quantification of the GFP^+ area showed that IVIG-treatment resulted in a small but significant increase in early remyelination (n = 17-22 OSC per group). Significances between the two groups were calculated using the student's t-test.

After a seven-day remyelination period, OSCs were fixed and stained for neurons (NF200) and the paranodal protein Caspr. Confocal analysis of the NF200 staining and the endogenous PLP-GFP signal confirmed, that OCSs which were incubated either in the presence or in the absence of IVIG build new myelin within one week **(Figure 28)**. Analysis of the immunohistochemical staining of the paranodal protein Caspr indicates the presence of Nodes of Ranvier in parts of the remyelinated areas, thereby referring to the functionality of new built myelin.

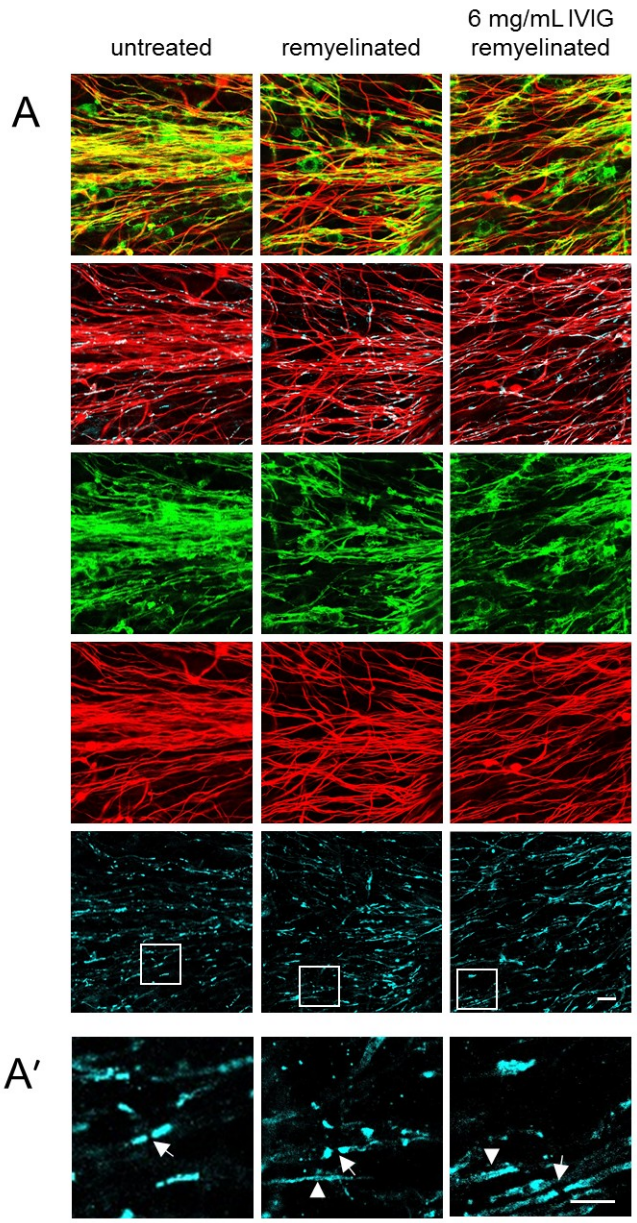

Figure 28. IVIG treatment of OSCs during remyelination.
OSCs were demyelinated for 3 days with 5 µg/mL anti-MOG antibody and 6% complement. After demyelination, remyelination was induced by a change to normal OSC medium with and without 6 mg/mL IVIG. At day 10, OSCs were fixed and stained for neurons (NF200) and the paranodal protein Caspr. Immunohistochemical stainings were analyzed by confocal microscopy. Representative confocal images: After 7 days of remyelination with or without IVIG treatment, axons showed remyelination and Caspr staining, indicating the functionality of the new built myelin. Untreated OSCs were still myelinated. **(A')** Magnification of boxed area: While Capsr formed short cylindrical structures (arrows), in untreated OSCs, in the remyelinated condition short (arrows), as well as longer (arrowheads) aggregates were present. Scale bars **(A)** 20 µm, **(A')** 10 µm.

3.14 IVIG prevents microglia migration in immune-mediated demyelination

To investigate the impact of demyelination and IVIG accompanied demyelination on microglia, OSC were prepared from heterozygous CX3CR1 mice. While the chemokine fractalkine (CX3CL1) in the brain is mainly expressed in neurons, its receptor (CX3CR1) is dominantly expressed in microglia (Harrison et al., 1998; Nishiyori et al., 1998). In homozygous CX3CR1 mice, CX3CR1 is replaced by GFP. Heterozygous CX3CR1 mice express GFP and CX3CR1 resulting in green microglia with a functional CX3CR1 (Jung et al., 2000). For visualization of myelin, OSCs of all conditions but the complement control were preincubated with cy3-coupled αMOG antibody for 1 day. After preincubation, all OSCs but the αMOG~cy3 control were treated with complement in the presence or absence of IVIG. Before the beginning of the experiment, microglia were evenly distributed in all conditions **(Figure 29)**. After two days of antibody and complement treatment, microglia migrated towards the site of demyelination. In OSCs, which were additionally incubated with IVIG, microglia migration was reduced. In contrast, microglia in control OSCs treated either with complement or with αMOG antibody remained evenly distributed.

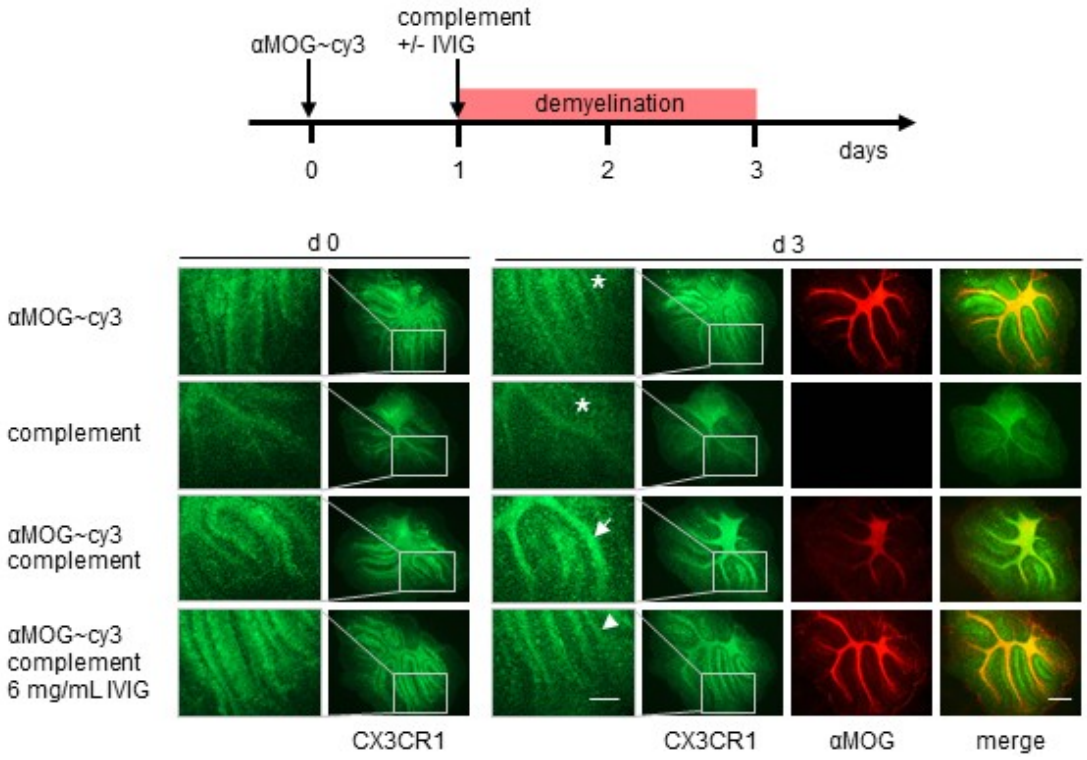

Figure 29. IVIG reduces the migration of microglia in OSCs during immune-mediated demyelination.
To visualize the distribution of microglia, OSCs were prepared from heterozygous CX3CR1 mice, expressing GFP and CX3CR1 in microglia. OSCs were treated as indicated. Pretreatment with αMOG~ cy3 occurred 1 day prior other treatments. Fluorescence microscopic images were acquired from living OSCs at day 0 and 3. Microglia migrated towards the sites of demyelination in OSCs treated with αMOG~cy3 and complement (arrow). Microglia migration was reduced in IVIG treated OSCs (arrow head). OSCs which were treated with complement or αMOG-antibody did not show significant microglia migration (asteriks). Scale bar 1 mm, enlargement 0.5 mm.

To verify that microglia migration following immune-mediated demyelination was not specific for heterozygous CX3CR1 mice, a similar experiment was performed with OSCs prepared from PLP-GFP mice. Therefore, these OSCs were demyelinated with and without 6 mg/mL of IVIG, incubated with complement only or were left untreated. After 2 days, OSCs were fixed with PFA and stained for cell nuclei with Hoechst and for microglia with Iba1 and CD68 antibodies. Immunohistochemistry proved that microglia in general (Iba1), as well as activated microglia (CD68) migrate to the sites of demyelination, after antibody and complement treatment. IVIG treatment during demyelination reduced microglia migration. Microglia do not migrate in untreated or complement-treated OSCs

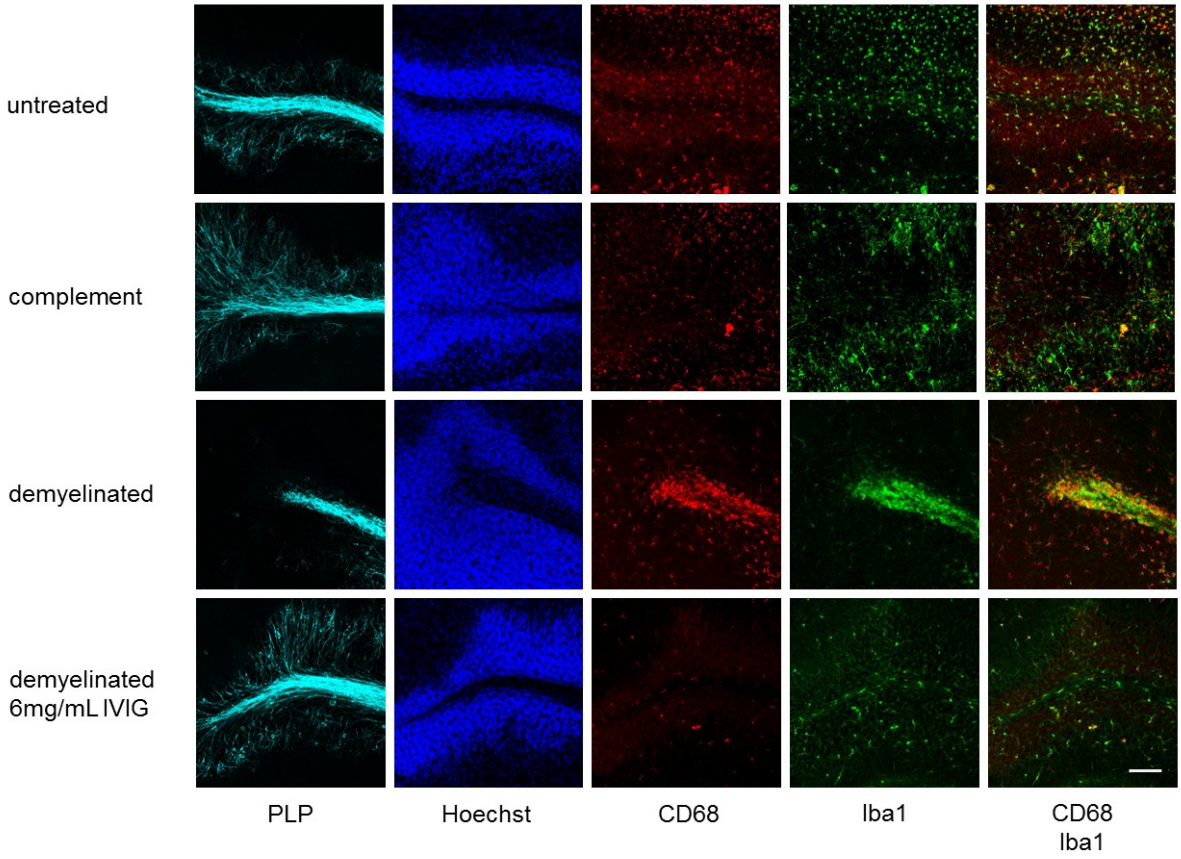

Figure 30. IVIG mediated reduction of microglia migration is independent of the mouse strain.
OSCs from PLP-GFP mice were demyelinated with and without 6 mg/mL of IVIG, incubated with complement only or were left untreated as indicated. After 2 days, OSCs were fixed and stained for cell nuclei with Hoechst and for microglia with antibodies against Iba1 and CD68. Thereafter OSCs were analyzed via confocal microscopy. Representative microscopic images: IVIG protects the myelin sheath from demyelination and thereby prevents the migration of Iba1-positive and CD68-positive microglia towards the site of demyelination. Scale bar 100 µm.

4 Discussion

4.1 Characterization and quantification of immune-mediated de- and remyelination in organotypic slice cultures (OSCs) of the cerebellum

De- and remyelination processes were investigated using the *ex vivo* model of OSCs. Immune-mediated demyelination was induced within 2-3 days by complement and a humanized anti-MOG antibody. Axons stayed largely intact, as shown before (Harrer et al.,2009). The replacement of complement and antibody containing medium with usual OSC medium started the remyelination process. A seven-day remyelination period resulted in an incomplete but remarkable remyelination. The use of PLP-GFP (Proteolipid-Protein; green fluorescent protein) -mice allowed live imaging of de- and remyelination processes due to the expression of GFP under regulatory elements of the PLP promoter. As a result, PLP positive oligodendrocytes were also positive for GFP (GFP^+) and could be imaged by fluorescence microscopy **(Figure 6)**. De- and remyelination was quantified by measuring the GFP^+ area above a defined threshold. During remyelination, not all oligodendrocyte precursor cells (OPCs) manage to remyelinate axons. OPCs need to undergo proliferation, migration, differentiation and finally remyelination to preserve the structure and function of axons. In spite of the ability of OPCs to differentiate into mature oligodendrocytes, some of them fail to migrate to the demyelinated axons (Boyd et al., 2013) or to myelinate them (Chang et al., 2002). In OSCs we monitored the remyelination of demyelinated axons by oligodendrocytes. Nevertheless, some oligodendrocytes express PLP and consequently GFP, but do not contribute to remyelination. To exclude those mature but not myelinating oligodendrocytes, the GFP^+ area was corrected by using size exclusion. **(Figure 6, Figure 7)**. The values for the GFP^+ area determined by the size exclusion method were lower compared to those generated by quantification without size exclusion **(Figure 7 B+C)**. However, both evaluation methods showed the same trend. Since the evaluation with size exclusion reflects better the incomplete remyelination **(Figure 6 A)**, this method was chosen for all remyelination experiments.

The paranodes as essential elements for the functionality of the myelin were investigated in untreated, demyelinated and remyelinated OSCs by confocal analysis of Caspr (Contactin associated protein 1) staining. Caspr forms together with two other adhesion proteins contactin 1 and neurofascin 155 the paranode, which is required for the formation of the nodes of Ranvier. Thus, a positive staining for Caspr is pointing towards intact nodes of Ranvier, which are critical for rapid and correct signal transduction in myelinated axons. Before demyelination, we observed in our model of cerebellar OSCs, that the expression pattern of Caspr formed the distinct cylindrical structure of the paranode. After immune-mediated demyelination Caspr staining was absent in OCSs and it reappeared after successful remyelination **(Figure 8)**. The same change in the Caspr expression pat-

tern has also been observed by Wolswijk and Balesar, 2003 who demonstrated that the Caspr staining is present in control tissue, absent in the demyelinated centre of human MS lesions and again present in the paranodal region after the formation of new myelin. Interestingly, after remyelination in our OSC model, Caspr not only formed short cylindrical aggregates but also extended structures. This phenomenon was also observed in studies by Wolswijk and Balesar, 2003 and Coman et al., 2006. Wolswijk and Balesar, 2003 detected the extended Caspr expression pattern in the borders of chronic lesions and speculated that they might be an early sign of upcoming myelin loss. Coman et al., 2006 found an extended Caspr expression pattern in partially remyelinated plaques and detected that this expression pattern was more often associated with demyelinated fibres than with myelinated fibres. Hence, they postulated that extended Caspr expression precedes the remyelination process. This theory is supported by axon glia co-culture experiments from Eisenbach et al., 2009. These experiments revealed that during myelination Caspr first accumulates at contact sites between axons and oligodendrocytes and that Caspr is restricted to the paranodes after the formation of compact myelin (Eisenbach et al., 2009).

4.2 Effect of IVIG on immune-mediated demyelination in OSCs

Quantification of the myelin (GFP^+ area) revealed that IVIG protected OSCs from immune-mediated demyelination in a dose dependent way **(Figure 9)**. These findings were supported by fluorescence microscopic colocalization of NF200 staining with the endogenous PLP-GFP signal **(Figure 10)**. While demyelination for two days resulted in a total loss of PLP-GFP signal, an additional treatment with IVIG protected OSCs dose-dependently from demyelination. A staining for the paranodal protein Caspr indicated that the protected myelin remained functional **(Figure 15)**. In addition, flow cytometry and gene expression experiments confirmed the protection of myelin by IVIG. Flow cytometric analysis of single cell suspensions demonstrated that the number of living oligodendrocytes was significantly reduced in OSCs which were demyelinated in the presence or absence of BSA as a control protein. In contrast, IVIG treatment during demyelination did not change the number of living oligodendrocytes in OSCs **(Figure 14)**. In line with these findings, the gene expression of two other myelin genes (MBP and CNPase) decreased following demyelination and was party rescued by IVIG **(Figure 13)**. Neither demyelination nor additional IVIG treatment significantly altered the gene expression of the oligodendrocyte progenitor marker Ng2. These findings are in line with the results of Liu et al., 2017, who showed that the amount and the morphology of Ng2+ and Olig2+ cells were not altered in cerebral OSCs treated with a myelin antibody and human complement. Demyelination and additional IVIG treatment caused no significant changes in gene expression of the axonal

marker neurofilament 200 (NF200). This is in harmony with previous experiments from Harrer et al., 2009, where axons were intact after immune-mediated demyelination.

4.3 Influence of IVIG on microglia and remyelination in OSCs

Immune-mediated demyelination and the additional treatment with IVIG reduced the gene expression of the microglial marker Iba1 in OSCs **(Figure 13)**. Although IVIG treatment rescued the reduction of gene expression partially, this effect did not reach statistical significance. A decrease in Iba1 gene expression was also measured by Silverman et al., 2015 in mouse brain tissue after an intraperitoneal lipopolysaccharide injection. In contrast to the declining gene expression, flow cytometric analysis of single cell suspension prepared from OSCs showed that the number of living $CD11b^+$ microglia did not significantly differ between conditions **(Figure 14)**. The different results of the gene expression and flow cytometric experiments might be explained by high scattering of the measured values in the flow cytometric experiment. However, the use of different microglia markers could also have contributed to the varying results. Demyelination of OSCs prepared from heterozygous CX3CR1 mice revealed that GFP^+ microglia migrate towards the site of demyelination within 2 days **(Figure 29)**. This migration was shown to be independent from a possible phenotype in heterozygous $CX3CR1^{+/-}$ mice, as it was also detectable in demyelinated OSCs prepared from PLP-GFP mice **(Figure 30)**. The entirety of microglia, stained with Iba1, as well as activated microglia stained with CD68 underwent migration to the area of demyelination. These findings are in line with experiments from Liu et al., 2017 which showed that treatment of cerebellar OSCs with human complement and a recombinant myelin-specific antibody resulted in an increase of $Iba1^+$ microglia in the focal areas of demyelination. Interestingly, we found in our experiments, that IVIG treatment during demyelination reduced microglia migration in OSCs. Apart from the migration, our group showed that IVIG treatment also influences microglia morphology following immune-mediated demyelination in OSCs (Winter et al., 2016). While microglia were rather swollen and rounded up following demyelination, microglia in OSCs incubated with IVIG during demyelination were still small and ramified similar to the untreated controls. Previously, it was shown that IVIG has activating but also inhibiting effects on the function of isolated microglia. On the one hand, it was shown that IVIG activates the production of tumor necrosis factor alpha (TNFα) and nitric oxide (NO) (Pul et al., 2002; Stangel and Compston, 2001). On the other hand, it was demonstrated that IVIG inhibits endocytosis of soluble MBP and Fc-receptor mediated phagocytosis of opsonised erythrocytes (Stangel, Joly et al., 2000). Interestingly, we found that IVIG treatment during remyelination caused a small but significant positive effect at the early remyelination **(Figure 27)**. These findings are

consistent with a study from Warrington et al., 2000, who showed that IVIG enhanced remyelination in the animal model of Theilers' Murine Encephalomyelitis. However, the underlying mechanisms are not clear yet. A study by Stangel et al., 1999 demonstrated that IVIG neither affects proliferation, nor differentiation or migration of cultured OPCs, making a direct interaction of IVIG with OPCs unlikely. The ability of microglia to clear myelin (Yamasaki et al., 2014) seems to be important for proper remyelination. Kotter et al., 2006 showed that myelin debris acts as an inhibitor for remyelination in a rat model of ethidium bromide induced demyelination. A different study by Lampron et al., 2015 demonstrated that the incomplete removal of myelin debris by microglia results in aberrant remyelination in CX3CR1-defficient mice using the cuprizone model of demyelination. Furthermore, microglia have been shown to increase their Matrix metalloproteinase-9 (MMP-9) secretion in response to IVIG treatment (Pul et al., 2009), which is together with the finding that MMP-9 is essential for proper remyelination (Larsen et al., 2003) supporting the hypothesis that remyelination is enhanced by an interaction of IVIG and microglia.
Taken together, the role of microglia in demyelinating diseases like MS is not fully understood. Our findings in an *ex vivo* system demonstrate that IVIG inhibits the migration and the activation of microglia, protects axons from demyelination and enhances remyelination. The question remains open whether the protection from demyelination and the promotion of remyelination is mediated via a direct interaction of IVIG and microglia or if IVIG interferes with the myelin and thereby prevents microglia migration and microglia activation.

4.4 Mechanism of action of IVIG in OSCs

Neither human serum albumine (HSA) nor bovine serum albumin (BSA) prevented OSCs from demyelination, proving that the protective effect of IVIG is not caused by a simple increase in protein concentration **(Figure 11)**. The incubation of OSC with complement alone did not lead to demyelination, indicating that complement alone is not sufficient for activation of the complement cascade in this model system **(Figure 12)**. Furthermore, the treatment of OSCs with IVIG alone did not influence the GFP^+ area, suggesting that IVIG does not contain an adequate amount of oligodendrocyte specific antibody for the mediation of antibody-dependent cellular cytotoxicity (ADCC). However, the fact that demyelination was also not induced in previous experiments from Harrer et al., 2009, where OSCs were incubated with anti-MOG antibody only, suggests that ADCC cannot be induced in our model of OSCs. In line with the findings of Stangel, Compston et al., 2000, combined treatment with IVIG and complement did not induce demyelination. This result implies that oligodendrocyte specific antibodies are not sufficiently present or have the wrong isotype (e.g. IgG4) for activation of the classical pathway of the complement cas-

cade. To further elucidate this aspect, we investigated whether IVIG could prevent demyelination by the competitive binding to the target epitope of the anti-MOG antibody. To this end, OSCs were preincubated for three days with IVIG and stained with biotinylated anti-MOG antibody afterwards. Fluorescence microscopic analysis however clearly revealed that IVIG preincubation did not affect the binding of anti-MOG antibody **(Figure 18)**. To further illucidate the protective effect of IVIG, the concentration of anti-MOG antibody or complement was varied in two different experiments. The evaluation revealed that rising concentrations of complement overruled IVIG-mediated protection of myelin in OSCs **(Figure 19)**. In contrast, OSCs treated with increasing concentration of anti-MOG antibody were still protected by IVIG from demyelination **(Figure 16, Figure 17, Figure 20).** These findings indicate that IVIG more likely interacts with the complement and does not block the idiotypes of anti-MOG antibodies. This is partially consistent with the literature. Urich et al., 2006 showed in an anti-MOG antibody enhanced experimental autoimmune encephalomyelitis (EAE) that the demyelination capacity of anti-MOG autoantibody is dependent on a functional complement cascade and independent on the Fcγ receptor. Furthermore, it was shown that IVIG binds activated complement components like C3b and C4b, thus scavenging them from cell-bound immune complexes (Frank et al., 1992; Frank et al., 2000). Nevertheless, the soluble complexes formed by IgG and C3b (C3b2-IgG) are even more effective in cleaving C3, arguing rather for an increase in complement activation than for a decrease (Jelezarova et al., 2000). However, *in vivo* and *in vitro* studies by Lutz and his group showed that IVIG moreover lowers the half-life of soluble C3bn-IgG complexes, resulting first in the decrease in concentration of C3-convertase and finally in attenuation of the complement cascade (Lutz et al., 1996; Lutz et al., 2004). Since there is clear evidence that IVIG interacts with complement, the question was raised whether autoantibodies directed against complement factors prevent the formation of membrane-bound C3b2-IgG complexes and thereby protect oligodendrocytes from lysis. To answer this question OSCs were demyelinated in the presence of IVIG derived variable antigen binding regions (Fab fragments) or constant Fc regions (Fc fragments) from a polyclonal IgG preparation. Interestingly, the constant Fc fragments **(Figure 23, Figure 24)** and not the Fab fragments protected OSCs from demyelination **(Figure 21, Figure 22)**. Other studies attribute immunomodulatory properties of IVIG to its Fab fragment, proposing different mechanisms of action. For example, autoantibodies directed against complement factors have been described to reduce inflammation and to attenuate complement activation. (Basta et al., 2003; Lutz and Späth, 2005). A different study from Rossi and Kazatchkine, 1989 detected in IVIG antiidiotypic antibodies which bind to human autoantibodies, arguing for the concept of a functional idiotypic network which regulates autoimmune responses. However, our findings show that the protection from demyelination is not

mediated by the variable antigen binding region of IVIG (Fab fragments). On the contrary, our results clearly indicate that the Fc fragment of IVIG interacts with the complement cascade. This is in line with experiments from Mollnes et al., 1995, who showed, that IVIG inhibited the lysis of erythrocytes in a dose-dependent manner via the classical complement pathway. There is evidence that therapeutic effects of IVIG are mediated through the glycosylation of its Fc fragment. Ravetch and colleagues showed that the linkage of sialyic acid to the Fc fragment is responsible for a reduced IgG cytotoxicity, as well as for anti-inflammatory activity in a mouse model of arthritis (Anthony, Nimmerjahn et al., 2008; Kaneko et al., 2006). Interestingly, a study by Youings et al., 1996 showed that the percentage incidence of sialylated oligosaccharides is considerably higher on Fab than on Fc fragments. However, according to the literature, only up to 29% of Fab fragments show glycosylation (Spiegelberg et al., 1970). Sialylated IgG binds to C-type lectin receptors like DC-SIGN (Dendritic Cell-Specific Intercellular adhesion molecule-3-Grabbing Non-integrin) expressed on human microglia (García-Vallejo et al., 2014) or to its murine homologue SIGN-R1 thereby mediating the anti-inflammatory properties of IVIG (Anthony, Wermeling et al., 2008). Studies from Park et al., 2009 showed that SIGN-R1 is expressed on microglia in mouse cerebellum, arguing for an interaction between IVIG and microglia. The immunotherapeutic, monoclonal (anti-CD20) antibody Rituximab was not able to protect OSCs from demyelination, which might be explained by the absence of sialyl residues in the recombinant antibody (Huang et al., 2012). However, Campbell et al., 2014 opened the discussion on the functionality of sialyl residues by demonstrating in two antibody and complement depending mouse models of arthritis that the therapeutic benefit of IVIG is dependent on the Fc fragments but not on their sialylation. According to our results, IVIG plays a central role in the complex microenvironment of the central nervous system (CNS) slice culture. Its various effects are mediated through the interaction with microglia and the complement system either by seperate or linked mechanisms. Taking into account all results, this study demonstrates that IVIG interfers with component of the CNS in several ways: The protection of OSCs from immune-mediated demyelination appears to be closely related to the suppression of the complement cascade by IVIG. Our data clearly show that the impact of IVG is mediated by its constant Fc fragment, while the variable Fab fragment is not needed for the myelin preservation. Furthermore, also the inhibition of microglia migration and microglia activation as well as the enhancement of early remyelination may be a notable consequence of IVIG treatment, although this hypothesis needs to be confirmed by future studies.

4.5 Medical relevance, perspectives and conclusion

4.5.1 Medical relevance

Since IVIG interacts with the complement cascade, efficient medical treatment of antibody and complement mediated diseases can only occur if the IVIG levels are sufficient to antagonize complement factors. While the empirical standard for the treatment of most autoimmune conditions (such as Myasthenia gravis) is 2 g IVIG/kg bodyweight, a multitude of dosage schemes used for clinical MS trials might have caused the inconsistent results. Consequently, one could think of a personalized dosage scheme based on the individual grade of complement deposition in diseases with antibody and complement mediated effector mechanisms. Furthermore, the question arises, whether also disease of the CNS like MS can benefit from IVIG treatment. There is little data available about what amount of serum IgG is able to cross the blood brain barrier (BBB). A study by van Engelen et al., 1994 measured a mean increase of 44% in cerebrospinal fluid (CSF) IgG concentration after systemic IVIG administration in epilepsy patients. In a patient with polyradiculitis after infusion of 30 g IVIG nearly 1% of the serum Ig was able to pass through the blood brain barrier (BBB) and to enter the CSF (Wurster and Haas, 1994). In the recent past, studies in wild type rodents showed that systemically administrated Igs reach therapeutically relevant concentration in the brain in the absence of BBB leakage (Pepinsky et al., 2011; St-Amour et al., 2013). While these studies favor the hypothesis that Igs can overcome the intact BBB, this might be even more the case during CNS inflammation, which is accompanied by an (at least partial) BBB breakdown. Regardless of these promising results, we are currently not able to estimate which ratio of systemically administered IVIG reaches the CNS, nor do we know which local concentration is required to achieve a therapeutic effect.

4.5.2 Perspectives

The pre-incubation of OSCs with IVIG revealed that IVIG does not block the binding sites of the anti-MOG antibody. Further pre-incubation studies followed by immunohistochemical co-stainings and subsequent microscopy, will be necessary to reveal possible interaction of IVIG with other cell types. A potential binding of IVIG to microglia could be verified via live imaging of fluorescence labeled IVIG in OSCs prepared from heterozygous CX3CR1 mice. Furthermore, we found in the present study, clear evidence for an Fc mediated protection from immune-mediated demyelination in OSCs. According to studies by Ravetch and colleagues anti-inflammatory activity of Fc fragments might be assigned to their sialylation (Anthony, Nimmerjahn et al., 2008; Kaneko et al., 2006). It is also known that glycosylation of Fc fragments is heterogeneous and that different glyco-

sylation patterns are associated with different effector functions (reviewed by Cymer et al., 2018). Therefore, in future studies, it would be interesting to associate distinct glycosylation patterns with the respective therapeutic effect. Results from these experiments could subsequently serve as an important basis for the development recombinant and specifically glycosylated molecules, which might be able to replace or to complement the limited supply of IVIG. Apart from the IVIG related experiments, we will use our *ex vivo* OSC model in the future to characterize patient derived antibodies. Intrahecal autoantibodies and oligoclonal immunoglobulins have been detected in the CSF of patients with autoimmune inflammatory disorders like MS (Büdingen et al., 2010; Obermeier et al., 2008). Since the role of these antibodies in disease is not clear yet, we have established in our group a method to rebuild these expanded autoantibodies in a recombinant and monoclonal form. Using the OSC model we would like to characterize the role of these autoantibodies in disease pathogenesis.

4.5.3 Conclusion

Finally, the present study demonstrates that the *ex vivo* system of cerebellar OSCs from PLP-GFP$^+$ mice is well suited for fluorescence microscopic live imaging in the same OSC. Immune-mediated demyelination can be induced by the addition of anti-MOG antibody and complement and is followed by spontaneous remyelination. De- and remyelination can be easily quantified by measuring the GFP$^+$ area of each OSC over the time. Even though, the OSC model might not be the best choice for high throughput drug screenings, it highly qualifies to investigate preselected pharmaceutical substances for their ability to protect from demyelination or to promote remyelination. Moreover, the present study reveals by the example of IVIG that the three-dimensional micro-architecture of OSC model is well suited to study effector mechanisms unimpaired by the BBB and peripheral immune components.

5 References

Achiron A, Gabbay U, Gilad R, Hassin-Baer S, Barak Y, Gornish M, Elizur A, Goldhammer Y, Sarova-Pinhas I. 1998. Intravenous immunoglobulin treatment in multiple sclerosis. Effect on relapses. Neurology 50(2):398–402.

Achiron A, Pras E, Gilad R, Ziv I, Mandel M, Gordon CR, Noy S, Sarova-Pinhas I, Melamed E. 1992. Open controlled therapeutic trial of intravenous immune globulin in relapsing-remitting multiple sclerosis. Archives of neurology 49(12):1233–1236.

Aktas O, Waiczies S, Grieger U, Wendling U, Zschenderlein R, Zipp F. 2001. Polyspecific immunoglobulins (IVIg) suppress proliferation of human (auto)antigen-specific T cells without inducing apoptosis. Journal of neuroimmunology 114(1-2):160–167.

Altman J, Das GD. 1966. Autoradiographic and histological studies of postnatal neurogenesis. I. A longitudinal investigation of the kinetics, migration and transformation of cells incorporating tritiated thymidine in neonate rats, with special reference to postnatal neurogenesis in some brain regions. The Journal of comparative neurology 126(3):337–389.

Anthony RM, Nimmerjahn F, Ashline DJ, Reinhold VN, Paulson JC, Ravetch JV. 2008. Recapitulation of IVIG anti-inflammatory activity with a recombinant IgG Fc. Science (New York, N.Y.) 320(5874):373–376.

Anthony RM, Wermeling F, Karlsson MCI, Ravetch JV. 2008. Identification of a receptor required for the anti-inflammatory activity of IVIG. Proceedings of the National Academy of Sciences of the United States of America 105(50):19571–19578.

Arancibia-Carcamo IL, Attwell D. 2014. The node of Ranvier in CNS pathology. Acta neuropathologica 128(2):161–175.

Babbe H, Roers A, Waisman A, Lassmann H, Goebels N, Hohlfeld R, Friese M, Schröder R, Deckert M, Schmidt S, Ravid R, Rajewsky K. 2000. Clonal expansions of CD8(+) T cells dominate the T cell infiltrate in active multiple sclerosis lesions as shown by micromanipulation and single cell polymerase chain reaction. The Journal of experimental medicine 192(3):393–404.

Ballow M. 2011. The IgG molecule as a biological immune response modifier: Mechanisms of action of intravenous immune serum globulin in autoimmune and inflammatory disorders. The Journal of allergy and clinical immunology 127(2):315-23; quiz 324-5.

Basta M, van Goor F, Luccioli S, Billings EM, Vortmeyer AO, Baranyi L, Szebeni J, Alving CR, Carroll MC, Berkower I, Stojilkovic SS, Metcalfe DD. 2003. F(ab)'2-mediated neutralization of C3a and C5a anaphylatoxins: A novel effector function of immunoglobulins. Nature medicine 9(4):431–438.

Batchelor PE, Porritt MJ, Martinello P, Parish CL, Liberatore GT, Donnan GA, Howells DW. 2002. Macrophages and Microglia Produce Local Trophic Gradients That Stimulate Axonal Sprouting Toward but Not beyond the Wound Edge. Molecular and cellular neurosciences 21(3):436–453.

Ben-Nun A, Wekerle H, Cohen IR. 1981. The rapid isolation of clonable antigen-specific T lymphocyte lines capable of mediating autoimmune encephalomyelitis. European journal of immunology 11(3):195–199.

Bin JM, Leong SY, Bull S-J, Antel JP, Kennedy TE. 2012. Oligodendrocyte precursor cell transplantation into organotypic cerebellar shiverer slices: A model to study myelination and myelin maintenance. PloS one 7(7):e41237.

Birgbauer E, Rao TS, Webb M. 2004. Lysolecithin induces demyelination in vitro in a cerebellar slice culture system. Journal of neuroscience research 78(2):157–166.

Blauth K, Soltys J, Matschulat A, Reiter CR, Ritchie A, Baird NL, Bennett JL, Owens GP. 2015. Antibodies produced by clonally expanded plasma cells in multiple sclerosis cerebrospinal fluid cause demyelination of spinal cord explants. Acta neuropathologica 130(6):765–781.

Booss J, Esiri MM, Tourtellotte WW, Mason DY. 1983. Immunohistological analysis of T lymphocyte subsets in the central nervous system in chronic progressive multiple sclerosis. Journal of the neurological sciences 62(1-3):219–232.

Bouslama-Oueghlani L, Wehrlé R, Sotelo C, Dusart I. 2003. The developmental loss of the ability of Purkinje cells to regenerate their axons occurs in the absence of myelin: An in vitro model to prevent myelination. The Journal of neuroscience : the official journal of the Society for Neuroscience 23(23):8318–8329.

Boyd A, Zhang H, Williams A. 2013. Insufficient OPC migration into demyelinated lesions is a cause of poor remyelination in MS and mouse models. Acta neuropathologica 125(6):841–859.

Brosnan CF, Raine CS. 2013. The astrocyte in multiple sclerosis revisited. Glia 61(4):453–465.

BROWNELL B, HUGHES JT. 1962. The distribution of plaques in the cerebrum in multiple sclerosis. Journal of neurology, neurosurgery, and psychiatry 25:315–320.

Büdingen H-C von, Gulati M, Kuenzle S, Fischer K, Rupprecht TA, Goebels N. 2010. Clonally expanded plasma cells in the cerebrospinal fluid of patients with central nervous system autoimmune demyelination produce "oligoclonal bands". Journal of neuroimmunology 218(1-2):134–139.

Burns J, Rosenzweig A, Zweiman B, Lisak RP. 1983. Isolation of myelin basic protein-reactive T-cell lines from normal human blood. Cellular immunology 81(2):435–440.

Buttmann M, Kaveri S, Hartung H-P. 2013. Polyclonal immunoglobulin G for autoimmune demyelinating nervous system disorders. Trends in pharmacological sciences 34(8):445–457.

Campbell IK, Miescher S, Branch DR, Mott PJ, Lazarus AH, Han D, Maraskovsky E, Zuercher AW, Neschadim A, Leontyev D, McKenzie BS, Käsermann F. 2014. Therapeutic effect of IVIG on inflammatory arthritis in mice is dependent on the Fc portion and independent of sialylation or basophils. Journal of immunology (Baltimore, Md. : 1950) 192(11):5031–5038.

Chang A, Nishiyama A, Peterson J, Prineas J, Trapp BD. 2000. NG2-positive oligodendrocyte progenitor cells in adult human brain and multiple sclerosis lesions. The Journal of neuroscience : the official journal of the Society for Neuroscience 20(17):6404–6412.

Chang A, Tourtellotte WW, Rudick R, Trapp BD. 2002. Premyelinating oligodendrocytes in chronic lesions of multiple sclerosis. The New England journal of medicine 346(3):165–173.

Colombo M, Dono M, Gazzola P, Roncella S, Valetto A, Chiorazzi N, Mancardi GL, Ferrarini M. 2000. Accumulation of clonally related B lymphocytes in the cerebrospinal fluid of multiple sclerosis patients. Journal of immunology (Baltimore, Md. : 1950) 164(5):2782–2789.

Coman I, Aigrot MS, Seilhean D, Reynolds R, Girault JA, Zalc B, Lubetzki C. 2006. Nodal, paranodal and juxtaparanodal axonal proteins during demyelination and remyelination in multiple sclerosis. Brain : a journal of neurology 129(Pt 12):3186–3195.

Cui Q-L, Kuhlmann T, Miron VE, Leong SY, Fang J, Gris P, Kennedy TE, Almazan G, Antel J. 2013. Oligodendrocyte progenitor cell susceptibility to injury in multiple sclerosis. The American journal of pathology 183(2):516–525.

Cymer F, Beck H, Rohde A, Reusch D. 2018. Therapeutic monoclonal antibody N-glycosylation - Structure, function and therapeutic potential. Biologicals : journal of the International Association of Biological Standardization 52:1–11.

Dean G, Kurtzke JF. 1971. On the risk of multiple sclerosis according to age at immigration to South Africa. British medical journal 3(5777):725–729.

Delmotte P, Gonsette R. 1977. Biochemical findings in multiple sclerosis IV. Isoelectric focusing of the CSF gamma globulins in multiple sclerosis (262 cases) and other neurological diseases (272 cases). Journal of neurology 215(1):27–37.

Eisenbach M, Kartvelishvily E, Eshed-Eisenbach Y, Watkins T, Sorensen A, Thomson C, Ranscht B, Barnett SC, Brophy P, Peles E. 2009. Differential clustering of Caspr by oligodendrocytes and Schwann cells. Journal of neuroscience research 87(15):3492–3501.

Elsone L, Panicker J, Mutch K, Boggild M, Appleton R, Jacob A. 2014. Role of intravenous immunoglobulin in the treatment of acute relapses of neuromyelitis optica: Experience in 10 patients. Multiple sclerosis (Houndmills, Basingstoke, England) 20(4):501–504.

Ephrem A, Chamat S, Miquel C, Fisson S, Mouthon L, Caligiuri G, Delignat S, Elluru S, Bayry J, Lacroix-Desmazes S, Cohen JL, Salomon BL, Kazatchkine MD, Kaveri SV, Misra N. 2008. Expansion of CD4+CD25+ regulatory T cells by intravenous immunoglobulin: A critical factor in controlling experimental autoimmune encephalomyelitis. Blood 111(2):715–722.

Farina C, Aloisi F, Meinl E. 2007. Astrocytes are active players in cerebral innate immunity. Trends in immunology 28(3):138–145.

Fassbender C, Klingel R, Köhler W. 2017. Immunoadsorption for autoimmune encephalitis. Atherosclerosis. Supplements 30:257–263.

Fazekas F, Deisenhammer F, Strasser-Fuchs S, Nahler G, Mamoli B. 1997. Randomised placebo-controlled trial of monthly intravenous immunoglobulin therapy in relapsing-remitting multiple sclerosis. Austrian Immunoglobulin in Multiple Sclerosis Study Group. Lancet (London, England) 349(9052):589–593.

Fazekas F, Lublin FD, Li D, Freedman MS, Hartung HP, Rieckmann P, Sørensen PS, Maas-Enriquez M, Sommerauer B, Hanna K. 2008. Intravenous immunoglobulin in relapsing-remitting multiple sclerosis: A dose-finding trial. Neurology 71(4):265–271.

Filippini G, Brusaferri F, Sibley WA, Citterio A, Ciucci G, Midgard R, Candelise L. 2000. Corticosteroids or ACTH for acute exacerbations in multiple sclerosis. The Cochrane database of systematic reviews(4):CD001331.

Foran DR, Peterson AC. 1992. Myelin acquisition in the central nervous system of the mouse revealed by an MBP-Lac Z transgene. The Journal of neuroscience : the official journal of the Society for Neuroscience 12(12):4890–4897.

Frank MM, Basta M, Fries LF. 1992. The effects of intravenous immune globulin on complement-dependent immune damage of cells and tissues. Clinical immunology and immunopathology 62(1 Pt 2):S82-6.

Frank MM, Miletic VD, Jiang H. 2000. Immunoglobulin in the control of complement action. Immunologic research 22(2-3):137–146.

Gähwiler BH, Capogna M, Debanne D, McKinney RA, Thompson SM. 1997. Organotypic slice cultures: A technique has come of age. Trends in neurosciences 20(10):471–477.

García-Vallejo JJ, Ilarregui JM, Kalay H, Chamorro S, Koning N, Unger WW, Ambrosini M, Montserrat V, Fernandes RJ, Bruijns SCM, van Weering JRT, Paauw NJ, O'Toole T, van Horssen J, van der Valk P, Nazmi K, Bolscher JGM, Bajramovic J, Dijkstra CD, Hart BA 't, van Kooyk Y. 2014. CNS myelin induces regulatory functions of DC-SIGN-expressing, antigen-presenting cells via cognate interaction with MOG. The Journal of experimental medicine 211(7):1465–1483.

Gelfand EW. 2012. Intravenous immune globulin in autoimmune and inflammatory diseases. The New England journal of medicine 367(21):2015–2025.

Gilhus NE, Owe JF, Hoff JM, Romi F, Skeie GO, Aarli JA. 2011. Myasthenia gravis: A review of available treatment approaches. Autoimmune diseases 2011:847393.

Hanisch U-K, Kettenmann H. 2007. Microglia: Active sensor and versatile effector cells in the normal and pathologic brain. Nature neuroscience 10(11):1387–1394.

Hansen MB, Svenson M, Abell K, Yasukawa K, Diamant M, Bendtzen K. 1995. Influence of interleukin-6 (IL-6) autoantibodies on IL-6 binding to cellular receptors. European journal of immunology 25(2):348–354.

Harrer MD, Büdingen H-C von, Stoppini L, Alliod C, Pouly S, Fischer K, Goebels N. 2009. Live imaging of remyelination after antibody-mediated demyelination in an ex-vivo model for immune mediated CNS damage. Experimental neurology 216(2):431–438.

Harrison JK, Jiang Y, Chen S, Xia Y, Maciejewski D, McNamara RK, Streit WJ, Salafranca MN, Adhikari S, Thompson DA, Botti P, Bacon KB, Feng L. 1998. Role for neuronally derived fractalkine in mediating interactions between neurons and CX3CR1-expressing microglia. Proceedings of the National Academy of Sciences of the United States of America 95(18):10896–10901.

Hartung H-P. 2008. Advances in the understanding of the mechanism of action of IVIg. Journal of neurology 255 Suppl 3:3–6.

Hauser SL, Waubant E, Arnold DL, Vollmer T, Antel J, Fox RJ, Bar-Or A, Panzara M, Sarkar N, Agarwal S, Langer-Gould A, Smith CH. 2008. B-cell depletion with rituximab in relapsing-remitting multiple sclerosis. The New England journal of medicine 358(7):676–688.

Hu Y, Turner MJ, Shields J, Gale MS, Hutto E, Roberts BL, Siders WM, Kaplan JM. 2009. Investigation of the mechanism of action of alemtuzumab in a human CD52 transgenic mouse model. Immunology 128(2):260–270.

Huang W, Giddens J, Fan S-Q, Toonstra C, Wang L-X. 2012. Chemoenzymatic glycoengineering of intact IgG antibodies for gain of functions. Journal of the American Chemical Society 134(29):12308–12318.

Jacobi C, Claus M, Wildemann B, Wingert S, Korporal M, Römisch J, Meuer S, Watzl C, Giese T. 2009. Exposure of NK cells to intravenous immunoglobulin induces IFN gamma release and degranulation but inhibits their cytotoxic activity. Clinical immunology (Orlando, Fla.) 133(3):393–401.

Janke AD, Giuliani F, Yong VW. 2006. IVIg attenuates T cell-mediated killing of human neurons. Journal of neuroimmunology 177(1-2):181–188.

Jelezarova E, Vogt A, Lutz HU. 2000. Interaction of C3b(2)--IgG complexes with complement proteins properdin, factor B and factor H: Implications for amplification. The Biochemical journal 349(Pt 1):217–223.

Jung S, Aliberti J, Graemmel P, Sunshine MJ, Kreutzberg GW, Sher A, Littman DR. 2000. Analysis of fractalkine receptor CX(3)CR1 function by targeted deletion and green fluorescent protein reporter gene insertion. Molecular and cellular biology 20(11):4106–4114.

Jurewicz A, Biddison WE, Antel JP. 1998. MHC class I-restricted lysis of human oligodendrocytes by myelin basic protein peptide-specific CD8 T lymphocytes. Journal of immunology (Baltimore, Md. : 1950) 160(6):3056–3059.

Kaneko Y, Nimmerjahn F, Ravetch JV. 2006. Anti-inflammatory activity of immunoglobulin G resulting from Fc sialylation. Science (New York, N.Y.) 313(5787):670–673.

Kapur R, Aslam R, Kim M, Guo L, Ni H, Segel GB, Semple JW. 2017. Thymic-derived tolerizing dendritic cells are upregulated in the spleen upon treatment with intravenous immunoglobulin in a murine model of immune thrombocytopenia. Platelets 28(5):521–524.

Keirstead HS, Blakemore WF. 1997. Identification of post-mitotic oligodendrocytes incapable of remyelination within the demyelinated adult spinal cord. Journal of neuropathology and experimental neurology 56(11):1191–1201.

Kessel A, Peri R, Haj T, Snir A, Slobodin G, Sabo E, Rosner I, Shoenfeld Y, Toubi E. 2011. IVIg attenuates TLR-9 activation in B cells from SLE patients. Journal of clinical immunology 31(1):30–38.

Kotter MR, Li W-W, Zhao C, Franklin RJM. 2006. Myelin impairs CNS remyelination by inhibiting oligodendrocyte precursor cell differentiation. The Journal of neuroscience : the official journal of the Society for Neuroscience 26(1):328–332.

Kremer D, Aktas O, Hartung H-P, Küry P. 2011. The complex world of oligodendroglial differentiation inhibitors. Annals of neurology 69(4):602–618.

Kuraku S, Zmasek CM, Nishimura O, Katoh K. 2013. aLeaves facilitates on-demand exploration of metazoan gene family trees on MAFFT sequence alignment server with enhanced interactivity. Nucleic acids research 41(Web Server issue):W22-8.

Kuusisto H, Kaprio J, Kinnunen E, Luukkaala T, Koskenvuo M, Elovaara I. 2008. Concordance and heritability of multiple sclerosis in Finland: Study on a nationwide series of twins. European journal of neurology 15(10):1106–1110.

Kwilasz AJ, Grace PM, Serbedzija P, Maier SF, Watkins LR. 2015. The therapeutic potential of interleukin-10 in neuroimmune diseases. Neuropharmacology 96(Pt A):55–69.

Lampron A, Larochelle A, Laflamme N, Préfontaine P, Plante M-M, Sánchez MG, Yong VW, Stys PK, Tremblay M-È, Rivest S. 2015. Inefficient clearance of myelin debris by microglia impairs remyelinating processes. The Journal of experimental medicine 212(4):481–495.

Larsen PH, Wells JE, Stallcup WB, Opdenakker G, Yong VW. 2003. Matrix metalloproteinase-9 facilitates remyelination in part by processing the inhibitory NG2 proteoglycan. The Journal of neuroscience : the official journal of the Society for Neuroscience 23(35):11127–11135.

Léger J-M, Guimarães-Costa R, Iancu Ferfoglia R. 2015. The pathogenesis of multifocal motor neuropathy and an update on current management options. Therapeutic advances in neurological disorders 8(3):109–122.

Lewańska M, Siger-Zajdel M, Selmaj K. 2002. No difference in efficacy of two different doses of intravenous immunoglobulins in MS: Clinical and MRI assessment. European journal of neurology 9(6):565–572.

Liang J, Takeuchi H, Jin S, Noda M, Li H, Doi Y, Kawanokuchi J, Sonobe Y, Mizuno T, Suzumura A. 2010. Glutamate induces neurotrophic factor production from microglia via protein kinase C pathway. Brain research 1322:8–23.

Linnington C, Webb M, Woodhams PL. 1984. A novel myelin-associated glycoprotein defined by a mouse monoclonal antibody. Journal of neuroimmunology 6(6):387–396.

Liu Y, Given KS, Harlow DE, Matschulat AM, Macklin WB, Bennett JL, Owens GP. 2017. Myelin-specific multiple sclerosis antibodies cause complement-dependent oligodendrocyte loss and de-myelination. Acta neuropathologica communications 5(1):25.

Lossi L, Alasia S, Salio C, Merighi A. 2009. Cell death and proliferation in acute slices and organotypic cultures of mammalian CNS. Progress in neurobiology 88(4):221–245. Figure 1c) was reprinted with permission from Elsevier

Lucchinetti C, Brück W, Parisi J, Scheithauer B, Rodriguez M, Lassmann H. 2000. Heterogeneity of multiple sclerosis lesions: Implications for the pathogenesis of demyelination. Annals of neurology 47(6):707–717.

Lucchinetti CF, Mandler RN, McGavern D, Bruck W, Gleich G, Ransohoff RM, Trebst C, Weinshenker B, Wingerchuk D, Parisi JE, Lassmann H. 2002. A role for humoral mechanisms in the pathogenesis of Devic's neuromyelitis optica. Brain : a journal of neurology 125(Pt 7):1450–1461.

Ludwin SK, Maitland M. 1984. Long-term remyelination fails to reconstitute normal thickness of central myelin sheaths. Journal of the neurological sciences 64(2):193–198.

Lünemann JD, Nimmerjahn F, Dalakas MC. 2015. Intravenous immunoglobulin in neurology--mode of action and clinical efficacy. Nature reviews. Neurology 11(2):80–89.

Lutz HU, Späth PJ. 2005. Anti-inflammatory effect of intravenous immunoglobulin mediated through modulation of complement activation. Clinical reviews in allergy & immunology 29(3):207–212.

Lutz HU, Stammler P, Bianchi V, Trüeb RM, Hunziker T, Burger R, Jelezarova E, Späth PJ. 2004. Intravenously applied IgG stimulates complement attenuation in a complement-dependent autoimmune disease at the amplifying C3 convertase level. Blood 103(2):465–472.

Lutz HU, Stammler P, Jelezarova E, Nater M, Späth PJ. 1996. High doses of immunoglobulin G attenuate immune aggregate-mediated complement activation by enhancing physiologic cleavage of C3b in C3bn-IgG complexes. Blood 88(1):184–193.

Maddur MS, Vani J, Hegde P, Lacroix-Desmazes S, Kaveri SV, Bayry J. 2011. Inhibition of differentiation, amplification, and function of human TH17 cells by intravenous immunoglobulin. The Journal of allergy and clinical immunology 127(3):823-30.e1-7.

Mathey EK, Park SB, Hughes RAC, Pollard JD, Armati PJ, Barnett MH, Taylor BV, Dyck PJB, Kiernan MC, Lin CS-Y. 2015. Chronic inflammatory demyelinating polyradiculoneuropathy: From pathology to phenotype. Journal of neurology, neurosurgery, and psychiatry 86(9):973–985.

Mausberg AK, Dorok M, Stettner M, Müller M, Hartung HP, Dehmel T, Warnke C, Meyer Zu Hörste G, Kieseier BC. 2013. Recovery of the T-cell repertoire in CIDP by IV immunoglobulins. Neurology 80(3):296–303.

McDonald WI, Compston A, Edan G, Goodkin D, Hartung HP, Lublin FD, McFarland HF, Paty DW, Polman CH, Reingold SC, Sandberg-Wollheim M, Sibley W, Thompson A, van den Noort S, Weinshenker BY, Wolinsky JS. 2001. Recommended diagnostic criteria for multiple sclerosis:

Guidelines from the International Panel on the diagnosis of multiple sclerosis. Annals of neurology 50(1):121–127.

Medana IM, Gallimore A, Oxenius A, Martinic MM, Wekerle H, Neumann H. 2000. MHC class I-restricted killing of neurons by virus-specific CD8+ T lymphocytes is effected through the Fas/FasL, but not the perforin pathway. European journal of immunology 30(12):3623–3633.

Mi S, Miller RH, Lee X, Scott ML, Shulag-Morskaya S, Shao Z, Chang J, Thill G, Levesque M, Zhang M, Hession C, Sah D, Trapp B, He Z, Jung V, McCoy JM, Pepinsky RB. 2005. LINGO-1 negatively regulates myelination by oligodendrocytes. Nature neuroscience 8(6):745–751.

Mollnes TE, Høgåsen K, Hoaas BF, Michaelsen TE, Garred P, Harboe M. 1995. Inhibition of complement-mediated red cell lysis by immunoglobulins is dependent on the IG isotype and its C1 binding properties. Scandinavian journal of immunology 41(5):449–456.

Munger KL, Zhang SM, O'Reilly E, Hernán MA, Olek MJ, Willett WC, Ascherio A. 2004. Vitamin D intake and incidence of multiple sclerosis. Neurology 62(1):60–65.

Neumann H, Kotter MR, Franklin RJM. 2009. Debris clearance by microglia: An essential link between degeneration and regeneration. Brain : a journal of neurology 132(Pt 2):288–295.

Nimmerjahn F, Ravetch JV. 2007. The antiinflammatory activity of IgG: The intravenous IgG paradox. The Journal of experimental medicine 204(1):11–15.

Nishiyori A, Minami M, Ohtani Y, Takami S, Yamamoto J, Kawaguchi N, Kume T, Akaike A, Satoh M. 1998. Localization of fractalkine and CX3CR1 mRNAs in rat brain: Does fractalkine play a role in signaling from neuron to microglia? FEBS letters 429(2):167–172.

Obermeier B, Mentele R, Malotka J, Kellermann J, Kümpfel T, Wekerle H, Lottspeich F, Hohlfeld R, Dornmair K. 2008. Matching of oligoclonal immunoglobulin transcriptomes and proteomes of cerebrospinal fluid in multiple sclerosis. Nature medicine 14(6):688–693.

Orton S-M, Herrera BM, Yee IM, Valdar W, Ramagopalan SV, Sadovnick AD, Ebers GC. 2006. Sex ratio of multiple sclerosis in Canada: A longitudinal study. The Lancet. Neurology 5(11):932–936.

Othy S, Hegde P, Topçu S, Sharma M, Maddur MS, Lacroix-Desmazes S, Bayry J, Kaveri SV. 2013. Intravenous gammaglobulin inhibits encephalitogenic potential of pathogenic T cells and interferes with their trafficking to the central nervous system, implicating sphingosine-1 phosphate receptor 1-mammalian target of rapamycin axis. Journal of immunology (Baltimore, Md. : 1950) 190(9):4535–4541.

Park J-Y, Choi H-J, Prabagar MGV, Choi W-S, Kim S-J, Cheong C, Park CG, Chin CY, Kang Y-S. 2009. The C-type lectin CD209b is expressed on microglia and it mediates the uptake of capsular polysaccharides of Streptococcus pneumoniae. Neuroscience letters 450(3):246–251.

Pepinsky RB, Shao Z, Ji B, Wang Q, Meng G, Walus L, Lee X, Hu Y, Graff C, Garber E, Meier W, Mi S. 2011. Exposure levels of anti-LINGO-1 Li81 antibody in the central nervous system and dose-efficacy relationships in rat spinal cord remyelination models after systemic administration. The Journal of pharmacology and experimental therapeutics 339(2):519–529.

Polman CH, Reingold SC, Banwell B, Clanet M, Cohen JA, Filippi M, Fujihara K, Havrdova E, Hutchinson M, Kappos L, Lublin FD, Montalban X, O'Connor P, Sandberg-Wollheim M, Thompson AJ, Waubant E, Weinshenker B, Wolinsky JS. 2011. Diagnostic criteria for multiple sclerosis: 2010 revisions to the McDonald criteria. Annals of neurology 69(2):292–302.

Polman CH, Reingold SC, Edan G, Filippi M, Hartung H-P, Kappos L, Lublin FD, Metz LM, McFarland HF, O'Connor PW, Sandberg-Wollheim M, Thompson AJ, Weinshenker BG, Wolinsky JS. 2005. Di-

agnostic criteria for multiple sclerosis: 2005 revisions to the "McDonald Criteria". Annals of neurology 58(6):840–846.

Pugliatti M, Sotgiu S, Rosati G. 2002. The worldwide prevalence of multiple sclerosis. Clinical neurology and neurosurgery 104(3):182–191.

Pul R, Kopadze T, Skripuletz T, Voss EV, Kieseier BC, Stangel M. 2009. Polyclonal immunoglobulins (IVIg) induce expression of MMP-9 in microglia. Journal of neuroimmunology 217(1-2):46–50.

Pul R, Nguyen D, Schmitz U, Marx P, Stangel M. 2002. Comparison of intravenous immunoglobulin preparations on microglial function in vitro: More potent immunomodulatory capacity of an IgM/IgA-enriched preparation. Clinical neuropharmacology 25(5):254–259.

Ross C, Svenson M, Hansen MB, Vejlsgaard GL, Bendtzen K. 1995. High avidity IFN-neutralizing antibodies in pharmaceutically prepared human IgG. The Journal of clinical investigation 95(5):1974–1978.

Rossi F, Dietrich G, Kazatchkine MD. 1989. Antiidiotypic suppression of autoantibodies with normal polyspecific immunoglobulins. Research in immunology 140(1):19–31.

Rossi F, Kazatchkine MD. 1989. Antiidiotypes against autoantibodies in pooled normal human polyspecific Ig. Journal of immunology (Baltimore, Md. : 1950) 143(12):4104–4109.

Ruff RL, Lisak RP. 2018. Nature and Action of Antibodies in Myasthenia Gravis. Neurologic clinics 36(2):275–291.

Sa JCC de, Airas L, Bartholome E, Grigoriadis N, Mattle H, Oreja-Guevara C, O'Riordan J, Sellebjerg F, Stankoff B, Vass K, Walczak A, Wiendl H, Kieseier BC. 2011. Symptomatic therapy in multiple sclerosis: A review for a multimodal approach in clinical practice. Therapeutic advances in neurological disorders 4(3):139–168.

Scalfari A, Neuhaus A, Daumer M, Muraro PA, Ebers GC. 2014. Onset of secondary progressive phase and long-term evolution of multiple sclerosis. Journal of neurology, neurosurgery, and psychiatry 85(1):67–75.

Schwab I, Nimmerjahn F. 2013. Intravenous immunoglobulin therapy: How does IgG modulate the immune system? Nature reviews. Immunology 13(3):176–189.

Silverman HA, Dancho M, Regnier-Golanov A, Nasim M, Ochani M, Olofsson PS, Ahmed M, Miller EJ, Chavan SS, Golanov E, Metz CN, Tracey KJ, Pavlov VA. 2015. Brain region-specific alterations in the gene expression of cytokines, immune cell markers and cholinergic system components during peripheral endotoxin-induced inflammation. Molecular medicine (Cambridge, Mass.) 20:601–611.

Skulina C, Schmidt S, Dornmair K, Babbe H, Roers A, Rajewsky K, Wekerle H, Hohlfeld R, Goebels N. 2004. Multiple sclerosis: Brain-infiltrating CD8+ T cells persist as clonal expansions in the cerebrospinal fluid and blood. Proceedings of the National Academy of Sciences of the United States of America 101(8):2428–2433.

Sofroniew MV. 2015. Astrocyte barriers to neurotoxic inflammation. Nature reviews. Neuroscience 16(5):249–263.

Sorensen PS, Haas J, Sellebjerg F, Olsson T, Ravnborg M. 2004. IV immunoglobulins as add-on treatment to methylprednisolone for acute relapses in MS. Neurology 63(11):2028–2033.

Sorensen PS, Wanscher B, Jensen CV, Schreiber K, Blinkenberg M, Ravnborg M, Kirsmeier H, Larsen VA, Lee ML. 1998. Intravenous immunoglobulin G reduces MRI activity in relapsing multiple sclerosis. Neurology 50(5):1273–1281.

Spiegelberg HL, Abel CA, Fishkin BG, Grey HM. 1970. Localization of the carbohydrate within the variable region of light and heavy chains of human gamma g myeloma proteins. Biochemistry 9(21):4217–4223.

St-Amour I, Paré I, Alata W, Coulombe K, Ringuette-Goulet C, Drouin-Ouellet J, Vandal M, Soulet D, Bazin R, Calon F. 2013. Brain bioavailability of human intravenous immunoglobulin and its transport through the murine blood-brain barrier. Journal of cerebral blood flow and metabolism : official journal of the International Society of Cerebral Blood Flow and Metabolism 33(12):1983–1992.

Stangel M, Compston A. 2001. Polyclonal immunoglobulins (IVIg) modulate nitric oxide production and microglial functions in vitro via Fc receptors. Journal of neuroimmunology 112(1-2):63–71.

Stangel M, Compston A, Scolding NJ. 1999. Polyclonal immunoglobulins for intravenous use do not influence the behaviour of cultured oligodendrocytes. Journal of neuroimmunology 96(2):228–233.

Stangel M, Compston A, Scolding NJ. 2000. Oligodendroglia are protected from antibody-mediated complement injury by normal immunoglobulins ("IVIg"). Journal of neuroimmunology 103(2):195–201.

Stangel M, Joly E, Scolding NJ, Compston DA. 2000. Normal polyclonal immunoglobulins ('IVIg') inhibit microglial phagocytosis in vitro. Journal of neuroimmunology 106(1-2):137–144.

Stoppini L, Buchs PA, Muller D. 1991. A simple method for organotypic cultures of nervous tissue. Journal of neuroscience methods 37(2):173–182.

Svenson M, Hansen MB, Bendtzen K. 1993. Binding of cytokines to pharmaceutically prepared human immunoglobulin. The Journal of clinical investigation 92(5):2533–2539.

Svenson M, Hansen MB, Ross C, Diamant M, Rieneck K, Nielsen H, Bendtzen K. 1998. Antibody to granulocyte-macrophage colony-stimulating factor is a dominant anti-cytokine activity in human IgG preparations. Blood 91(6):2054–2061.

Tackenberg B, Jelcic I, Baerenwaldt A, Oertel WH, Sommer N, Nimmerjahn F, Lünemann JD. 2009. Impaired inhibitory Fcgamma receptor IIB expression on B cells in chronic inflammatory demyelinating polyneuropathy. Proceedings of the National Academy of Sciences of the United States of America 106(12):4788–4792.

Teitelbaum D, Aharoni R, Arnon R, Sela M. 1988. Specific inhibition of the T-cell response to myelin basic protein by the synthetic copolymer Cop 1. Proceedings of the National Academy of Sciences of the United States of America 85(24):9724–9728.

Teksam M, Tali T, Kocer B, Isik S. 2000. Qualitative and quantitative volumetric evaluation of the efficacy of intravenous immunoglobulin in multiple sclerosis: Preliminary report. Neuroradiology 42(12):885–889.

Thacker EL, Mirzaei F, Ascherio A. 2006. Infectious mononucleosis and risk for multiple sclerosis: A meta-analysis. Annals of neurology 59(3):499–503.

Tha-In T, Metselaar HJ, Tilanus HW, Boor PPC, Mancham S, Kuipers EJ, Man RA de, Kwekkeboom J. 2006. Superior immunomodulatory effects of intravenous immunoglobulins on human T-cells and dendritic cells: Comparison to calcineurin inhibitors. Transplantation 81(12):1725–1734.

Thompson AJ, Banwell BL, Barkhof F, Carroll WM, Coetzee T, Comi G, Correale J, Fazekas F, Filippi M, Freedman MS, Fujihara K, Galetta SL, Hartung HP, Kappos L, Lublin FD, Marrie RA, Miller AE, Miller DH, Montalban X, Mowry EM, Sorensen PS, Tintoré M, Traboulsee AL, Trojano M,

Uitdehaag BMJ, Vukusic S, Waubant E, Weinshenker BG, Reingold SC, Cohen JA. 2018. Diagnosis of multiple sclerosis: 2017 revisions of the McDonald criteria. The Lancet. Neurology 17(2):162–173.

Trapp BD, Peterson J, Ransohoff RM, Rudick R, Mörk S, Bö L. 1998. Axonal transection in the lesions of multiple sclerosis. The New England journal of medicine 338(5):278–285.

Urich E, Gutcher I, Prinz M, Becher B. 2006. Autoantibody-mediated demyelination depends on complement activation but not activatory Fc-receptors. Proceedings of the National Academy of Sciences of the United States of America 103(49):18697–18702.

van Engelen BG, Renier WO, Weemaes CM, Lamers KJ, Gabreels FJ, Meinardi H. 1994. Cerebrospinal fluid examinations in cryptogenic West and Lennox-Gastaut syndrome before and after intravenous immunoglobulin administration. Epilepsy research 18(2):139–147.

van Oosten BW, Lai M, Hodgkinson S, Barkhof F, Miller DH, Moseley IF, Thompson AJ, Rudge P, McDougall A, McLeod JG, Adèr HJ, Polman CH. 1997. Treatment of multiple sclerosis with the monoclonal anti-CD4 antibody cM-T412: Results of a randomized, double-blind, placebo-controlled, MR-monitored phase II trial. Neurology 49(2):351–357.

Wada J, Shintani N, Kikutani K, Nakae T, Yamauchi T, Takechi K. 2001. Intravenous immunoglobulin prevents experimental autoimmune myositis in SJL mice by reducing anti-myosin antibody and by blocking complement deposition. Clinical and experimental immunology 124(2):282–289.

Walsh MJ, Tourtellotte WW. 1986. Temporal invariance and clonal uniformity of brain and cerebrospinal IgG, IgA, and IgM in multiple sclerosis. The Journal of experimental medicine 163(1):41–53.

Warrington AE, Asakura K, Bieber AJ, Ciric B, van Keulen V, Kaveri SV, Kyle RA, Pease LR, Rodriguez M. 2000. Human monoclonal antibodies reactive to oligodendrocytes promote remyelination in a model of multiple sclerosis. Proceedings of the National Academy of Sciences of the United States of America 97(12):6820–6825.

Wekerle H. 2017. B cells in multiple sclerosis. Autoimmunity 50(1):57–60.

Willer CJ, Dyment DA, Risch NJ, Sadovnick AD, Ebers GC. 2003. Twin concordance and sibling recurrence rates in multiple sclerosis. Proceedings of the National Academy of Sciences of the United States of America 100(22):12877–12882.

Winter M, Baksmeier C, Steckel J, Barman S, Malviya M, Harrer-Kuster M, Hartung H-P, Goebels N. 2016. Dose-dependent inhibition of demyelination and microglia activation by IVIG. Annals of clinical and translational neurology 3(11):828–843.

Wioland L, Dupont J-L, Doussau F, Gaillard S, Heid F, Isope P, Pauillac S, Popoff MR, Bossu J-L, Poulain B. 2015. Epsilon toxin from Clostridium perfringens acts on oligodendrocytes without forming pores, and causes demyelination. Cellular microbiology 17(3):369–388.

Wolswijk G, Balesar R. 2003. Changes in the expression and localization of the paranodal protein Caspr on axons in chronic multiple sclerosis. Brain : a journal of neurology 126(Pt 7):1638–1649.

Wurster U, Haas J. 1994. Passage of intravenous immunoglobulin and interaction with the CNS. Journal of neurology, neurosurgery, and psychiatry 57 Suppl:21–25.

Yamasaki R, Lu H, Butovsky O, Ohno N, Rietsch AM, Cialic R, Wu PM, Doykan CE, Lin J, Cotleur AC, Kidd G, Zorlu MM, Sun N, Hu W, Liu L, Lee J-C, Taylor SE, Uehlein L, Dixon D, Gu J, Floruta CM, Zhu M, Charo IF, Weiner HL, Ransohoff RM. 2014. Differential roles of microglia and monocytes in the inflamed central nervous system. The Journal of experimental medicine 211(8):1533–1549.

Youings A, Chang SC, Dwek RA, Scragg IG. 1996. Site-specific glycosylation of human immunoglobulin G is altered in four rheumatoid arthritis patients. The Biochemical journal 314 (Pt 2):621–630.

Yuki N, Hartung H-P. 2012. Guillain-Barré syndrome. The New England journal of medicine 366(24):2294–2304.

Zamvil S, Nelson P, Trotter J, Mitchell D, Knobler R, Fritz R, Steinman L. 1985. T-cell clones specific for myelin basic protein induce chronic relapsing paralysis and demyelination. Nature 317(6035):355–358.

6 Appendix

6.1 List of figures

6.2 List of tables

6.3 Abbreviations

ADCC	Antibody-depdendent cytotoxicity
BBB	Blood brain barrier
BC	Bicinchoninic acid
BDNF	Brain-derived neurotrophic factor
BSA	Bovine serum albumin
Ca^{2+}	Calcium ions
Caspr	Contactin associated protein 1
CD11b	Cluster of differentiation molecule 11B
CDC	Complement dependent cytotoxicity
cDNA	Complementary DNA
CNPase	2',3'-Cyclic-nucleotide 3'-phosphodiesterase
CNS	Central nervous system
CSF	cerebrospinal fluid
CX3CL1	Fractalkine
CX3CR1	Fractalkine receptor
d	day
DC-SIGN	Dendritic Cell-Specific Intercellular adhesion molecule-3-Grabbing Non-integrin
dH_2O	distilled water
DMF	dimethyl fumarate
DNA	Deoxyribonucleic acid
DTT	Dithiothreitol
EAE	Experimental autoimmune encephalitis
EBV	Epstein-Barr virus

EDTA	Ethylenediaminetetraacetic acid
EGL	External granule layer
ELISA	Enzyme-linked Immunosorbent Assay
Fab	Fab fragment
Fc	Fc fragment
FCS	Fetal calf serum
FS	Freestyle
GAPDH	Glyceraldehyde 3-phosphate dehydrogenase
GC	Granule cells
GDNF	Glial cell line derived neurotrophic factor
GFP	Green fluorescent protein
GFP^+	GFP-positive
HCl	Hydrogen chloride
HEK-FS cells	Human embryonic kidney FreeStyle™ cells
HEPES	4-(2-hydroxyethyl)-1-piperazineethanesulfonic acid
HLA	Human leukocyte antigen
HSA	Human serum albumin
hu	Human
hu818c5	Humanized anti MOG-antibody clone 818c5
Iba1	Ionized calcium-binding adapter molecule 1
Ig	Immunoglobulin
IGL	Internal granular layer
IL-10	Interleukin 10
IL-1β	Interleukin 1 beta
IVIG	Intravenous immunoglobulin

LINGO-1	Leucine rich repeat and immunoglobulin-like domain-containing protein 1
MBP	Myelin basic protein
MEM	Minimal essential medium
Mg^{2+}	Magnesium ions
MHC	Major histocompatibility complex
ML	Molecular layer
MMP-9	Matrix metalloproteinase-9
MOG	Myelin oligodendrocyte glycoprotein
MS	Multiple sclerosis
NaCl	Sodium chloride
NF155	Neurofascin 155
NF200	Neurofilament 200
Ng2	Neuron-glial antigen 2
NGF	Neuronal growth factor
NgR1	Nogo receptor 1
NO	Nitric oxide
Nrf2	Nuclear factor erythroid 2-related factor 2
ns	not significant
OCB	Oligoclonal bands
OD	Optical density
OPC	Oligogendrocyte precursor cell
OSC	Organotypic slice culture
P	Postnatal day
PAGE	Polyacrylamide gel electrophoresis

PBS	Phosphate-buffered saline
PC	Purkinje cells
PCL	Purkinje cell layer
PCR	Polymerase chain reaction
PEI	Polyethylenimine
Pen	Penicillin
PLP	Proteolipid Protein
PNS	Peripheral nervous system
PP	Primary progressive
RNA	Ribonucleic acid
Rnase	Ribonuclease
RPMI	Roswell Park Memorial Institute medium
RR	Relapsing-remitting
S1PR1	Sphingosine-1-phosphate receptor 1
SDS	Sodium dodecyl sulfate
SEM	Standard error of the mean
SP	Secondary progressive
Strep	Streptomycin
TBE	Tris-borate-EDTA
TMB	3,3',5,5'-Tetramethylbenzidine
TNF α	Tumor necrosis factor alpha
Tris	Tris(hydroxymethyl)aminomethane
U	Enzyme units

7 Acknowledgements

First, I would like to thank Prof. Dr. Norbert Goebels for the opportunity to do my PhD studies in the field of neurology. I appreciated my freedom of action and independency during the time of my PhD as well as his contagious enthusiasm for research.

Many thanks go also to Prof. Dr. Peter Proksch for being my second research supervisor.

I would like to thank all current and former members of the AG Goebels. My special thanks go to Julia Steckel for the many years of support in all major and minor projects. Thanks to Sumanta Barman, Henrike Diel and Md. Nur A Alam Siddique for the production of recombinant antibodies and for being wonderful colleagues. I would also like to thank Tatjana Males for helping me with the organotypic slice culture (OSC) experiments and for doing a great job getting the lab more organized. Thanks to Armin Scheffler for his imperturbable calm and his untiring friendliness. Thanks to Anna Coordt for her inescapable good spirits and of course for being the never-ending source of those delicious flapjacks. Further, I would like to thank Marcel Brauweiler and Pia Sporkmann for being the best medical students one could think of in the lab. Thanks to Manish Malviya, who taught me how to produce monoclonal recombinant antibodies and to Meike Winter who introduced me to the world of OSCs.

I would also like to thank all current and former colleagues of the Life Science Center for their help during productive and unproductive times. Especially, I would like to thank Klaudia Lepka not only for many productive discussions and scientific advices but also for the great time we had together in our shared office. Thanks to my iBrain colleague Maxi Hofrichter for the delicious meetings. Further, I would like to thank Marcel Kohlhaas for his fast and uncomplicated help with technical problems.

For financial, support I would like to thank the iBrain Graduate School from the Heinrich-Heine-University Düsseldorf.

My sincere thanks go to my parents who supported me on my ways to this day.

Finally, I would like to express my heartfelt thanks to Heiko Luckmann, who was always at my side in good as well as in bad times.

8 Declarations

Ich versichere an Eides Statt, dass die Dissertation von mir selbstständig und ohne unzulässige fremde Hilfe unter Beachtung der "Grundsätze zur Sicherung guter wissenschaftlicher Praxis an der Heinrich-Heine-Universität Düsseldorf" erstellt worden ist.

Die Dissertation wurde weder in dieser noch in einer abgewandelten Form bereits einer anderen Fakultät vorgelegt. Ich habe bisher keine erfolglosen Promotionsversuche unternommen.

Daten der vorliegenden Dissertation wurden von Winter et al., 2016 veröffentlicht. Die Verwendung dieser Daten in der vorliegenden Dissertation, wurde an den entsprechenden Stellen kenntlich gemacht. Zur Generierung der von Winter et al., 2016 veröffentlichten Daten habe ich unten stehende Beiträge geleistet und dadurch die geteilte Erstautorenschaft erlangt.

- Präparation von organotypischen Schnittkulturen aus dem Cerebellum (OSCs) von postnatalen Mäusen
- Durchführung von Demyelinisierungsversuchen an OSCs
- Dokumentation der Demyelinisierung in lebenden OSCs mit Hilfe von Fluoreszenzmikroskopie
- Quantifizierung der Demyeliniserung anhand von fluoreszenzmikroskopischen Aufnahmen
- Dissoziation von OSCs und anschließende immunhistochemische Färbung der Einzelzellsuspension zur Analyse mittels Durchflusszytometrie
- Analysen zur Genexpression in OSCs mittels quantitativer Echtzeit-PCR
- Immunhistochemische Färbungen von OSCs
- Statistiche Auswertung der generierten Daten
- Korrektur des Manuskripts

_____ _____

Ort, Datum Unterschrift (Christine Baksmeier)